



REVIEW ARTICLE

# Progress on phthalocyanine-conjugated Ag and Au nanoparticles: Synthesis, characterization, and photo-physicochemical properties

Shereen A. Majeed<sup>a,\*</sup>, Kutloano Edward Sekhosana<sup>b</sup>, Ahmad Tuhl<sup>c</sup>

<sup>a</sup> Department of Chemistry, Kuwait University, P.O. Box 5969, Safat 13060, Kuwait

<sup>b</sup> Nanotechnology and Water Sustainability (NanoWS) Research Unit, College of Science, Engineering and Technology (CSET), University of South Africa, Cnr Christiaan De Wet and Pioneer Avenue, Florida, Roodepoort 1709, South Africa

<sup>c</sup> Department of Chemistry, Acadia University, Wolfville, NS 902-993-0017, Canada

Received 16 July 2020; accepted 4 October 2020

Available online 15 October 2020

## KEYWORDS

Phthalocyanine;  
Nanoconjugate;  
Fluorescence;  
Singlet oxygen;  
Triplet;  
Nonlinear optics

**Abstract** Phthalocyanine (Pc) complexes are an important class of dyes with numerous (e.g., biological, photophysical, and analytical) applications. Among the methods used to improve the properties of these complexes, one should mention the introduction of different substituents, variation of the central metal ion, ligand exchange, and conjugation to nanomaterials (e.g., carbon-based nanomaterials and metal nanoparticles (NPs)). This work briefly reviews Pc complex conjugation to Ag and Au NPs, highlights the different NP shapes, and discusses the diversity of conjugation approaches. Moreover, the use of UV–Vis spectroscopy, powder X-ray diffraction, X-ray photoelectron spectroscopy, transmission electron microscopy, atomic force microscopy, dynamic light scattering and Fourier transform infrared spectroscopy to characterize Pc-NP hybrids is summarized. The effect of conjugation on Pc photo-physicochemical properties (fluorescence, singlet oxygen generation, triplet state formation, and optical limiting behavior) is discussed, and future perspectives for the synthesis and applications of new hybrids are provided.

© 2020 The Author(s). Published by Elsevier B.V. on behalf of King Saud University. This is an open access article under the CC BY-NC-ND license (<http://creativecommons.org/licenses/by-nc-nd/4.0/>).

\* Corresponding author.

E-mail address: [sh.sh.a.majeed@gmail.com](mailto:sh.sh.a.majeed@gmail.com) (S.A. Majeed).

Peer review under responsibility of King Saud University.



Production and hosting by Elsevier

## Contents

1. Introduction . . . . .	8849
2. Synthesis and characterization of NPs and their Pc conjugates . . . . .	8850
2.1. NP synthesis. . . . .	8850
2.2. Conjugation of Pcs to Ag and Au NPs. . . . .	8857
2.3. Characterization . . . . .	8858
2.3.1. UV-Vis spectroscopy . . . . .	8858
2.3.2. Powder X-ray diffraction (PXRD) . . . . .	8861
2.3.3. X-ray photoelectron spectroscopy (XPS) . . . . .	8861
2.3.4. Transmission electron microscopy (TEM) . . . . .	8867
2.3.5. Dynamic light scattering (DLS) . . . . .	8867
2.3.6. Atomic force microscopy (AFM) . . . . .	8869
2.3.7. Fourier transform infrared (FT-IR) spectroscopy . . . . .	8869
3. Photo-physicochemical properties . . . . .	8870
3.1. Background of Pc photophysical studies . . . . .	8870
3.2. Fluorescence studies . . . . .	8870
3.2.1. Background . . . . .	8870
3.2.2. Determination of the fluorescence quantum yield of Pc complexes . . . . .	8870
3.2.3. Effect of Ag and Au NPs on the fluorescence properties . . . . .	8871
3.3. Triplet and singlet oxygen generation . . . . .	8872
3.3.1. Background . . . . .	8872
3.3.2. Determination of singlet oxygen and triplet oxygen quantum yields of Pc complexes . . . . .	8872
3.3.3. Effect of Ag and Au NPs on triplet and singlet oxygen generation . . . . .	8873
3.3.4. Photothermal conversion efficiency . . . . .	8874
3.4. Nonlinear optical limiting . . . . .	8874
3.4.1. Background . . . . .	8874
3.4.2. Calculation of NLO parameters. . . . .	8876
3.4.3. Effect of Ag and Au NPs . . . . .	8877
4. Conclusion and future perspectives . . . . .	8878
Declaration of Competing Interest . . . . .	8879
Acknowledgments . . . . .	8879
References . . . . .	8879

## 1. Introduction

Phthalocyanines (Pcs) have been intensively studied as prospective compounds for the photodynamic therapy (PDT) of cancer (Allen et al., 2001; Khoza et al., 2020; Lee et al., 2020; Li et al., 2018a, 2018b, 2019a, 2019b; Lukyanets, 1999; Miller et al., 2007; Moeno et al., 2014; Negrimovsky et al., 2015), near-infrared (NIR) imaging (Lobo et al., 2016; Pansare et al., 2012), organic-based solar cells (Ghadari et al., 2020; Ince et al., 2014; Singh et al., 2005; Walter et al., 2010; Yuen et al., 2012), and organic light-emitting diodes (Bae et al., 2012; Kao et al., 2006; Wang et al., 2015).

Pc properties can be enhanced through the modification of peripheral (*p*) and nonperipheral (*np*) positions and the central metal (*M*) (Fig. 1). In particular, Pcs can be conjugated to nanomaterials such as carbon nanotubes (Pillay and Ozoemena, 2009; Yang et al., 2004), fullerenes (Bottari et al., 2013; Yoshimoto et al., 2008; Yuen et al., 2012), graphene quantum dots (GQDs) (Achadu and Nyokong, 2017; Bankole et al., 2017a; Fomo et al., 2018; Majeed et al., 2019b), nanodiamonds (Matshitse and Nyokong, 2020), and metal nanoparticles (NPs) (Ashokkumar et al., 2014; Castro-Latorre et al., 2020; Cheng et al., 2019; Fashina et al., 2013; Hong et al., 2018; Matlou et al., 2019; Mpetta et al., 2020; Mphuthi et al., 2017; Zasedatelev et al., 2016) via *p*, *np*, or axial ligands.

Self-assembly has also attracted remarkable interest in nanomedicine due to noteworthy potential in phototheranostic and PDT applications (Li et al., 2018a, 2019b; Lovell et al.,

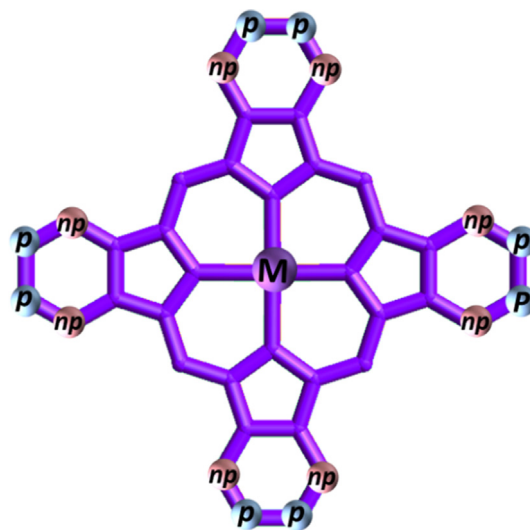


**Fig. 1** Pc structure illustrating the positions of different substitution sites.

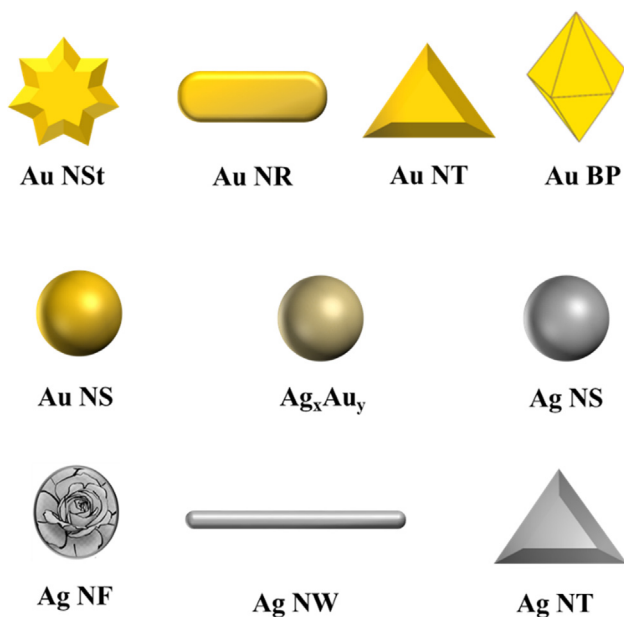


**Fig. 2** Schematic structures of Ag and Au nanomaterials used to enhance the photo-physicochemical properties of Pc complexes.

2011; Ma and Zhao, 2015; Zou et al., 2017). This method generally refers to a self-cyclic arrangement of an organic compound either by encapsulating a biomolecule into the cavity or by forming a completely new nanohybrid from itself with the exposed substituents enhancing the solubility. Self-assembly nanohybrids are stable, and can be well-dispersed in neutral solvents (Li et al., 2018a). As such, these nanohybrids do not suffer from aggregation. Among these approaches, conjugation to Ag and Au NPs has been extensively employed to improve the photophysical properties of Pcs through the heavy atom effect, which, in turn, increases the extent of intersystem crossing (ISC) to the triplet state and thus improves singlet oxygen generation and nonlinear optical (NLO) parameters (Nwaji et al., 2017d). Thus, the above NPs have been widely used in drug delivery imaging, sensing medicine, preclinical, clinical anti-arthritis, antimicrobial, anticancer, antiparasitic, anti-HIV, and other biological applications (Chen et al., 2010; Hone et al., 2002; Khoza et al., 2020; Shaw, 1999; Terentyuk et al., 2014; Wieder et al., 2006).

Free electrons on the surface of metal NPs can be excited by the electric field of light to create collective free conduction oscillation modes. This localized surface plasmon resonance (LSPR) endows metal NPs with certain optical properties such as light absorption and scattering in a certain wavelength range (visible to infrared wavelengths in the case of noble metal NPs) (Kulyk et al., 2019; Majeed, 2020; Teixeira et al., 2015; Waszkowska et al., 2020). The SPR is known to impact the fluorescence properties of fluorophores (Kang et al., 2011). In some instances, at a controlled distance between the fluorophore and the nanoparticle surface, the quenching of fluorescence occurs (Swierczewska et al., 2011). The improvement of fluorescence through metal-enhanced fluorescence phenomenon has also been reported (García Calavia et al., 2018), with this phenomenon observed in Pcs conjugated to Au NPs leading to an increased production of singlet oxygen.

For polymer nanofibers formed from phthalocyanines linked to Au NPs, singlet oxygen quantum yield has been observed to increase significantly (Tombe et al., 2013b).

Herein, we summarize the methods used to synthesize and characterize the conjugates of Pcs with Ag and Au NPs, further describing the effect of this conjugation on Pc photophysical properties (fluorescence, triplet state formation, singlet oxygen formation, and NLO parameters).

## 2. Synthesis and characterization of NPs and their Pc conjugates

### 2.1. NP synthesis

Since the introduction of the two-phase system by Faraday (Faraday, 1857), many approaches such as the Turkevich method (Turkevich et al., 1951) and Brust's two-phase reduction method (Brust et al., 1994) have been employed to synthesize functionalized NPs with well-controlled morphology and variable size/shape and thus tune their surface plasmon resonance (SPR), which affects NP physicochemical properties (Lee et al., 2008; Widoniak et al., 2005), especially for NPs with aspect ratios (length/width) of  $> 1$  (Nikoobakht and El-Sayed, 2003). Thermal annealing has also been shown to afford Au NPs (Jia et al., 2017). Herein, we focus on the methods used for conjugating Pc complexes to Ag and Au NPs (Fig. 2) to enhance the photophysical properties of these complexes.

**Nanospheres (NSs):** Spherical Au and Ag NPs can be synthesized using different capping agents and surfactants (Frens, 1973). According to the widely used Brust protocol, chloroaurate ions are transferred from an aqueous medium into an organic solvent with the help of phase-transfer agents (e.g., tetraalkylammonium salts), reduced, and capped by alkanethiols/alkylamines (Brust et al., 1994). Tetraoctylammonium bromide (TOABr, Fig. 3) is widely used in the synthesis of Au and Ag NSs as a phase-transfer agent (Brust et al., 1994), while methoxypolyethylene glycol thiol (MPEG-SH, Fig. 3) is used as a capping agent in the synthesis of Au NSs by the Frens method (Frens, 1973), and 4-hexadecylaniline (HDA, Fig. 3) is commonly used as a stabilizing agent (Osifeko and Nyokong, 2016).

**Nanorods (NRs):** During seed-mediated growth – the most common method of synthesizing NPs of different shapes – small spherical Au NPs prepared in the seeding step are grown in the desired shape by controlling the type and concentration of added reagents (Jana et al., 2001). The most broadly used surfactant is cetyltrimethylammonium bromide (CTAB, Fig. 3), as its adsorption at the crystal faces of Au inhibits growth in the direction perpendicular to the longer axis, thus supporting growth at the ends of nonspherical particles (Murphy et al., 2005). Templates such as alumina (Martin et al., 1999; van der Zande et al., 2000), carbon nanotubes (Fullam et al., 2000; Govindaraj et al., 2000), micelles (Pileni et al., 1998), and polycarbonates (Cepak and Martin, 1998) are widely employed to synthesize Au NRs and nanowires (NWs) in addition to electrochemical (Yu et al., 1997), photochemical (Esumi et al., 1995), and reduction methods (Nikoobakht and El-Sayed, 2003). Notably, additives such as  $\text{Ag}^+$  ions and cyclohexane strongly favor the formation of Au NRs/NWs (Hao Ming Chen et al., 2009; Mthethwa and Nyokong, 2015). Ascorbic acid and HDA are also used to

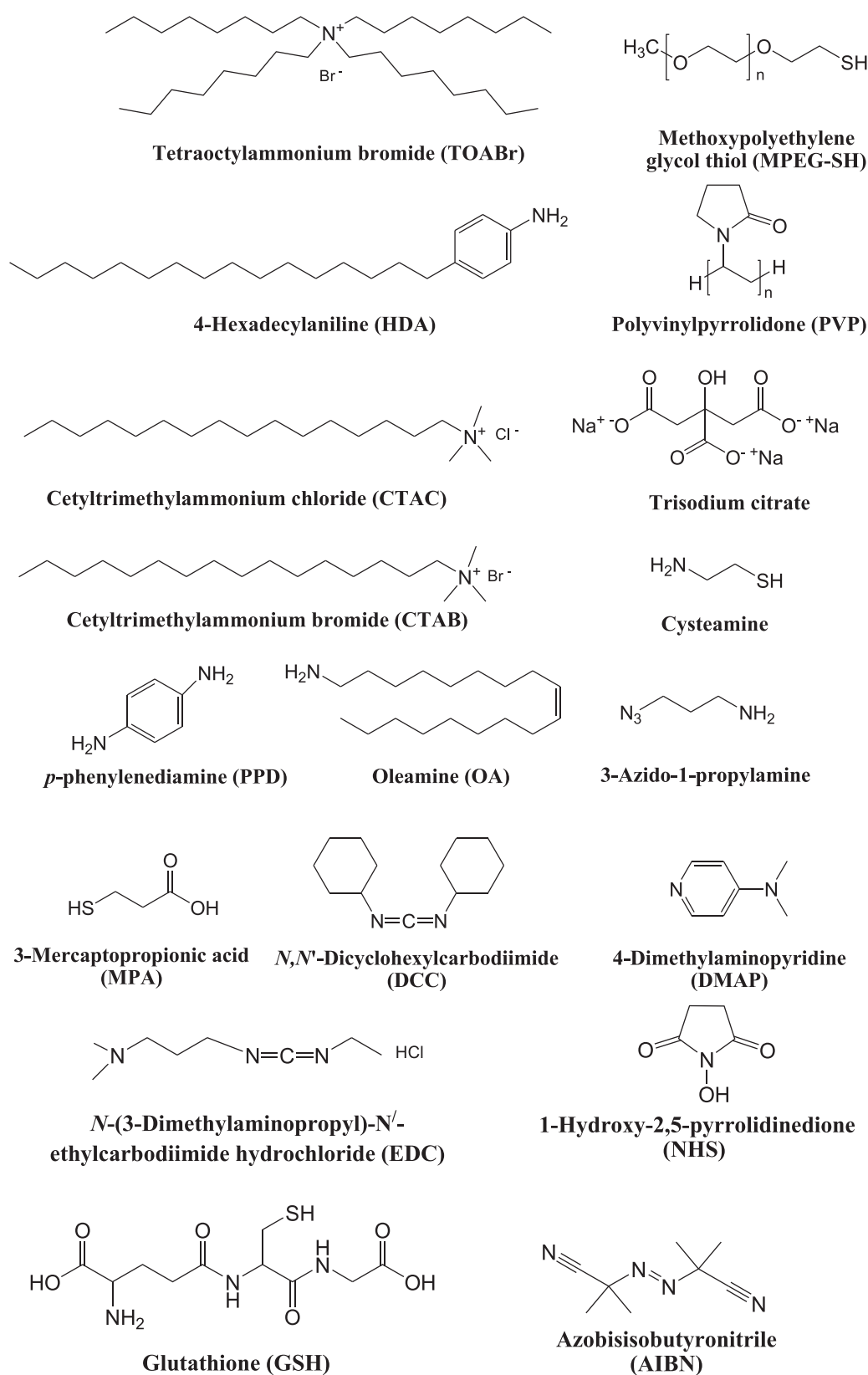
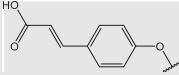
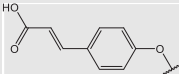
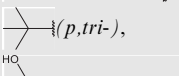


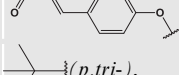
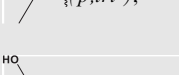
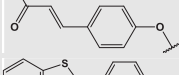
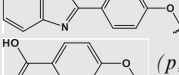
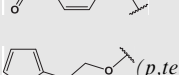
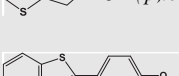
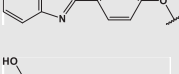
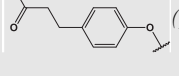
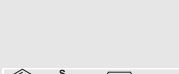
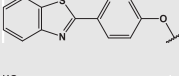
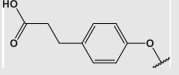
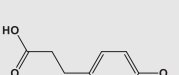
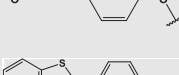
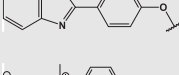


Fig. 3 General reagents used in nanomaterial synthesis.

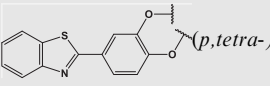
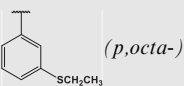
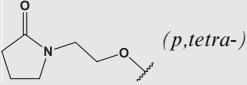
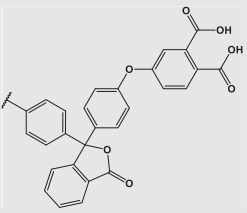
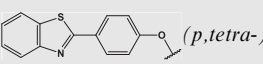
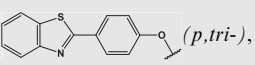
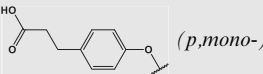
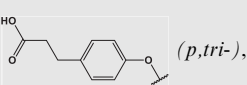
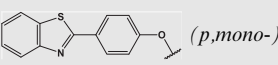
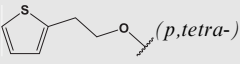
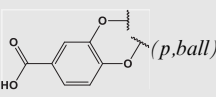
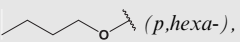
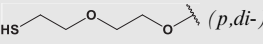
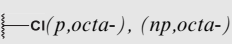
reduce and transfer Au ions to organic media to form Au NRs through seeded growth (Chandran et al., 2007; Mthethwa and Nyokong, 2015; Selvakannan et al., 2002; Zhou et al., 2016).

**Bipyramidal branched Au nanocrystals and nanostars (NSts):** Au bipyramids (BPs) can be synthesized by adding Au seed particles to a mixture of  $\text{HAuCl}_4$ , ascorbic acid, a capping sur-

**Table 1** Summary of substituents introduced to Pc complexes and the type/size of NPs used for Pc conjugation.

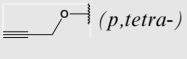
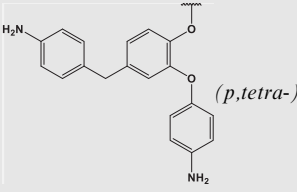
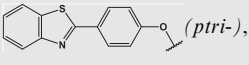
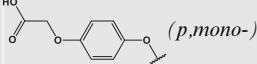
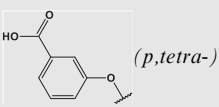
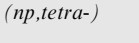
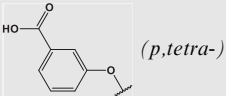
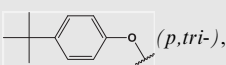
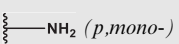
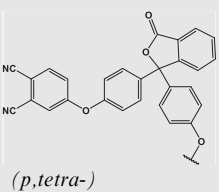
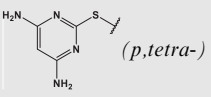
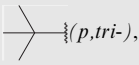
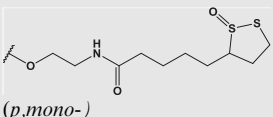
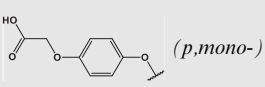
Substituent structure, position, no	M	NPs	Estimated NPs size (nm)	Stabilizer	Ref.
 ( <i>p,tetra-</i> )	Zn	Ag NS	11.68 (TEM) 11.88 (PXRD)	OA Ex. cysteamine	(Matlou and Nyokong, 2020)
 ( <i>p,mono-</i> )	Zn				
 ( <i>p,tri-</i> ),					
 ( <i>p,mono-</i> )	Zn				
 ( <i>p,tri-</i> ),					
 ( <i>p,mono-</i> )	Zn				
 ( <i>p,tri-</i> ),					
 ( <i>p,mono-</i> )	Zn	Ag NS	11.68 (TEM) 11.88 (PXRD)	OA Ex. cysteamine	(Matlou et al., 2019)
 ( <i>p,tri-</i> ),					
 ( <i>p,mono-</i> )	Zn	Ag NS <sup>a</sup> Au NS <sup>a</sup>	– –	Pc	(Nwahara et al., 2019)
 ( <i>p,tetra-</i> )	Zn, InCl	Au NS, Au NT	15.2 (TEM) 52.7(TEM)	TOABr CTAC	(Dube and Nyokong, 2019a)
 ( <i>p,tetra-</i> )	Zn, InCl				
 ( <i>p,tetra-</i> )	Zn	Au NS, Au NT	17.7 (TEM) 33.2 (TEM)	TOABr Ex. GSH CTAC Ex.GSH	(Dube and Nyokong, 2019b)
 ( <i>p,tri-</i> ),					
 ( <i>p,mono-</i> )	Zn				
 ( <i>P,mono-</i> )	Zn				
 ( <i>p,tetra-</i> )	Zn InCl	Au NS	4.51 (PXRD) 78.4 (TEM)	CTAB	(Dube et al., 2019c)
 ( <i>p,tetra-</i> )	InCl	Ag NP <sup>b</sup> , Ag NP <sup>c</sup>	10 (TEM) 5 (TEM)	OA	(Magadla et al., 2019)
 ( <i>p,tetra-</i> )	Zn InCl	Ag NT	26 (TEM)	Sodium citrate Ex. GSH	(Mafukidze et al., 2019)

**Table 1** (continued)

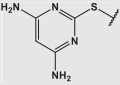
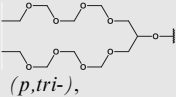
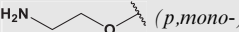
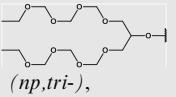
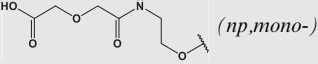
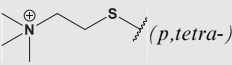
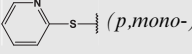
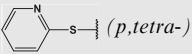
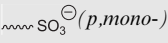
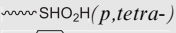
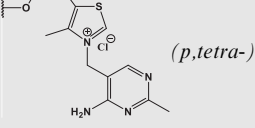
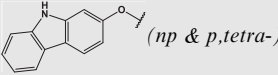
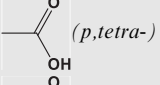
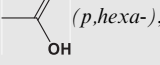
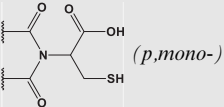
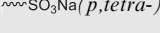
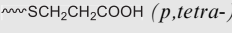
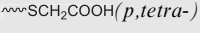
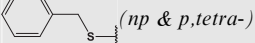
Substituent structure, position, no	M	NPs	Estimated NPs size (nm)	Stabilizer	Ref.
 (p,tetra-)	Zn, GaCl, InCl	Ag NS, Au NS	10.5(TEM) 9.3(PXRD) 12.4(TEM) 10.7(PXRD)	OA	(Nwaji et al., 2018)
 (p,octa-)	TbOAc, ErOAc, LuOAc	Au NS	30	Commercial	(Dubinina et al., 2018)
 (p,tetra-)	Zn, Cu, Co, Ni	Au NS	14.9 (TEM)	MPEG-SH	(Chen et al., 2018)
–	Zn	Ag NW	60–200 <sup>d</sup> (TEM)	PVP	(Zhang et al., 2018)
 (p,tetra-)	Zn	Ag NS	50 (TEM)	CTAB	(Zhou et al., 2018)
 (p,tetra-)	Zn	Au NT	62.3 (TEM)	CTAC	(Dube et al., 2018a)
 (p,tri-),					
 (p,mono-)					
 (p,tri-),					
 (p,mono-)					
 (p,tetra-)	Zn	Au NS <sup>c</sup>	4.51 (PXRD) 78.4 (TEM)	CTAB	(Dube et al., 2018c)
 (p,ball)	InCl	Ag NS, Au NS	7.61 (PXRD) 14.77 (PXRD)	TOABr Ex. GSH Sodium borohydride Ex. GSH	(Nwaji et al., 2017d)
 (p,hexa-),  (p,di-)	2H	Ag NS	7.4 (TEM)	OA	(Oluwole et al., 2017b)
 (p,octa-), (np,octa-)	ErOAc EuOAc LuOAc	Au NS	20 & 30 (TEM)	Commercial	(Kuzmina et al., 2017)

(continued on next page)

**Table 1** (continued)

Substituent structure, position, no	M	NPs	Estimated NPs size (nm)	Stabilizer	Ref.
 ( <i>p,tetra-</i> )	Zn, InCl	Au NS	5.0 (TEM)	TOABr Ex. 3-azido-1-prop-ylamine	(Bankole and Nyokong, 2017b)
 ( <i>p,tetra-</i> )	Zn	Ag NS, Au NS	9.02 (TEM) 9.84 (PXRD) 10.5 (TEM) 10.9 (PXRD)	OA Ex. GSH	(Nwaji et al., 2017b)
 ( <i>p,tri-</i> ),  ( <i>p,mono-</i> )	Zn	Ag NS, Au NS	8.03 (TEM) 9.88 (DLS) 10.5 (TEM) 10.25(DLS)	OA Ex. GSH	(Nwaji and Nyokong, 2017c)
 ( <i>p,tetra-</i> )  ( <i>np,tetra-</i> )	InCl	Ag NS <sup>f</sup>	14.1 (PXRD)	OA Ex. GSH	(Oluwole et al., 2017a)
 ( <i>p,tetra-</i> )	InOH	Ag <sub>x</sub> Au <sub>y</sub> <sup>g</sup>	9.0 (TEM)	OA Ex. GSH	(Dube et al., 2017)
 ( <i>p,tri-</i> ),  ( <i>p,mono-</i> )	Zn	Ag NP <sup>b</sup> , Ag NP <sup>c</sup>	10 (TEM) 5 (TEM)	OA Ex. MPA	(Bankole and Nyokong, 2016a)
 ( <i>p,tetra-</i> )	Zn	Au NR	2.1 <sup>d</sup> (TEM)	CTAB	(Zhou et al., 2016)
 ( <i>p,tetra-</i> )	Zn, InCl	Au NS	5.35 (TEM)	HDA	(Osifeko and Nyokong, 2016)
 ( <i>p,tri-</i> ),  ( <i>p,mono-</i> )	Zn	Au NS	2.0–2.5 (TEM)	TOABr	(Baldovi et al., 2016)
 ( <i>p,mono-</i> )	Zn	Ag NS, Ag <sub>x</sub> Au <sub>y</sub>	14.2 (TEM) 11.3 (PXRD) 20.9 (TEM) 11.6 (PXRD)	OA Ex. cysteamine OA	(Oluwole et al., 2016)

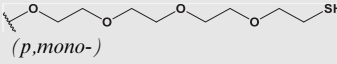
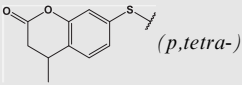
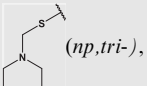
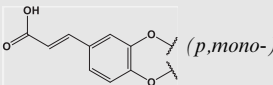
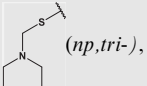
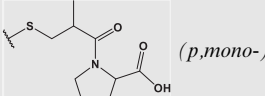
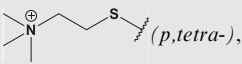
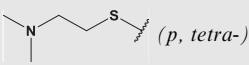
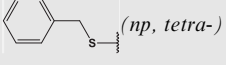
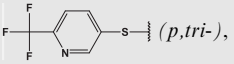
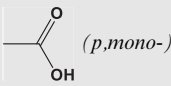
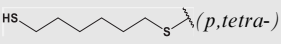
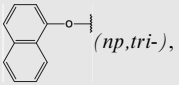
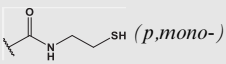
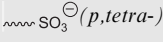
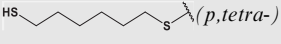
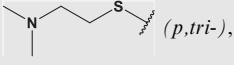
**Table 1** (continued)

Substituent structure, position, no	M	NPs	Estimated NPs size (nm)	Stabilizer	Ref.
 ( <i>p,tetra-</i> )	Zn	Ag <sub>x</sub> Au <sub>y</sub>	9.0 (TEM)	OA	(Bankole et al., 2016c)
 ( <i>p,tri-</i> ),	Zn	Ag NF	20 (TEM) 17 (PXRD)	PVP/PPD	(D'Souza et al., 2015a)
 ( <i>p,mono-</i> )					
 ( <i>np,tri-</i> ),	Zn				
 ( <i>np,mono-</i> )					
 ( <i>p,tetra-</i> )	Zn				
 ( <i>p,mono-</i> )	Zn	AgNS	40 (TEM) 33 (PXRD)	Trisodium citrate	(D'Souza et al., 2015b)
 ( <i>p,tetra-</i> )	Zn	Ag NT, Ag NF	40 (TEM) -	PVP PVP/PPD	
 ( <i>p,mono-</i> )	AlCl	Au NS	20–80 (TEM)	Trisodium citrate & CTAB	(Teixeira et al., 2015)
 ( <i>p,tetra-</i> )	AlCl	Au Het.	10.4 (TEM)	GO <sup>h</sup>	(M. et al., 2015)
 ( <i>p,tetra-</i> )	Zn	Au NS, Au NR	2.1 (TEM) 2.0 <sup>d</sup> (TEM) 4.7 <sup>d</sup> (TEM) 7.1 <sup>d</sup> (TEM)	CTAB	(Mthethwa et al., 2014)
 ( <i>np &amp; p,tetra-</i> )	Zn	Ag NS	2–7 (TEM)	Citric acid	(Khoza and Nyokong, 2014)
 ( <i>p,tetra-</i> )	Al	Au NR <sup>i</sup>	46.8 X 9.4 (TEM)	CTAB	(Ke et al., 2014)
 ( <i>p,hexa-</i> ),					
 ( <i>p,mono-</i> )	Zn	Au NS	2, 5, 15 (TEM)	Trisodium citrate	(Dement'eva et al., 2014)
 ( <i>p,tetra-</i> )	Zn, AlOH	Au NS	20 (TEM) 75 (AFM)	Trisodium citrate	(D'Souza et al., 2013)
 ( <i>p,tetra-</i> )	Zn	Au NS <sup>t</sup>	38 (TEM)	CTAC	
 ( <i>p,tetra-</i> )	Zn				
 ( <i>np &amp; p,tetra-</i> )	Zn	Au NS	2–5 (TEM)	TOABr	(Tombe et al., 2013a)

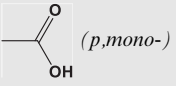
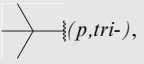
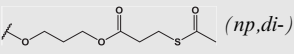
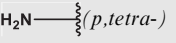
(continued on next page)



**Table 1** (continued)

Substituent structure, position, no	M	NPs	Estimated NPs size (nm)	Stabilizer	Ref.
 ( <i>p,mono-</i> )	Zn				
 ( <i>p,tetra-</i> )	Zn	Au NS	5.0 (TEM)	TOABr	(Tombe et al., 2013b)
 ( <i>np,tri-</i> ),					
 ( <i>p,mono-</i> )	Zn	Ag NS	5.4 (PXR) 5.4 (TEM)	Sodium borohydride Ex. GSH	(Rapulenyane et al., 2013)
 ( <i>np,tri-</i> ),					
 ( <i>p,mono-</i> )	Zn				
 ( <i>p,tetra-</i> ),	Mg, AlOH	Au NS	5.4 (PXR)	Trisodium citrate	(Mthethwa et al., 2012)
 ( <i>p, tetra-</i> )					
 ( <i>np, tetra-</i> )	Zn	AuNS	3–5 (TEM) 4.5 (AFM)	TOABr	(Tombe et al., 2012)
 ( <i>p,tri-</i> ),					
 ( <i>p,mono-</i> )	2H	Au NS	5.37 (PXR) 3.5–4.5 (AFM) 5.97–7.87 (TEM)	TOABr	(Nombona et al., 2011a)
 ( <i>p,tetra-</i> )	Zn				
 ( <i>np,tri-</i> ),					
 ( <i>p,mono-</i> )	Zn				
 ( <i>p,tetra-</i> )	AlOH	Au NS	22 (AFM)	Trisodium citrate	(Teixeira et al., 2011)
 ( <i>p,tetra-</i> )	Zn	Au NS	4.96 (PXR)	TOABr	(Sharon Moeno et al., 2011)
 ( <i>p,tri-</i> ),	Ge (OH) <sub>2</sub> ,	Au NS	5.2 (PXR)	TOABr Ex. GSH	(Masilela and Nyokong, 2011)

**Table 1** (continued)

Substituent structure, position, no	M	NPs	Estimated NPs size (nm)	Stabilizer	Ref.
 ( <i>p,mono-</i> )	OTi, Sn(ac) <sub>2</sub>				
 ( <i>p,tri-</i> ),					
 ( <i>np,di-</i> )	2H	Au NS	5.0 (TEM)	TOABr	(Kotiaho et al., 2010)
 ( <i>p,tetra-</i> )	Co	Au NS, Ag NS	1.5 (TEM) 4.0 (TEM)	CoPcTa	(Lokesh et al., 2009)

Ex.: Ligand exchange. Het.: Heterogeneous shape. <sup>a</sup>Pc@GQDs-MnO<sub>2</sub>, <sup>b</sup>Fe<sub>3</sub>O<sub>4</sub>@Ag, <sup>c</sup>Fe<sub>3</sub>O<sub>4</sub>-Ag hybrid, <sup>d</sup>Aspect ratio for nonspherical particles, <sup>e</sup>Au-speckled silica NPs, <sup>f</sup>Ag<sub>2</sub>Se/ZnS-GSH QDs, <sup>g</sup>Doped into Si NPs, <sup>h</sup>Growth on graphene oxide (GO), <sup>i</sup>2.1-, 10.6-, and 28.2-nm silica shell.

factant such as cetyltrimethylammonium chloride (CTAC, Fig. 3), and AgNO<sub>3</sub> (Jana et al., 2002; Kou et al., 2007; Xiaoshan Kou et al., 2006; Liu and Guyot-Sionnest, 2005). However, the overgrowth of Au BPs and related penta-branched particles can afford NSTs. A similar method was also used to synthesize Au BPs by introducing AgNO<sub>3</sub> to the reaction and replacing CTAC with CTAB (Wu et al., 2009).

**Nanotriangles (NTs):** Triangular NPs have attracted much attention among nanostructures with other shapes, as the NT SPR bands can be tuned by controlling the particle aspect ratio (Pastoriza-Santos and Liz-Marzán, 2008). Two main methods have been utilized for Ag NT synthesis, namely the chemical reduction of Ag salts and photochemical growth (Bastys et al., 2006; Jin et al., 2001; Wu et al., 2008). The former method was used to prepare Ag NTs in high yields from aqueous solutions of AgNO<sub>3</sub>, NaBH<sub>4</sub>, polyvinylpyrrolidone (PVP), trisodium citrate (Fig. 3), and H<sub>2</sub>O<sub>2</sub> (Syafiuddin et al., 2017). Au NTs can be capped with CTAC (Chen et al., 2014).

**Nanoflowers (NFs):** Amines (e.g., primary amines, amino acids, and amine-functionalized polymers (Bastys et al., 2006; Wu et al., 2008; Xia et al., 2009)) have been widely used in NP synthesis as reducing agents and stabilizers because of their presence in biological and environmental systems (Newman and Blanchard, 2006). *p*-Phenylenediamine (PPD, Fig. 3) has been used to prepare Au and Ag NPs with different shapes (Sun, 2010; Sun et al., 2004; Sun et al., 2005). Flower-like Ag nanostructures can also be synthesized by reducing AgNO<sub>3</sub> with PPD in the presence of PVP at room temperature, in which case PPD acts as a reducing agent and a soft template in combination with PVP to induce Ag NF formation (D'Souza et al., 2015b).

**NWs:** Among the differently shaped Ag NPs, Ag NWs have received much attention because of their electrical/optical applications (Shi et al., 2019) and high mechanical flexibility attributable to their one-dimensional architecture and high aspect ratio (Zhang et al., 2017). Ag NWs can be prepared by UV light irradiation (Choo and Kim, 2017), template (Liu et al., 2009), solvothermal (Banica et al., 2017), and polyol (Prabukumar and Bhat, 2018) methods, among which the

polyol method has been used to synthesize Ag NWs in the presence of PVP as a capping agent by Sun et al. (Knight et al., 2007; Sun et al., 2003).

**Alloys:** The LSPR wavelengths of Au and Ag NPs are approximately equal 530 and 400 nm, respectively, and can be tuned in this range (400–530 nm) through the formation of Au-Ag alloy NPs. Oleamine (OA), Fig. 3, is used as a reducing and stabilizing agent in the synthesis of such alloys, as its amine group can reduce Au and Ag ions at high temperature to produce NPs (Liu et al., 2011) with compositions dependent on the Ag: Au precursor ratio (Bankole et al., 2016c).

## 2.2. Conjugation of Pcs to Ag and Au NPs

Different substituents have been introduced into Pc complexes to make them suitable for conjugation to NPs, as summarized in Table 1. Two main approaches are available for such conjugation, namely (i) self-assembly through direct electrostatic interaction between the Pc S or N and the NP surface, and (ii) covalent amide bond formation between carboxylic and amino groups. In particular, covalent linkages to Pcs can be established by capping NPs with functionalized agents such as cysteamine (Oluwole et al., 2016), glutathione (GSH) (Dube et al., 2017; Mafukidze et al., 2019; Nwaji et al., 2017b, 2017d; Nwaji and Nyokong, 2017c; Oluwole et al., 2017a; Rapulenyane et al., 2013), 3-azido-1-propylamine (Bankole and Nyokong, 2017b), and 3-mercaptopropionic acid (MPA) (Bankole and Nyokong, 2016a) (Fig. 3).

In the self-assembly approach, ligand exchange takes place on the NP surface via the direct coordination of Pc S and/or N to the NP. Both single solvents such as dimethyl sulfoxide (DMSO) (D'Souza et al., 2015b; Khoza and Nyokong, 2014; Lokesh et al., 2009), *N,N*-dimethylformamide (DMF) (Tombe et al., 2013b), toluene (Nwaji et al., 2017b; Tombe et al., 2012), tetrahydrofuran (THF) (Nombona et al., 2011a), CHCl<sub>3</sub> (Nombona et al., 2011a), and water (pH-adjusted to 9) (Mthethwa et al., 2014), and different solvent mixtures have been used for Pc-NP mixing, e.g., NPs in toluene, Pc in 10:1 (v/v) DMF:toluene (Nwaji et al., 2018), NPs in water, Pc in THF (Zasedatelev et al., 2016), NPs in

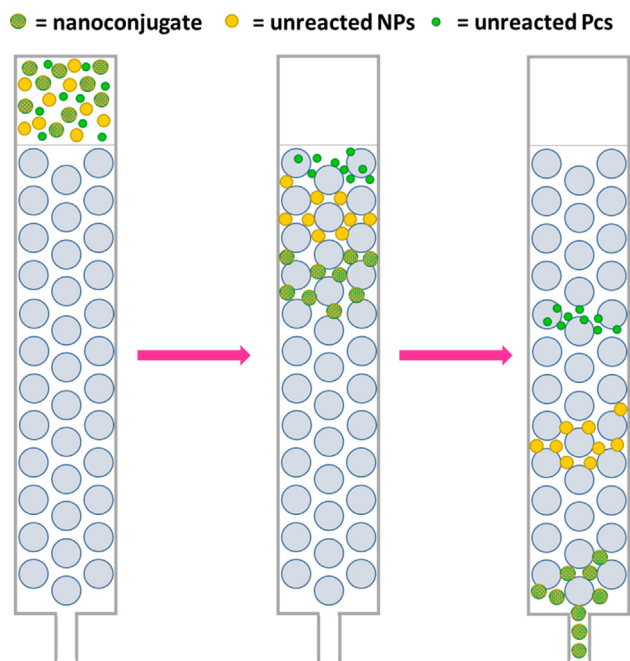


Fig. 4 Principle of size-exclusion chromatography.

THF, Pc in DMSO (Bankole et al., 2016c), and NPs in water, Pc in DMF (Bankole and Nyokong, 2016a; Dube et al., 2018a). Lokesh et al. have used tetraaminocobaltphthalocyanine (CoPcTa) in a one-step process to stabilize Au and Ag NPs and prevent their aggregation through the four amino groups in the peripheral positions of this Pc (Lokesh et al., 2009).

For covalent linkage through amide bond formation, the carboxylic group needs to be activated for its reaction with the amino group. Hydrophobic reagents such as *N,N*-dicyclohexylcarbodiimide (DCC, Fig. 3) are widely used to activate  $\text{—COOH}$  groups in DMF, and the activated carboxylic coupling partner is then reacted with a mixture of the amino partner and 4-dimethylaminopyridine (DMAP, Fig. 3), which acts as a coupling agent (Dube et al., 2017; Masilela and Nyokong, 2011; Nwaji et al., 2017b, 2017d; Nwaji and Nyokong, 2017c; Oluwole et al., 2017a, 2016). Hydrophilic reagents such as *N*-(3-dimethylaminopropyl)-*N'*-ethylcarbodiimide hydrochloride (EDC, Fig. 3) and 1-hydroxy-2,5-pyrrolidinedione (NHS, Fig. 3) were also used for the cross-linking of (i) a carboxyl-functionalized Pc to an amino-functionalized Au NR@SiO<sub>2</sub> hybrid (Ke et al., 2014) and (ii) an amino-functionalized Pc to a carboxyl-functionalized Fe<sub>3</sub>O<sub>4</sub>/Ag hybrid (Bankole and Nyokong, 2016a).

Other methods of linking Pcs to NPs are also known, as exemplified by the click reaction between alkyne-functionalized Pcs and azide-derivatized Au NPs (Bankole and Nyokong, 2017b). The conjugation of pyrrolidinonyl metal phthalocyanines (PyMPc) to thiolated methoxy-polyethylene glycol-capped Au NPs (Au NPs-MPEG) was achieved through a donor-acceptor interaction between the Pc C=O groups and the NP surface (Chen et al., 2018). Baldovi et al. synthesized a silica matrix shell through a radical chain reaction by linking a Pc to silyl- and vinyl-modified Au NPs using azobisisobutyronitrile (AIBN, Fig. 3) as a

radical initiator (Baldovi et al., 2016). Moreover, electrostatic attraction is known to occur between negatively charged Pcs and positively charged Au NPs (D'Souza et al., 2013; Zhou et al., 2016, 2018). Kuzmina et al. prepared Au NPs surrounded by Pc shells through axial ligand exchange of acetate on the lanthanide ion with the citrate OH group of the NP surface (Kuzmina et al., 2017).

Nanoconjugate purification can be achieved by addition of methanol and centrifugation to separate NPs (Bankole and Nyokong, 2016a; Bankole et al., 2016c; Dubinina et al., 2018; Nwaji et al., 2017b, 2018; Nwaji and Nyokong, 2017c; Oluwole et al., 2017a, 2016) or by size-exclusion chromatography on a Bio-Beads S-X1 column using different eluents, e.g., pH 9 buffer (Mthethwa et al., 2014), DMSO (Mthethwa and Nyokong, 2015; Mthethwa et al., 2012), toluene (Forteach et al., 2012; Kotiaho et al., 2010; Sharon Moeno et al., 2011; Mthethwa et al., 2013; Tombe et al., 2012), DMF (Tombe et al., 2013b), THF, or CHCl<sub>3</sub> (Nombona et al., 2011a). Silica beads modified with poly(*N*-isopropyl acrylamide) are known to effectively separate aromatic compounds by employing water as an eluent (Liu et al., 2012; Mitchell et al., 2001). During this chromatographic separation, the elution order is largest nanoconjugate → unreacted NPs → unreacted Pcs (Fig. 4).

### 2.3. Characterization

#### 2.3.1. UV-Vis spectroscopy

The SPR absorption bands of Au NSs appear in the visible region and are shifted upon the change of NP shape to non-spherical. Au NRs feature two (transverse and longitudinal) characteristic SPR peaks (Huang et al., 2007), as exemplified by the peaks at 513 and 749 nm observed by Mthethwa et al. (Mthethwa and Nyokong, 2015). Fig. 5A compares the UV-Vis spectra of Au NSs and Au NRs with different aspect ratios (Mthethwa et al., 2014), showing that with increasing aspect ratio, the absorption maximum shifts to the NIR region (Mthethwa et al., 2014). In contrast, Au NSTs lack a prominent longitudinal absorption band in their UV-Vis spectra because of the short branches and the thick body of these NSTs. Wu et al. observed the absorption band of Au NSTs centered at 590 nm and featuring a long tail in the NIR region (Fig. 5B) (Wu et al., 2009), while two SPR bands were observed for Au BPs by the same authors (Fig. 5B) (Wu et al., 2009), and one band at 548 nm was detected by Mthethwa et al. (Mthethwa and Nyokong, 2015).

The SPR absorption bands of Ag NSs were observed in the range of 400–430 nm (Nwaji et al., 2018), while those of Ag NWs were observed at 353 and 378 nm (Fig. 5C) (Zhang et al., 2018). Furthermore, SPR absorption bands at 416 and 452 nm were detected for Ag NSs and Ag NTs, respectively, whereas two broad peaks were observed for Ag NFs (Fig. 5D) (D'Souza et al., 2015b).

The SPR bands were found to be affected by the capping agent used for NP synthesis. For example, when OA was replaced with a larger capping ligand, GSH, the SPR band of OA-Au NSs shifted to higher wavelengths (Fig. 5E) (Nwaji and Nyokong, 2017c), while the SPR band of GSH-Ag NSs was found to be broad and blue-shifted compared to that of OA-Ag NSs. This broadening was attributed to the variation of NP size (Fig. 5F) (Alqadi et al., 2014).

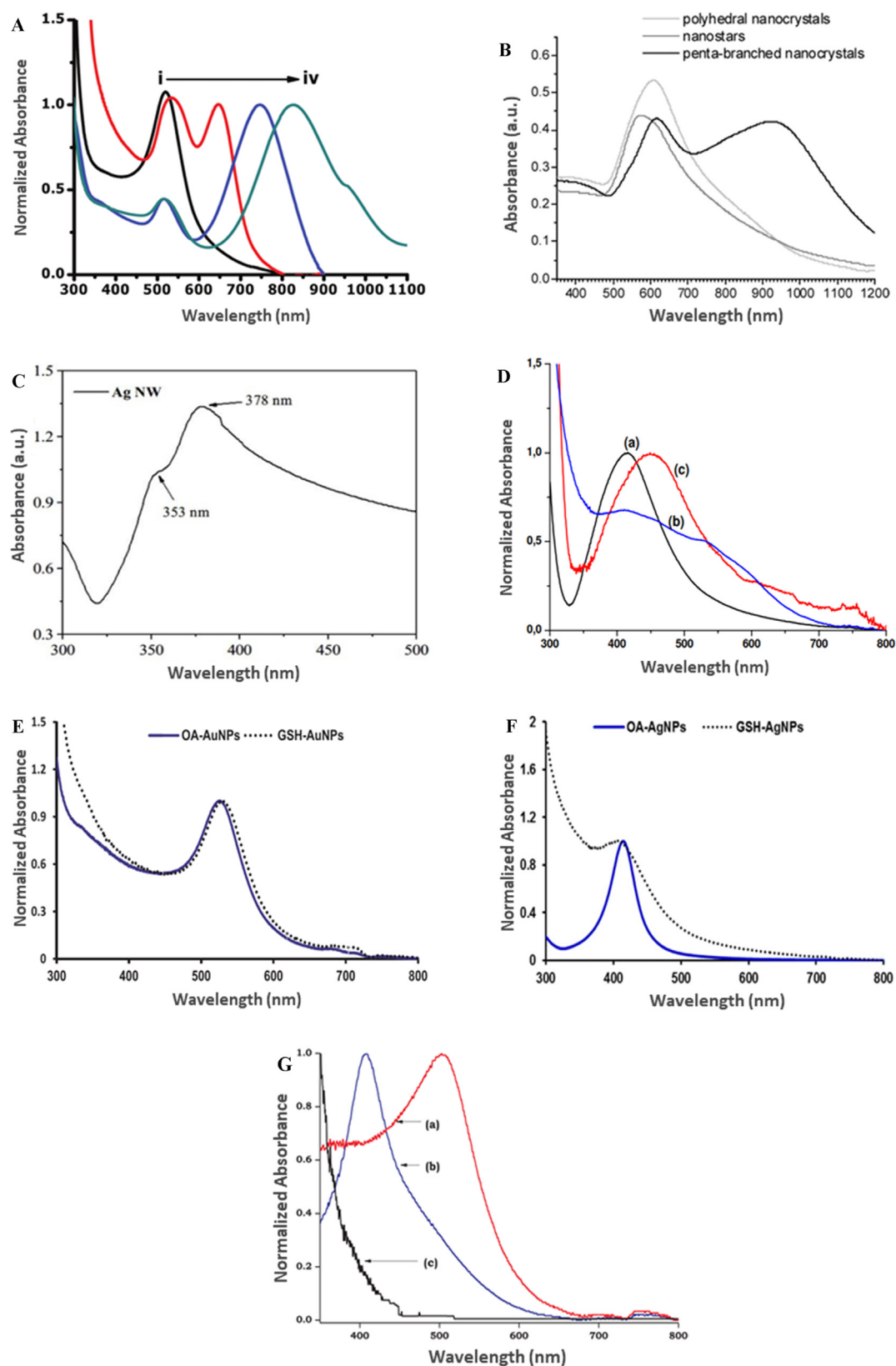


**Fig. 5** UV-Vis absorption spectra of (A) (i) Au NSs, Pc-Au NRs with an aspect ratio of (ii) 2.0, (iii) 4.7, and (iv) 7.1. Reproduced with permission from ref. (Mthethwa et al., 2014). Copyright 2014 Elsevier; (B) polyhedral Au nanocrystals, NSs, and penta-branched nanocrystals. Reproduced from ref. (Wu et al., 2009). Copyright 2009 American Chemical Society; (C) Ag NWs. Reproduced with permission from ref. (Zhang et al., 2018). Copyright 2018 Elsevier; (D) (a) Ag NSs, (b) Ag NFs, and (c) Ag NTs. Reproduced with permission from ref. (D'Souza et al., 2015b). Copyright 2015 Elsevier; (E) OA- and GSH-functionalized Au NSs; (F) OA- and GSH-functionalized Ag NSs. Reproduced with permission from ref. (Nwaji and Nyokong, 2017c). Copyright 2017 Elsevier; (G) (a) AuAg-GSH, (b) AgAu-GSH, and (c) AgAu-Si NP. Reproduced with permission from ref. (Dube et al., 2017). Copyright 2017 Elsevier.

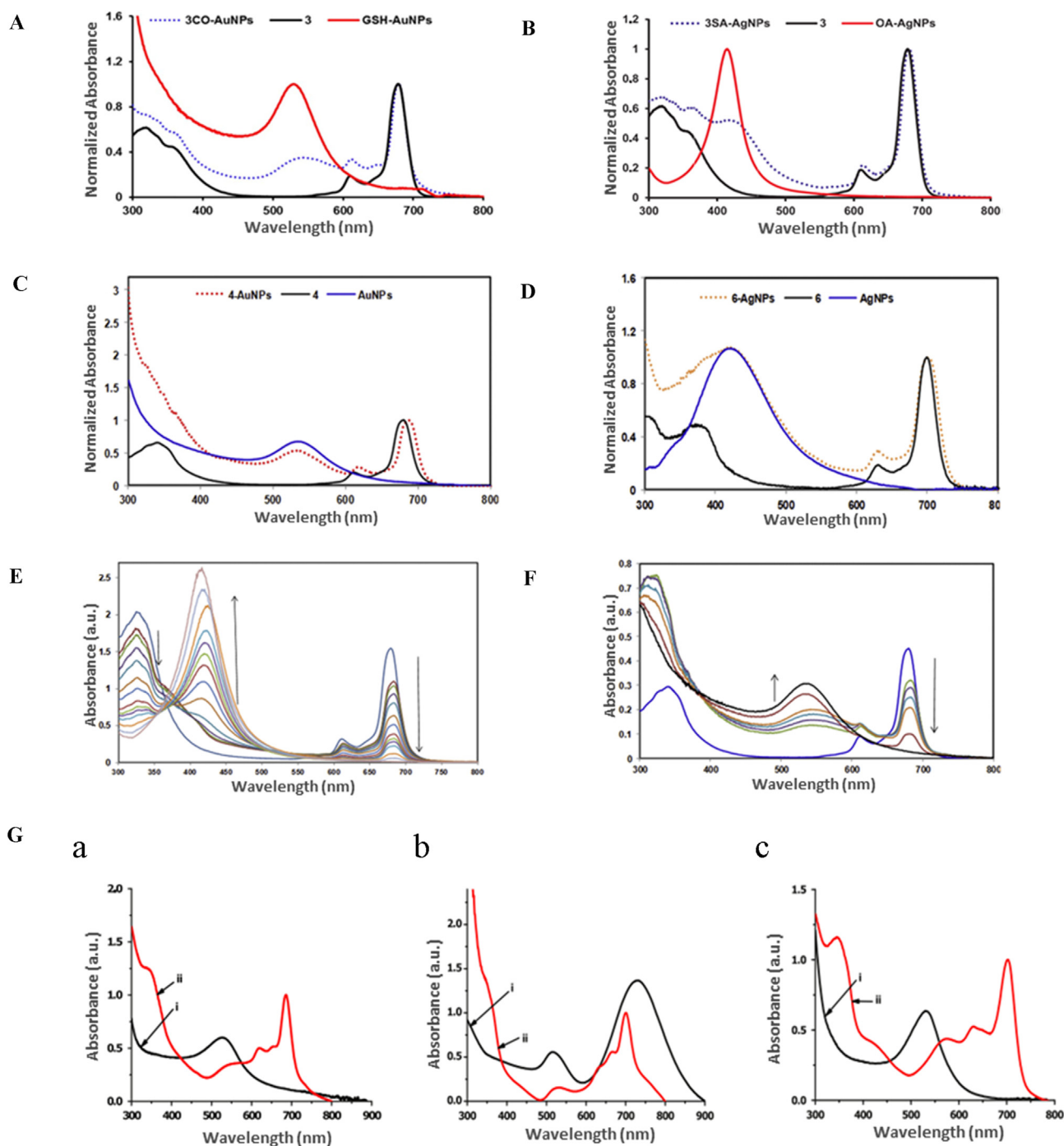


**Fig. 6** UV-Vis absorption spectra of different Pc conjugates showing a shift in SPR wavelength. (A) GSH-Au NSs, Pc, Pc-CB-Au NSs, (B) OA-Ag NSs, Pc, and Pc-SA-Ag NSs. Reproduced with permission from ref. (Nwaji and Nyokong, 2017c). Copyright 2017 Elsevier; (C) Pc, Au NSs, and Pc-Au NSs, (D) Pc, Ag NSs, and Pc-Ag NSs. Reproduced with permission from ref. (Nwaji et al., 2018). Copyright 2018 Elsevier. (E) Disappearance of the Pc Q-band in aqueous solution at different Pc:Au NS and (F) Pc:Ag NS molar ratios. Reproduced with permission from ref. (Nwaji et al., 2018). Copyright 2018 Elsevier. (G) Effects of Au NP shape on the shift of the Pc Q-band in the corresponding conjugates: (a) Au NSs, (b) Au NRs, and (c) Au BPs. (i): Pc, (ii): Pc conjugates. Reproduced with permission from ref. (Mthethwa and Nyokong, 2015). Copyright 2015 Elsevier.

Alloy formation has been achieved by Ag and Au co-reduction with OA to afford NPs with a plasmon band at 420–485 nm (depending on composition) (Bankole et al., 2016; Chen et al., 2006), which is very close to the SPR absorptions of Ag NSs and Au NSs (Papagiannouli et al., 2015). Dube

et al. observed the SPR peaks of Ag- and Au-rich alloys at 410 and 506 nm, respectively, revealing that alloy doping into Si NPs induced no significant change in SPR peak position and thus confirming that AgAu NPs were not exposed and successfully embedded within Si NPs (Fig. 5G) (Dube et al., 2017).

Pc conjugation to GSH-capped Au NSs through covalent bonding (CB) was reported to result in a red shift of the corresponding SPR from 529 to 532 nm, while a shift from 523 to 539 nm was observed for the self-assembly of Pc to OA-Au NSs (Fig. 6A) (Nwaji and Nyokong, 2017c). In the case of Pc conjugation to Ag NSs, both CB through GSH and self-assembly through OA resulted in a red shift of SPR bands from 400 to 428 nm and from 407 to 415 nm, respectively (Fig. 6B) (Nwaji and Nyokong, 2017c). Even though the NP SPR bands are usually slightly red-shifted upon conjugation to Pcs, a blue shift was also reported (Fig. 6C and D) (Nwaji et al., 2018).

The red shifts of SPR were attributed to the increase in NP size due to  $\pi$ - $\pi$  interactions between the NPs and dye molecules (Thomas et al., 2008), while bathochromic SPR shifts were attributed to the modest aggregation of NPs in hybrids (Mishra et al., 2010), the very low surface curvature, and large particle size, which facilitated orbital overlap to afford a stiffer plasmon surface and induced the damping of electrons of NPs with high-energy resonance (Fleger and Rosenbluh, 2009; Thomas et al., 2008).

The Pc Q-band maximum showed either no shift or a slight red shift upon conjugation, which, in the latter case, was ascribed to the molecular orientation of Pcs to NPs (Vukovic et al., 2009). However, when the Pc molecule (1 nm) is saturated with metallic NPs (> 10 nm), the Q-band might disappear. Tebello et al. recorded the disappearance of the Q-band at molar ratio ranges from 5.2 to 8.5 of downloading Au NPs or Ag NPs to the complex (Fig. 6E and F) (Nwaji et al., 2018). The spectra of conjugates usually feature an elevated B-band intensity (Dubinina et al., 2018). A broadening of the Pc Q-band in the spectra of conjugates was also observed by the same group and was attributed to the tight Pc packing on NPs (Kotiaho et al., 2010). These authors also recorded a blue shift of the Q-band in the presence of Au NSs and a red shift in the presence of nonspherical Au NPs, suggesting that the orientation of Pc bonding to the surface of Au NSs was different to that in the case of other NPs because of the longitudinal dipole moment arrangement of both Pc and Au NPs (Vukovic et al., 2009) (Fig. 6G) (Mthethwa and Nyokong, 2015). On the other hand, a blue shift of the Q-band upon conjugation was reported and attributed to the involvement of the sulfur groups of the thio-functionalized Pc in the formation of links to Au NPs (Sharon Moeno et al., 2011).

### 2.3.2. Powder X-ray diffraction (PXRD)

PXRD is widely used to study the phase composition and unit cell dimensions of crystalline materials, e.g., the Debye-Scherrer equation (Eq. (1)) can be used to determine the sizes of NPs (Ron Jenkins, 1996):

$$d = \frac{K\lambda}{\beta \cos\theta} \quad (1)$$

where  $\lambda$  is the wavelength of the X-ray source (1.5404 Å),  $\kappa$  is an empirical constant equaling 0.9,  $\beta$  is the full width at half-maximum of the diffraction peak, and  $\theta$  is the angular position of the peak.

The NP to Pc ratio can also be determined from PXRD data using Eqs. (1)–(3) (Liu et al., 2007). The average number

of Au atoms ( $N$ ) in the conjugates can be determined by assuming a spherical structure as

$$N = \frac{\pi\rho D^3}{6M}, \quad (2)$$

where  $\rho$  is the density of face-centered cubic Au (19.3 g/cm<sup>3</sup>) (Liu et al., 2007),  $M$  is the atomic weight of Au, and  $D$  is the average core diameter determined by PXRD.

The initial concentration of NPs ( $C$ ) can then be calculated as

$$C = \frac{N_{Total}}{NVN_A} \quad (3)$$

where  $N_{Total}$  is the number of atoms in the initial amount of Au salt added to the reaction mixture,  $V$  is the volume of the reaction solution [L], and  $N_A$  is Avogadro's constant. The NP molar extension coefficient ( $\varepsilon$ ) can be calculated using Eq. (4) (Liu et al., 2007) and be subsequently used to determine the NP to Pc ratio.

$$\ln\varepsilon = \kappa\ln D + \alpha \quad (4)$$

where  $\kappa = 3.32111$ ,  $\alpha = 10.80505$ , and  $D$  is the NP core diameter.

PXRD peaks corresponding to reflections from 111, 200, 220, 311, and 222 planes were attributed to the face-centered cubic structures of metallic Au and Ag (Fig. 7A) (Nwaji et al., 2017b). Moreover, D'Souza et al. probed the effect of Ag NP shape on the corresponding PXRD patterns (Fig. 7B) (D'Souza et al., 2015b), whereas no such comparison has been performed for variable-shape Au NPs.

The broad band at  $2\theta = 11$ – $25^\circ$  was assigned to the amorphous form of Pc in the conjugate (Fig. 7C) (Bankole et al., 2016c; Mthethwa et al., 2012; Snow et al., 1984). It was reported that the change in crystallinity degree and interplanar spacing indicates a new Pc or a new crystal form (Yang et al., 2004). Thus, the conjugation of NPs with Pcs is usually accompanied by a change in peak position and  $d$ -spacing as well as by the emergence of new peaks.

### 2.3.3. X-ray photoelectron spectroscopy (XPS)

As a highly sensitive method of probing the chemical states of elements, XPS has been used to investigate the interactions of Pc groups with the NP surface and confirm the formation of new bonds (Nwaji et al., 2017b).

Moreover, XPS has been used to study the expected atomic compositions and the corresponding binding energies (Dube et al., 2017). For instance, this technique was employed to confirm the coating of Ag<sub>x</sub>Au<sub>y</sub> alloys with Si NPs by comparing the atomic composition of this alloy with that of alloy–Si NPs. As a result, a significant decrease in the contents of Ag, Au, and C accompanied by an increase in O content were observed for alloy–Si NPs (Fig. 8A) (Dube et al., 2017), which was attributed to the grafting of the Ag<sub>x</sub>Au<sub>y</sub> alloy into the pores of Si NPs (Dube et al., 2017). Similarly, the X-ray photoelectron spectra of Ag<sub>x</sub>Au<sub>y</sub> showed peaks at 368.0 eV (Ag 3d) and 82.6 eV (Au 4f), and a higher metal mole ratio was recorded for the metal-rich alloy (Bankole et al., 2016c). The additional peak at 455 eV in the nanoconjugate spectrum was assigned to In metal in the Pc complex, confirming successful conjugation (Oluwole et al., 2017a). In the spectra of ZnPc and its conjugates, Zn 2p peaks were positioned at

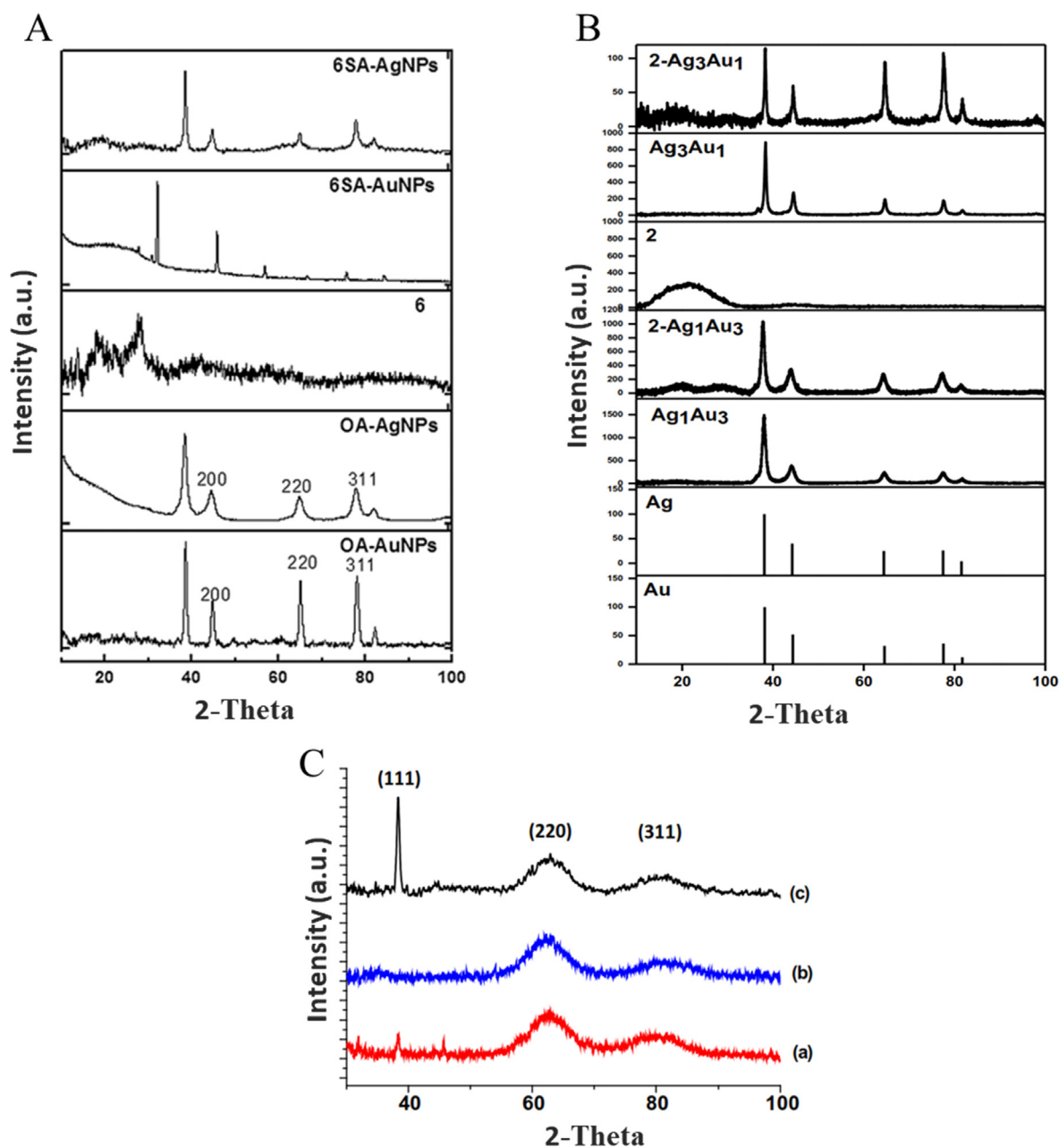


**Fig. 7** XRD patterns of (A) Ag NSs, Au NSs, and their nanoconjugates. Reproduced with permission from ref. (Nwaji et al., 2017b). Copyright 2017 Royal Society of Chemistry; (B) (a) Ag NSs, (b) Ag NFs, and (c) Ag NTs. Reproduced with permission from ref. (D'Souza et al., 2015b). Copyright 2015 Elsevier; (C) Ag<sub>x</sub>Au<sub>y</sub> alloys and their nanoconjugates. Reproduced with permission from ref. (Bankole et al., 2016c). Copyright 2016 Elsevier.

~1022 eV (Zn 2p<sub>3/2</sub>) and 1046 eV (Zn 2p<sub>1/2</sub>) (Bankole and Nyokong, 2016a).

The formation of amide-type covalent linkages was confirmed by the shift of N—C, N—H, and N—C=O N 1s sub-peaks (from 395.8, 397.7, and 400.0 eV, respectively, to 396.5, 398.8, and 399.2 eV, respectively) and the intensity gain of the N—C=O peak upon going from GSH-Au NSs to Pc-CB-Au NSs (Fig. 8B) (Nwaji and Nyokong, 2017c). Concomitantly, the N—H peak (due to amide bond formation) lost intensity, while the N—C peak (due to the increasing amount of carbon from Pcs) gained intensity (Nwaji and Nyokong, 2017c).

Similarly, the formation of covalent bonds between the primary amine groups of GSH-functionalized NPs and Pc carboxylic groups was confirmed by appearance of an additional —HN—C=O amide sub-peak at 401.94 eV in the N 1s deconvoluted spectrum of the hybrid (Fig. 8C) and the by a decrease in the peak intensity of —N—H compared to that of —N—C (Fig. 8C) (Oluwole et al., 2017a).

The N 1s spectrum of an amine-functionalized complex described in ref. (Nwaji et al., 2017b) showed N—C and N—H peaks at 396.1 and 397.5 eV, respectively, while two sets of N 1s doublets (at 397.7 and 400.8 eV) were observed in the spectrum of the corresponding Au nanoconjugate after surface

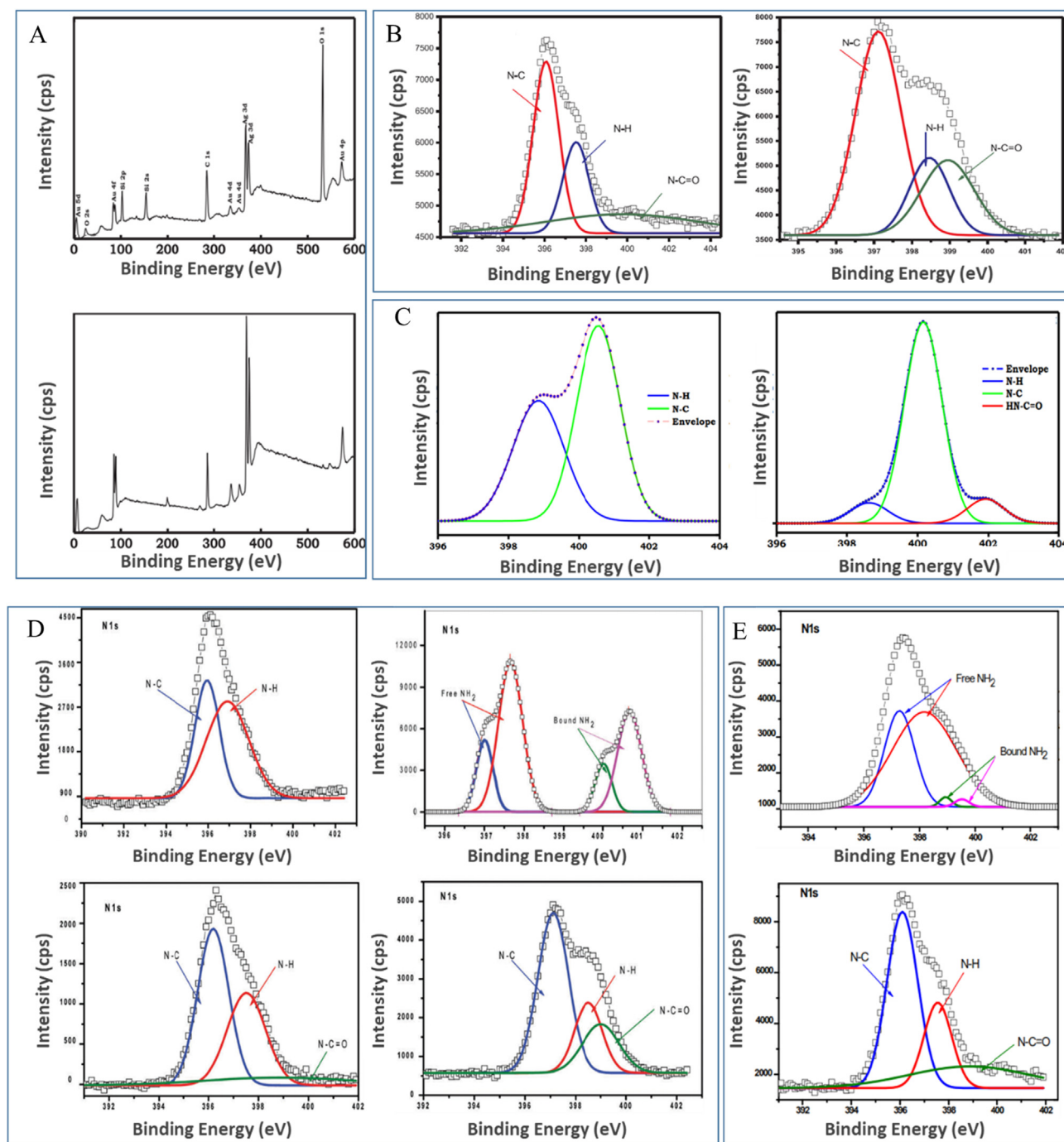


**Fig. 8** (A) X-ray photoelectron survey spectra of  $\text{Ag}_x\text{Au}_y$  (top) and  $\text{Ag}_x\text{Au}_y\text{-Si}$  NPs (bottom) used to compare the corresponding elemental compositions. Reproduced with permission from ref. (Dube et al., 2017). Copyright 2017 Elsevier. Deconvoluted N 1s spectra confirming the covalent linking of NPs to Pc: (B) GSH-Au NSs (left) and Pc-CB-Ag NSs (right). Reproduced with permission from ref. (Nwaji and Nyokong, 2017c). Copyright 2017 Elsevier; (C) GSH-NPs (left) and Pc-CB-NPs (right). Reproduced with permission from ref. (Oluwole et al., 2017a). Copyright 2017 Elsevier. Deconvoluted N 1s spectra showing self-assembly and covalent bonding between NPs and Pc: (D) Pc (top left), GSH-Au NSs (bottom left), Pc-SA-Au NSs (top right), and Pc-CB-Au NSs (bottom right). Reproduced with permission from ref. (Nwaji et al., 2017b). Copyright 2017 Royal Society of Chemistry. (E) N 1s spectra of Pc-SA-Ag NSs (left) and Pc-CB-Ag NSs (right). Reproduced with permission from ref. (Nwaji et al., 2017b). Copyright 2017 Royal Society of Chemistry. (F) N 1s and (G) S  $2p_{3/2}$  and  $2p_{1/2}$  spectra of Pc (left), Pc- $\text{Ag}_1\text{Au}_3$  (middle), and Pc- $\text{Ag}_3\text{Au}_1$  (right). Reproduced with permission from ref. (Bankole et al., 2016c). Copyright 2016 Elsevier. (H) N 1s and (I) S 2p spectra of (a) Pc and (b) Pc-Au NPs. Reproduced with permission from ref. (Mthethwa et al., 2014). Copyright 2014 Elsevier.



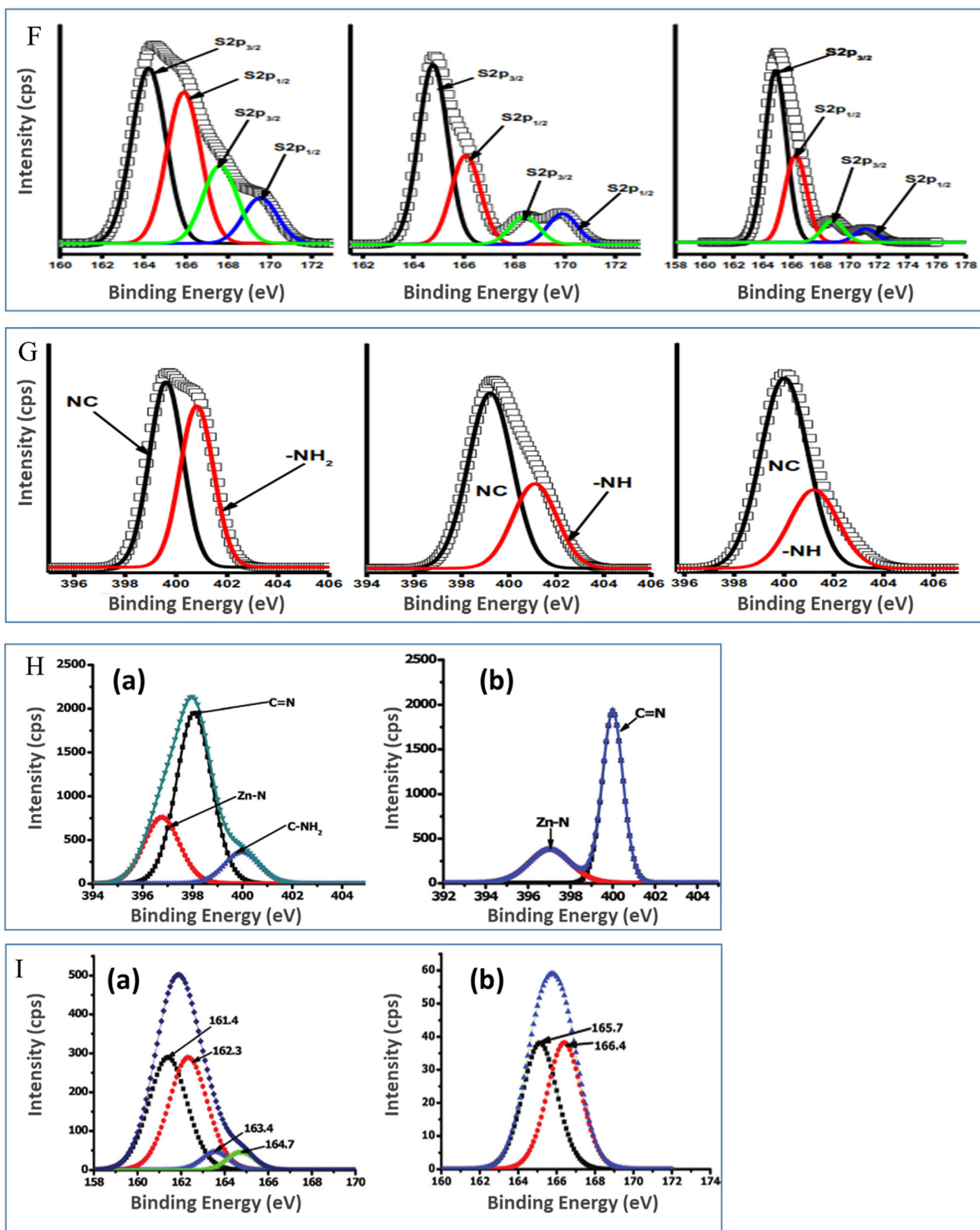
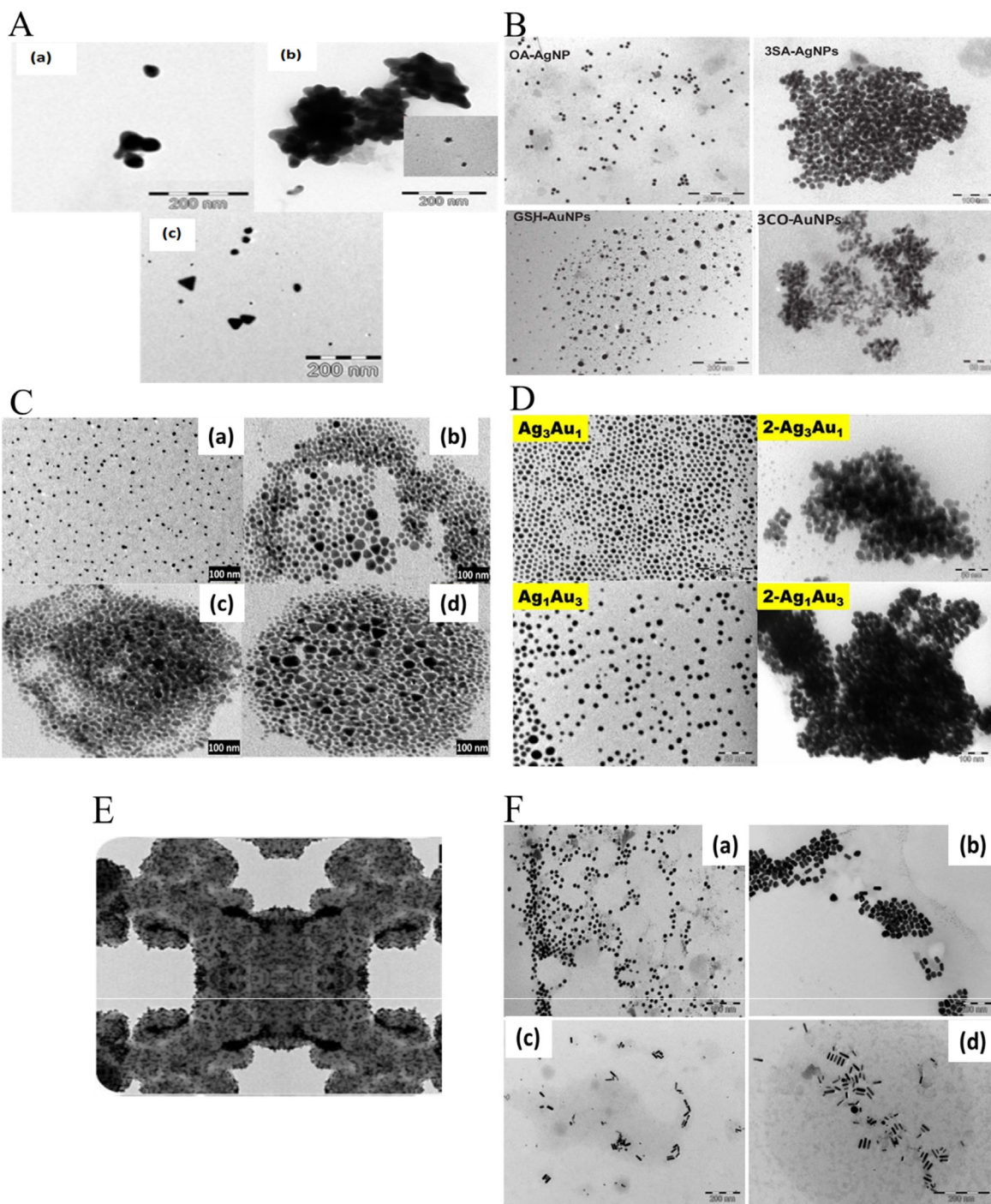


Fig. 8 (continued)

assembly (Fig. 8D) (Nwaji et al., 2017b). Similar behavior was observed for the corresponding Ag nanoconjugates, in which case the two sets of doublets appeared at 397.3 and 399.7 eV

(Fig. 8E) (Nwaji et al., 2017b), indicating the presence of amino nitrogen in two different environments characterized by the formation or non-formation of N–Au and N–Ag



**Fig. 9** TEM images of (A) (a) Ag NSs, (b) Ag NFs, and (c) Ag NTs. Reprinted with permission from ref. (D'Souza et al., 2015b). Copyright 2015 Elsevier. (B) TEM images showing a slight increase in NP size upon the conjugation of OA-Ag NSs and GSH-Au NSs to Pc. Reproduced with permission from ref. (Nwaji and Nyokong, 2017c). Copyright 2017 Elsevier, Images of (C) Au NSs bearing different capping agents and Pcs: (a) TOABr-Au NSs, (b) azide-functionalized Au NSs, (c) ZnPc-Au NSs, and (d) InPc-Au NSs. Reproduced with permission from ref. (Bankole et al., 2017b). Copyright 2017 Elsevier; (D)  $Ag_xAu_y$  alloy NPs and their nanoconjugates. Reproduced with permission from ref. (Bankole et al., 2016c). Copyright 2016 Elsevier; (E) Pc-GSS. Reproduced with permission from ref. (Dube et al., 2018c). Copyright 2018 John Wiley and Sons. (F) TEM images showing the smaller increase in the size of nonspherical Au NPs compared to that observed for Au NSs: (a) Pc-Au NSs, Pc-Au NRs with aspect ratios of (b) 2.0, (c) 4.7, and (d) 7.1. Reproduced with permission from ref. (Mthethwa et al., 2014). Copyright 2014 Elsevier. (G) TEM images of (a) Au NSs, (b) Au NRs, and (c) Au BPs: (i) Au NPs, (ii) Au NP conjugates. Reproduced with permission from ref. (Mthethwa and Nyokong, 2015). Copyright 2015 Elsevier. (H) Effect of silica shell thickness ((a) 2.1, (b) 6.2, (c) 10.6, (d) 14.7, (e) 18.9, and (f) 28.2 nm) on the aggregation of Au NRs@SiO<sub>2</sub>. Reproduced with permission from ref. (Ke et al., 2014). Copyright 2014 SpringerOpen. (I) Au NSs covered by a Pc shell (a and b) and the corresponding bare Au NSs (c and d). Reproduced with permission from ref. (Dubinina et al., 2018). Copyright 2018 Elsevier.

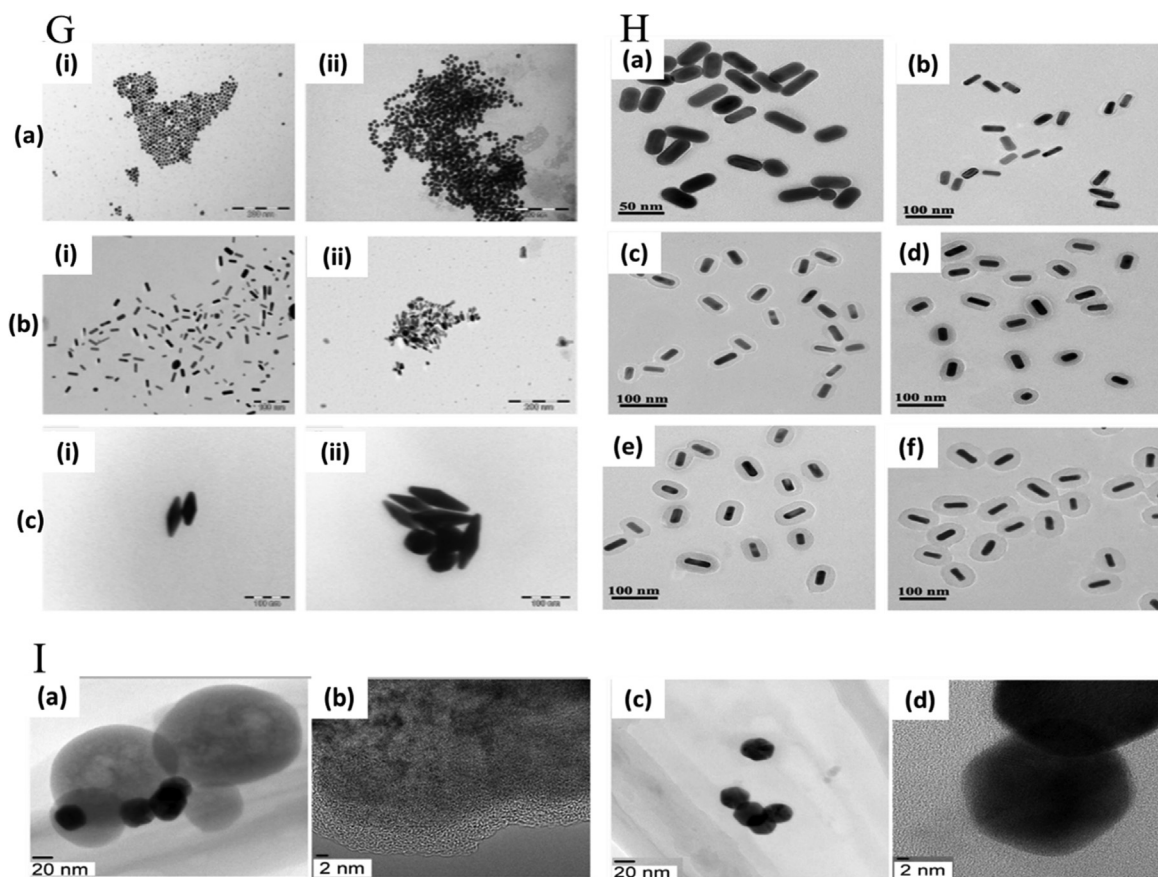


Fig. 9 (continued)

bonds of complex amino “arms.” The set with the higher binding energy was attributed to unbound nitrogen.

The peaks of N—C, N—H, and N—C=O units in GSH-Au NPs were observed at 396.3, 397.8, and 400.2 eV, respectively (Fig. 8D) (Nwaji et al., 2017b), and the establishment of a Pc-NP linkage resulted in a significant intensity gain and position shift of the amide bond signal. The intensity increase was ascribed to the conversion of the COOH groups of GSH-functionalized NPs to amide bonds and the resulting decrease in bond polarizability.

The probable attachment centers of the thio-amine-functionalized Pc synthesized in ref. (Bankole et al., 2016c) were elucidated by investigation of deconvoluted N 1s and S 2p spectra (Fig. 8F and 8G) (Bankole et al., 2016c). Specifically, the N 1s spectrum of Pc was deconvoluted into two peaks at 399.13 and 400.97 eV corresponding to N—C (Pc ring) and —NH<sub>2</sub> (unprotonated amine) units, respectively (Fig. 8F) (Bankole et al., 2016c), while the N 1s core-level spectra of Pc-Ag<sub>1</sub>Au<sub>3</sub> showed two peaks at 399.61 and 401.09 eV, corresponding to N—C and —NH units, respectively. Similarly, the deconvoluted N 1s spectrum of Pc-Ag<sub>3</sub>Au<sub>1</sub> featured N—C and —NH peaks at 400.01 and 401.20 eV, respectively. The high-binding-energy N 1s peaks observed in the spectra of hybrids at ~401 eV were attributed to protonated amine/amide species and thus indicated the successful conjugation of Pc to the alloy (Das et al., 2012; Lim et al., 2010; Ramanathan et al., 2005).

The S 2p spectra of Pc and the corresponding alloy conjugates featured two doublets, one at 161.7–163.39 eV, and the

other at 165.01–167.22 eV (Fig. 8G) (Bankole et al., 2016c). In the case of Pc-Ag<sub>1</sub>Au<sub>3</sub>, these signals were shifted to 162.08 and 163.38 eV, respectively, while a shift to 161.95 and 163.25 eV, respectively, was observed for Pc-Ag<sub>3</sub>Au<sub>1</sub>. Signals at ~162 and 163 eV were assigned to thiolated species immobilized and physisorbed on bimetallic NPs in the alloy hybrid, respectively (Castner et al., 1996; Weidner et al., 2008; Zharnikov et al., 2000), while the peaks of other unbound thiols observed at higher binding energies (> 164 eV) were attributed to the S—C bonds of the Pc ring (Yam et al., 2002, 2001).

The self-assembly of Pc synthesized in ref. (Mthethwa et al., 2014) and Ag NPs or Au NPs to form hybrids was manifested by the disappearance of the Pc C—NH<sub>2</sub> peak in the N 1s spectrum of the hybrid (Fig. 8H(ii)) (Mthethwa et al., 2014). In the case of sulfur coordination, deconvoluted S 2p spectra are known to exhibit doublet peaks due to spin-orbit coupling (Lim et al., 2010). Notably, upon conjugation, the doublet peaks at 161.4 and 162.3 eV (S 2p<sub>3/2</sub>) and at 163.4 and 164.7 (S 2p<sub>1/2</sub>) in the spectrum of Pc (Castner et al., 1996) (Fig. 8I(i)) (Mthethwa et al., 2014) disappeared (S 2p<sub>3/2</sub>) and shifted to higher binding energies of 165.7 and 166.4 eV, respectively (S 2p<sub>1/2</sub>) (Fig. 8I(ii)) (Mthethwa et al., 2014).

#### 2.3.4. Transmission electron microscopy (TEM)

TEM, during which an electron beam is passed through a specimen to form an image, is widely used to study NP morphology and size distribution, as exemplified by data obtained for Ag NPs (Fig. 9A) (D’Souza et al., 2015b).

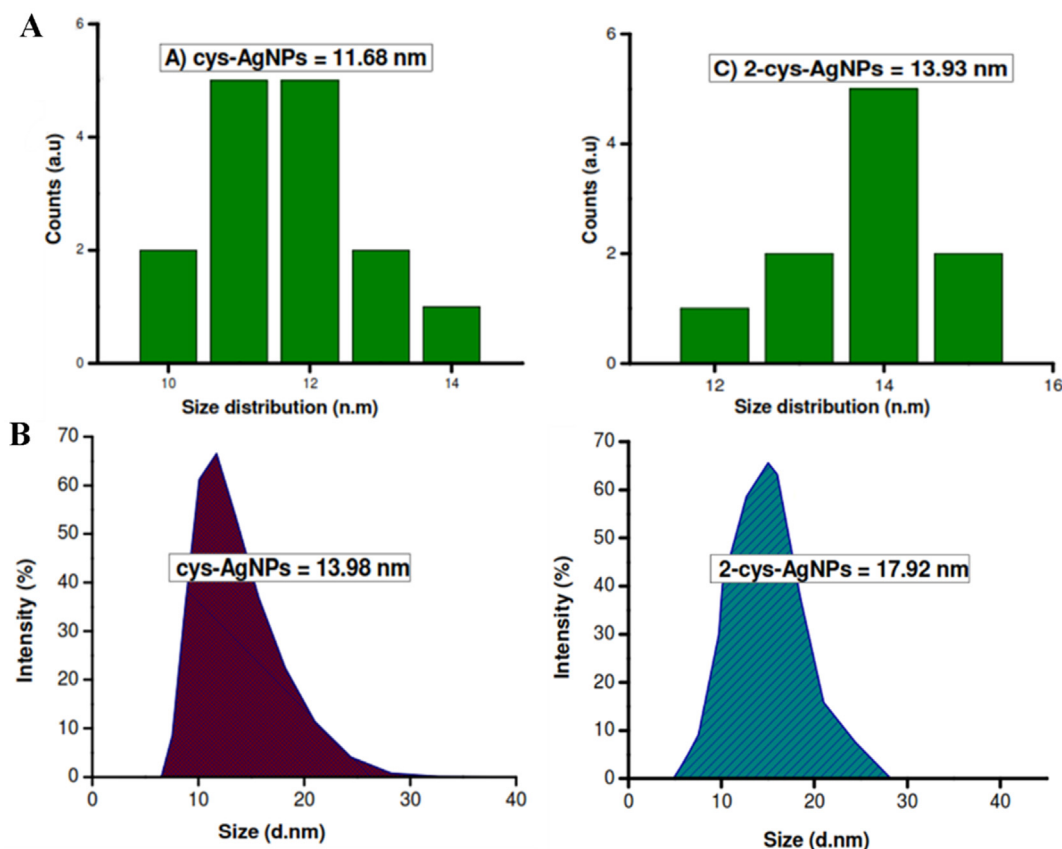


**Fig. 10** (A) TEM histograms and (B) DLS micrographs depicting the average size distributions of Ag NP and its corresponding nanoconjugate. Reproduced with permission from ref. (Matlou and Nyokong, 2020). Copyright 2020 Elsevier.

The number of Au or Ag atoms per particle ( $N_x$ ) can be determined from the average size measured by TEM as (Alvarez et al., 1997)

$$N_x = (59 \text{ nm}^{-3})(\pi/6)(\text{DMS})^3, \quad (5)$$

where DMS is the mean diameter of particles determined by TEM, and  $x$  is an index referring to the metal of the NP.

As Ag NPs are smaller than Au NPs with the same number of atoms and thus feature a higher surface to volume ratio, more Pc molecules can be loaded into the surface of the former NPs (Nwaji et al., 2018).

Generally, a slight increase in size was observed upon the conjugation of NPs to Pcs, which was attributed to  $\pi$ - $\pi$  stacking between Pc molecules to form H-aggregates (Fig. 9B) (J. et al., 1989; Nwaji and Nyokong, 2017c).

Surface modification of TOABr-Au NSs with 3-azido-1-propylamine was shown to induce agglomeration and increase the average NP size (Fig. 3) because of the concomitant reduction in interparticle distance (Fig. 9C and 9D) (Ashjari et al., 2015; Bankole and Nyokong, 2017b; Bankole et al., 2016c). Moreover, extensive NP aggregation was observed after conjugation to Pcs because of the formation of larger single or twinned crystals due to interactions between the neighboring nanocrystals and  $\pi$ - $\pi$  interactions between Pc complexes (Fig. 9C(C) and 9C(D)) (Ashjari et al., 2015; J. et al., 1989; Moon et al., 2010). The same aggregation was also noticed in the case of alloy nanoconjugates (Fig. 9D) (Bankole et al., 2016c) and Pcs conjugated to a silica core speckled with irreg-

ular Au nanodomains (Au-speckled silica, GSS) (Fig. 9E) (Dube et al., 2019c, 2018c). The increase in NP size due to conjugation increased in the order of Au BPs < Au NRs < Au NSs (Fig. 9F and 9G) (Mthethwa et al., 2014; Mthethwa and Nyokong, 2015). In this case, upon conjugation (which was accompanied by a certain extent of aggregation), the average aspect ratio of Au BPs (2.5) and Au NRs (3.2) slightly increased to 2.9 and 3.7, respectively. On the other hand, Ke et al. reported that the silica shells around Au NRs act as spacer layer between the NPs and inhibit their aggregation (Fig. 9H) (Ke et al., 2014).

Nonetheless, axial ligand exchange at the lanthanide metal center was suggested to be a probable route of hybrid formation, which explained the formation of a Pc shell on Au NSs (Fig. 9I) (Dubinina et al., 2018). The growth of these shells was attributed to  $\pi$ - $\pi$  stacking interactions between Pc molecules (Dubinina et al., 2018).

### 2.3.5. Dynamic light scattering (DLS)

In DLS technique, a monochromatic beam is directed to nanoparticles, and the light scattered at a certain angle is detected, giving information about the physical characteristics of the sample (Carvalho et al., 2018). It was reported that the sizes recorded by DLS are larger than those recorded by TEM (Cheng et al., 2019; Dube et al., 2019c; Matlou et al., 2019; Nwahara et al., 2019; Nwaji and Nyokong, 2017c; Ray et al., 2015) because the particles are measured in solution in DLS while they are measured in solid state in TEM.

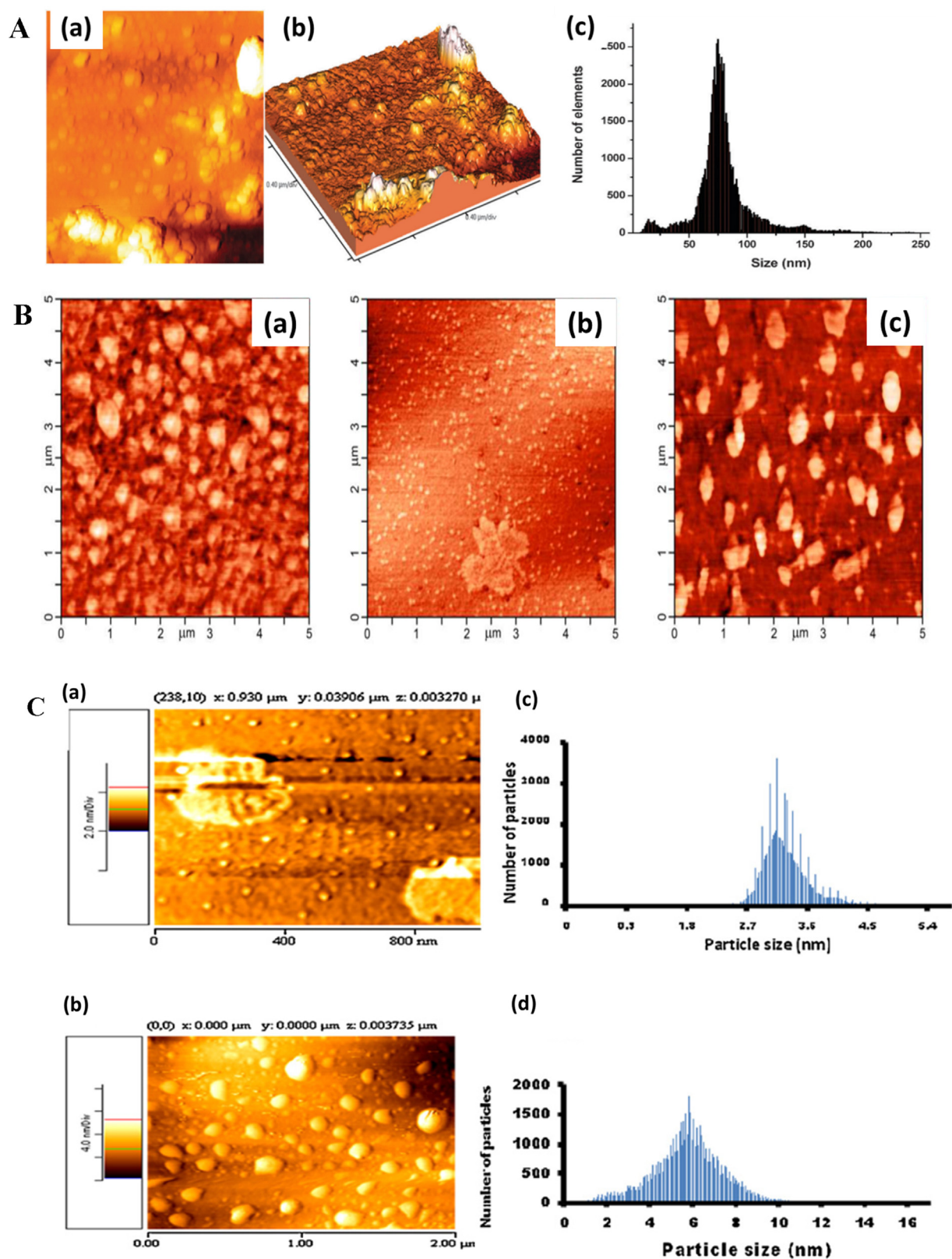


**Fig. 11** (A) AFM images of Au NSs: (a) 2D and (b) 3D (height profile), and the corresponding size distribution (c). Reproduced with permission from ref. (D'Souza et al., 2013). Copyright 2013 Royal Society of Chemistry. (B) AFM images of (a) a thin film, (b) Au NPs, and (c) hybrid particles, featuring an "island-type" texture. Reproduced with permission from ref. (Dubinina et al., 2018). Copyright 2018 Elsevier. (C) Surface topographies and sizes of (a) TOABr-Au NSs and (b) the corresponding nanoconjugates. (c) and (d) the histograms of the nanoparticles and nanoconjugates, respectively. Reproduced with permission from ref. (Tombe et al., 2012). Copyright 2012 Elsevier.

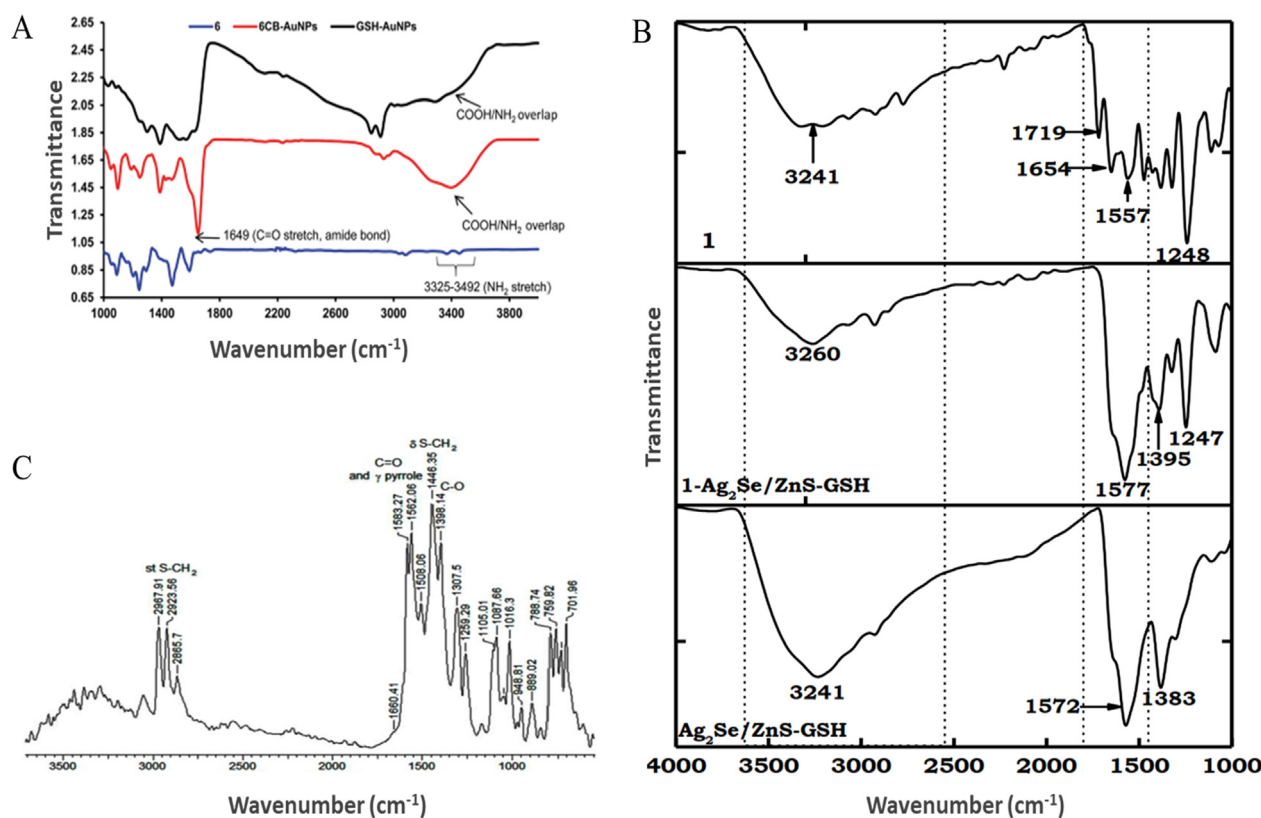


**Fig. 12** FT-IR spectra representing (A) amide bond formation between an amine-functionalized Pc and GSH-functionalized NPs. Reproduced with permission from ref. (Nwaji et al., 2017b). Copyright 2017 Royal Society of Chemistry; (B) amide bond formation between a carboxy-functionalized Pc and GSH-functionalized NPs. Reproduced with permission from ref. (Oluwole et al., 2017a). Copyright 2017 Elsevier, (C) the self-assembly of a Pc-NP conjugate through sulfur. Reproduced with permission from ref. (Dubinina et al., 2018). Copyright 2018 Elsevier.

Matlou et al. reported bigger sizes of Ag NPS and the nanoconjugates measured by DLS compared to TEM results, Fig. 10 (Matlou and Nyokong, 2020). The variance in sizes was attributed to the interference of the dispersant into the hydrodynamic diameter of the particles in DLS measurements which skew to larger particles.

### 2.3.6. Atomic force microscopy (AFM)

AFM is a very-high-resolution type of scanning probe microscopy that provides the possibilities of (i) force measurement, (ii) manipulation, and (iii) imaging, and is used to obtain 3D representations (topographies) of the sample surface and estimate NP size (Fig. 11A) (D'Souza et al., 2013).

A higher-order island-type texture observed by AFM for some Pc-Au NP hybrids was ascribed to the aggregation of Pcs around the Au core (Fig. 11B) (Dubinina et al., 2018) and was also observed for films deposited from dilute solutions (D'Souza et al., 2013; Dubinina et al., 2012; Wang et al., 2010).

The conjugation of Au NSs with Pcs was found to change surface topography (Fig. 11C(A) vs. 11C(B)) (Tombe et al., 2012), increase the average NP size, and elevate average roughness ( $R_a$ ) by facilitating aggregation.

### 2.3.7. Fourier transform infrared (FT-IR) spectroscopy

FT-IR spectroscopy is used to confirm the conjugation of Pcs to NPs through amide bond formation (Bankole and Nyokong, 2016a; Dube and Nyokong, 2019a). In this case, the two primary amine stretches in the spectra of amine-functionalized Pcs are replaced by a sharp single vibration band in the spectra of the corresponding nanoconjugates, which indicates the conversion of primary amine moieties into amide units upon bonding to carboxy-functionalized NPs (Fig. 12A) (Nwaji et al., 2017b). Moreover, the increased intensity and broadening observed between 3432 and 3500  $\text{cm}^{-1}$  upon nanoconjugate formation was shown to reflect the overlap of the nanoconjugate  $\text{NH}_2$  peak with the COOH stretch of GSH-Au NSs (Fig. 12A) (Nwaji et al., 2017b). Similarly, in the case of a carboxy-functionalized Pc, the  $\text{C}=\text{O}$  band at 1719  $\text{cm}^{-1}$  was replaced by new bands of the amide moiety at 3241 and 1577  $\text{cm}^{-1}$  upon conjugation (Fig. 12B) (Oluwole et al., 2017a).

The disappearance of the S-H band in the Pc-NP conjugate spectrum was also used to confirm the self-assembly of Pc and NPs through sulfur and suggested the formation of metal-sulfur bonds (Fig. 12C) (Oluwole et al., 2017b).

### 3. Photo-physicochemical properties

#### 3.1. Background of Pc photophysical studies

Photophysical processes have been widely reported for Pc complexes because of their high molar absorptivity in the visible region (Stillman and Thomson, 1974), with the origin of these processes illustrated by the Perrin-Jablonski diagram (Fig. 13).

UV-visible absorption and emission spectroscopy involve the excitation of an electron from the ground state to an excited state. Transitions with no change in spin ( $\Delta S = 0$ ), such as singlet-singlet and triplet-triplet ones, are allowed, whereas singlet-triplet transitions are forbidden, as they result in a spin change. Singlet and triplet states are represented by  $S_n$  and  $T_n$ , respectively. The lifetime of a state is defined as the average time the excited molecule spends in this state prior to deactivation to afford another state (Berberan-Santos, 2013).

#### 3.2. Fluorescence studies

##### 3.2.1. Background

Similarly to UV-visible absorption spectroscopy, fluorescence spectroscopies also involve the excitation of an electron from a low-energy occupied orbital (ground state) to a higher-energy unoccupied orbital (excited state) and relaxation (emission) which is reverse process. A transition which occurs with no change in spin and maintains spin pairing affords a singlet excited state, represented by  $S$ , with  $S_0$  being the lowest-energy excited singlet state. A transition involving a spin change gives rise to unpaired spins and affords a triplet ( $T$ ) excited state, with  $T_0$  being the lowest-energy triplet state. The selection rule for a radiative transition is  $\Delta S = 0$ , i.e., singlet-singlet and triplet-triplet transitions are allowed, while singlet-triplet ones ( $\Delta S \neq 0$ ) are forbidden.

In the case of fluorescence, electrons in the excited singlet state lose energy, i.e., are transferred to lower-energy states and ultimately to the ground state via a mechanism called

internal conversion (IC) (Albani, 2008). In the case of phosphorescence, electrons in the singlet state undergo ISC, and the spins are aligned in the same direction to afford a triplet state (Berberan-Santos, 2013). Vibrational relaxation of electrons is also likely to occur via collision and rotation before the return to the ground state ( $S_0$ ). Moreover, IC provides yet another way of returning to lower energy levels (Berberan-Santos, 2013).

##### 3.2.2. Determination of the fluorescence quantum yield of Pc complexes

For Pc complexes, fluorescence quantum yield ( $\Phi_F$ ) is mostly determined by the comparative method (Fery-Forgues and Lavabre, 1999; Maree et al., 2002):

$$\Phi_{Fs} = \Phi_{Fr} \frac{F_s \cdot A_r \cdot n_s^2}{F_r \cdot A_s \cdot n_r^2} \quad (6)$$

where  $F_s$  and  $F_r$  are the areas under the fluorescence emission curves of the sample and the reference, respectively;  $A_s$  and  $A_r$  are the absorbances of the sample and standard at the excitation wavelength, respectively; and  $n_s$  and  $n_r$  are the refractive indices of solvents used for the sample and the reference, respectively. Unsubstituted ZnPc is commonly employed as a reference ( $\Phi_F = 0.20$  in DMSO (Ogunsipe et al., 2004), 0.17 in DMF (Ogunsipe et al., 2003), 0.25 in THF (Saka et al., 2011), and 0.07 in toluene (Ogunsipe et al., 2003)).

William's comparative method provides another way to determine fluorescence quantum yield (Williams et al., 1983) using the absorbance and emission spectra of the reference and the sample measured at different concentrations. The integrated fluorescence intensities are plotted vs. the absorbance of the reference and the sample, and  $\Phi_F$  is calculated according to Eq. (7) (Topal et al., 2014), where subscripts  $r$  and  $s$  designate the reference and the sample, respectively, Grad is the plot gradient, and  $n$  is the solvent refractive index.

$$\Phi_{Fs} = \Phi_{Fr} \frac{\text{Grad}_s \cdot n_s^2}{\text{Grad}_r \cdot n_r^2} \quad (7)$$

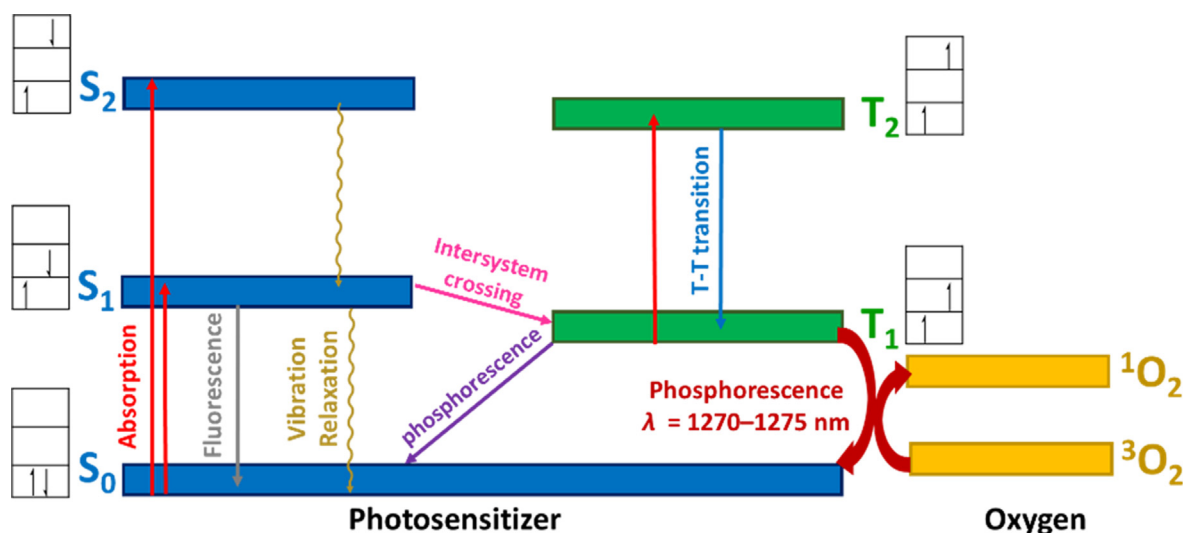


Fig. 13 Perrin-Jablonski diagram of Pc photosensitizer and singlet oxygen generation.

$\Phi_F$  can also be determined from the ratio of the number of photons emitted to the number of photons absorbed upon direct excitation (de Mello et al., 1997) using Eq. (8) (Suzuki et al., 2009):

$$\Phi_{Fs} = \frac{E_B - E_A}{S_A - S_B} \quad (8)$$

where  $E_A$  and  $E_B$  are the integrated intensities of solvent (blank) and sample emission peaks, respectively, while  $S_A$  and  $S_B$  are the integrated intensities of solvent and sample scattering peaks, respectively. Such measurements are commonly performed using an integrating sphere coated by polytetrafluoroethylene (Majeed et al., 2019a, 2019b).

### 3.2.3. Effect of Ag and Au NPs on the fluorescence properties

In general, Pcs form face-to-face-oriented H-aggregates (non-fluorescent) but can sometimes form side-by-side-oriented J-aggregates (fluorescent) (Kadish et al., 2003), the fluorescence behavior of which is affected by factors such as NP size and NP-Pc distance (Swierczewska et al., 2011).

Changes in both fluorescence quantum yields and fluorescence lifetimes of Pcs upon conjugation to Ag and Au NPs (Nwaji et al., 2018) were attributed to the interaction between the free electrons of the metallic surface and the fluorophore when the latter is excited in the presence of nearby metallic NPs, which changes the electric field around the molecule and affects fluorescence behavior (Geddes and Lakowicz, 2002). Thus, depending on the geometry or distance between the metal and the Pc molecule, the fluorescence quantum yield and lifetime increase or decrease.

Accordingly, fluorescence quenching after the conjugation of Pcs to Ag and Au NPs has been recorded and ascribed to the close packing of Pcs on the NP surface. Additionally, the heavy atom effect of Au and Ag NPs promotes ISC and contributes to the reduction in fluorescence quantum yield and lifetime (Bankole and Nyokong, 2017b; Bankole et al., 2016c; Chen et al., 2018; Dube and Nyokong, 2019a, 2019b; Dube et al., 2019c; Khoza and Nyokong, 2014; Mafukidze et al., 2019; Nwaji et al., 2018; Nwaji and Nyokong, 2017c; Oluwole et al., 2017a, 2016).

The fluorescence quantum yields of covalently linked nanoconjugates were observed to be lower than those of conjugates produced via the surface assembly of Pcs and Ag NSs/Au NSs, which was attributed to aggregation and fluorescence quenching due to the higher number of Pc molecules loaded via the covalent approach (Nwaji et al., 2017b). A similar trend of fluorescence quenching was recorded when Pcs were covalently bonded to GSH-capped Au NSs and Au NTs (Dube and Nyokong, 2019b). However, when Pcs were conjugated through surface assembly, the Pc-Au NS hybrids featured lower  $\Phi_F$  values than the corresponding Pc-Au NT hybrids (Dube and Nyokong, 2019a), which was attributed to the smaller size of Au NSs and, hence, their larger extent of fluorescence quenching (Xue et al., 2013). In addition, more Pc molecules could be loaded on Au NSs than on Au NTs, which resulted in more pronounced aggregation in the former case (Dube and Nyokong, 2019a). Asymmetric Pc complexes also display lower  $\Phi_F$  values than symmetric ones, which suggests that asymmetric structures can enhance ISC to the triplet state (Dube et al., 2018a). No clear change in fluorescence quantum yields was observed upon Pc conjugation to Ag

NTs and Ag NFs (D'Souza et al., 2015b), and the red shift observed in the excitation spectra of Ag nanoconjugates for the corresponding absorption indicated a change in nuclear configuration upon excitation or different Pc packing on Ag NSs (Khoza and Nyokong, 2014). Nonetheless, fluorophore quenching is not always due to conjugation. Despite the fact that Pc fluorescence quantum yields are known to decrease in the presence of Ag and Au NPs (Kotiaho et al., 2010), this quenching competes with the promotional effect of surface plasmon coupling (Mthethwa and Nyokong, 2015). Thus, the quenching efficiency is also related to NP shape, e.g., Au NRs and Au BPs, which have a higher number of coordinated Pc molecules per NP, showed a smaller quenching efficiency than Au NSs with a lower number of coordinated Pc molecules. The field around the excited complex is affected by the edges around nonspherical NPs and is therefore inhomogeneous, in contrast to the homogenous field created in the presence of spherical NPs (Mthethwa and Nyokong, 2015).

Pc-Au NR conjugates were found to feature fluorescence quantum yields slightly higher than those of nonconjugated Pcs in pH 9 buffer + Triton X-100, as the reduced aggregation and modified local field around the fluorescent molecule in the former case resulted in excitation occurring at a larger distance (Chen et al., 2018; Lakowicz, 2005). Moreover, fluorescence quantum yields slightly increased with increasing aspect ratio (Mthethwa et al., 2014), as polarization along NR length exceeds that of NSs (Ming et al., 2011). The ability of aggregates to convert electronic excitation energy to vibrational energy decreases fluorescence quantum yield (Lacey and Phillips, 2002).

The fluorescence of a CoPc complex (Lokesh et al., 2009) was not quenched upon conjugation with Au NSs, whereas quenching was observed upon conjugation with Ag NSs, which was ascribed to NP size differences. Moreover, Au NPs stabilized by thiol-derivatized Pcs did not quench fluorescence (Hone et al., 2002). The capping agent used for NP synthesis also affects the fluorescence spectra of Pc-NP conjugates. For example, TOABr was found to encourage ISC and decrease fluorescence intensity because of the presence of Br (Hone et al., 2002) and was suggested to promote the Pc-to-Au NP energy transfer and thus decrease the fluorescence lifetime of free Pc molecules (Camerin et al., 2010). Some studies revealed that thiol or amino derivatives of Pcs can stabilize Au NPs, in which case Pc fluorescence is not quenched (Hone et al., 2002; Lokesh et al., 2009).

Metal-enhanced fluorescence (MEF) has also been studied for NP-Pc systems, e.g., the increase in fluorescence intensity and decrease in fluorescence lifetime recorded in the presence of Au NPs were enhanced upon the addition of a Au NP@GO solution (M. et al., 2015). Teixeira et al. designed polyelectrolyte-modified Au NPs for the plasmonic enhancement of fluorescence emission from a Pc dye (Teixeira et al., 2015) and observed approximately three-orders-of-magnitude emission enhancements for an optimum number of 13–15 polyelectrolyte bilayers, which was attributed to hot spot formation via Au NP clustering during the layer-by-layer polyelectrolyte deposition. Ke et al. reported the MEF of a tetra-substituted carboxyl aluminum Pc conjugated to silica-coated Au NRs (Au NRs@SiO<sub>2</sub>) with a core-shell structure. At a separation distance of 10.6 nm, the fluorescence enhancement factor changed from 7 to 2.1 as the thickness of the silica shell changed from 2.1 to 28.6 nm (Ke et al., 2014).



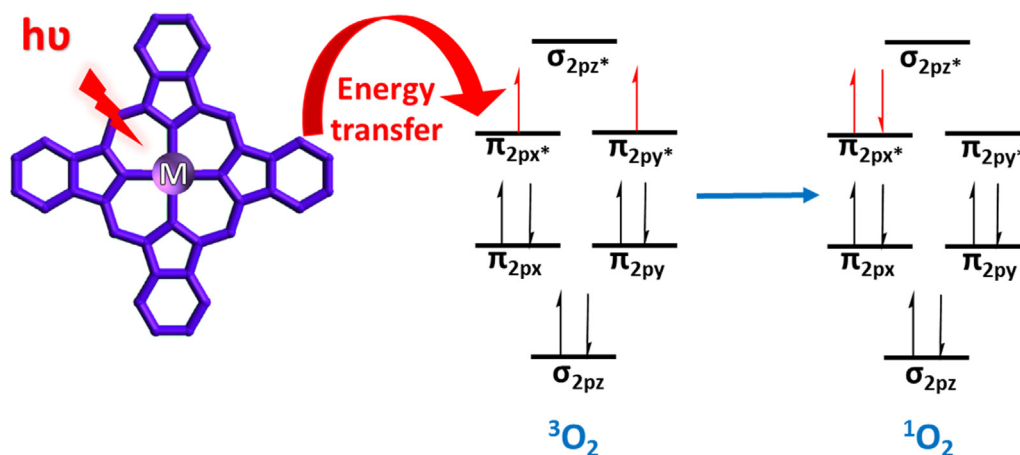


Fig. 14 Energy transfer from Pc to triplet oxygen ( $^3\text{O}_2$ ) to generate singlet oxygen ( $^1\text{O}_2$ ).

Fluorescence lifetime ( $\tau_F$ ) refers to the average time that a molecule stays in its excited state before fluorescing, is positively correlated to  $\Phi_F$  (Nwaji et al., 2017b; Tombe et al., 2013a), and is affected by the shape and size of the metal NP. For example, spherical and nonspherical NPs exhibit large differences in  $\tau_F$ , which is attributed to the induction of multipolar excitation by excited anisotropic NPs (D'Souza et al., 2013).

The general lowering of Pc  $\tau_F$  upon conjugation to NPs was ascribed to the close packing of Pc molecules on the NP surface (Chen et al., 2018). The  $\tau_F$  decay curve showed monoexponential behavior with a single excited state lifetime, while bi-exponential curves were observed for some conjugates, in which case the two lifetimes were attributed to the different orientations and packing of Pc molecules on the NP surface (Bankole and Nyokong, 2017b; D'Souza et al., 2013; D'Souza et al., 2015b; Dube et al., 2018a, 2019c, 2017; Dube and Nyokong, 2019a, 2019b; Forteach et al., 2012; Mthethwa et al., 2012, 2013; Nwaji et al., 2017b; Oluwole et al., 2017a; Tombe et al., 2013a, 2012) or the presence of free Pcs in addition to conjugated Pc molecules (Mthethwa et al., 2012). However, biexponential decay was also detected for nonconjugated Pcs and ascribed to the quenching of monomer fluorescence by the formation of a nonfluorescent aggregated form (Lacey and Phillips, 2002). The fact that only one lifetime was obtained for a Pc and its conjugates with nonspherical NPs was attributed to the higher surface area of these NPs compared to that of spherical ones and the decreased stacking in the former case (Mthethwa and Nyokong, 2015).

### 3.3. Triplet and singlet oxygen generation

#### 3.3.1. Background

Singlet oxygen ( $^1\text{O}_2$ ) is a highly reactive form of reactive oxygen species that interacts with most biomolecules such as lipids, proteins, and DNA/RNA with a preference for electron-rich regions, which results in a certain selectivity (Li et al., 2016). As singlet oxygen is generated when energy is transferred from the triplet state of a photosensitizer to the ground state of molecular oxygen (Fig. 14), Pcs are promising photocatalysts for green chemistry (Fernández et al., 2016) that can be used to photodegrade pollutants (e.g., pesticides,

petroleum hydrocarbons, phenols, plasticizers, chlorinated biphenyls, and detergents) in water (Ali et al., 2012). Pcs have also been used to develop antibacterial/antiviral biomolecular degradation methods and cancer PDT (Alpugan et al., 2019).

#### 3.3.2. Determination of singlet oxygen and triplet oxygen quantum yields of Pc complexes

The singlet oxygen quantum yield ( $\Phi_\Delta$ ) can be measured by optical, chemical, and calorimetric methods. In particular, optical determination can be performed by two main methods.

- (1) Indirect measurements are based on the use of chemical quenchers (Shinohara et al., 2006) in a literature-described experimental setup (Brannon and Magde, 1980; Seotsanyana-Mokhosi et al., 2001). The sample containing a singlet oxygen quencher, e.g. 1,3-diphenylisobenzofuran (DPBF) in organic solvents or anthracene-9,10-bis-methylmalonate (ADMA) in aqueous media (Fig. 15), is irradiated in the Q-band region of the photosensitizer.  $\Phi_\Delta$  is determined by the relative method using unsubstituted ZnPc as a reference (Eq. (9)):

$$\Phi_{\Delta s} = \Phi_{\Delta r} \frac{R_s \cdot I_{abs}^r}{R_r \cdot I_{abs}^s} \quad (9)$$

where  $\Phi_{\Delta r}$  is the singlet oxygen quantum yield of the reference ( $\Phi_\Delta = 0.67$  in DMSO (Kuznetsova et al., 2000), 0.56 in DMF (Spiller et al., 1998), 0.58 in toluene (Ogunsipe et al., 2003), 0.53 in THF (Saka et al., 2011), and 0.61 in pyridine) (Ogunsipe et al., 2004);  $R_s$  and  $R_r$  are the photobleaching rates in the presence of the sample and the reference, respectively; and  $I_{abs}^s$  and  $I_{abs}^r$  are the light absorption efficiencies of the sample and the reference, respectively.

- (2) The direct method relies on the monitoring of  $^1\text{O}_2$  phosphorescence at 1270–1280 nm and the direct optical detection of NIR  $^1\text{O}_2$  luminescence. The phosphorescence of singlet molecular oxygen in the NIR region at 1276 nm generated by the Pc sample is compared with that generated by the reference ZnPc, and  $\Phi_\Delta$  is then calculated as (Losev et al., 1988)

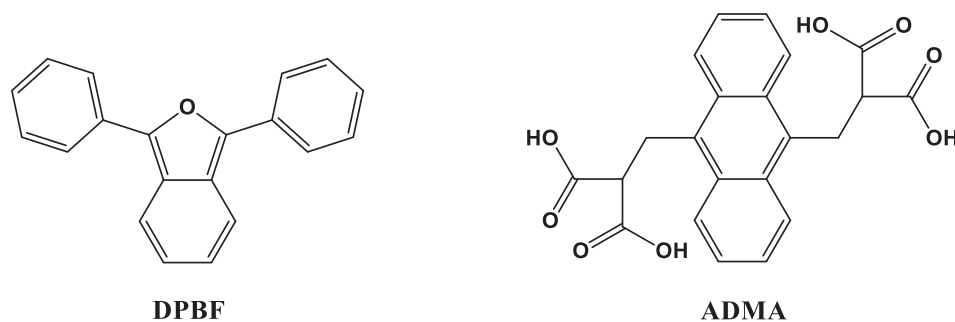


Fig. 15 Structures of singlet oxygen quenchers.

$$\Phi_{\Delta_s} = \Phi_{\Delta_r} \frac{n_s^2 A_r I_s}{n_r^2 A_s I_r} \quad (10)$$

where  $\Phi_{\Delta_s}$  and  $\Phi_{\Delta_r}$  are the quantum yields of the sample and reference, respectively;  $n_s$  and  $n_r$  are the refractive indices of solvents used for sample and reference measurements, respectively;  $A_s$  and  $A_r$  are the absorbances of the sample and the reference, respectively; and  $I_s$  and  $I_r$  are the integrated areas under the emission spectra of the sample and the reference, respectively.

A comparative method using ZnPc as a reference ( $\Phi_T = 0.68$  in DMSO) (Kossanyi and Chahraoui, 2000) was employed for the calculation of triplet quantum yield ( $\Phi_T$ ) according to Eq. (11) (Tran Thi et al., 1989):

$$\Phi_{T_s} = \Phi_{T_r} \frac{\Delta A_{T_s} \varepsilon_{T_r}}{\Delta A_{T_r} \varepsilon_{T_s}} \quad (11)$$

where  $\Delta A_T$  and  $\Delta A_T^r$  are the changes in the triplet state absorbance of the sample and the reference, respectively;  $\varepsilon_T$  and  $\varepsilon_T^r$  are the triplet state molar extinction coefficients for the sample and the reference, respectively; and  $\phi_T^r$  is the triplet quantum yield for the reference.  $\varepsilon_T$  and  $\varepsilon_T^r$  are determined from the molar extinction coefficients of the respective ground singlet states ( $\varepsilon_S$  and  $\varepsilon_S^r$ ), the changes in absorbance of these states ( $\Delta A_S$  and  $\Delta A_S^r$ ), and changes in the triplet state absorbance ( $\Delta A_T$  and  $\Delta A_T^r$ ), in accordance with Eqs. (12) and (13):

$$\varepsilon_T = \varepsilon_S \frac{\Delta A_T}{\Delta A_S}, \quad (12)$$

$$\varepsilon_T^r = \varepsilon_S^r \frac{\Delta A_T^r}{\Delta A_S^r} \quad (13)$$

### 3.3.3. Effect of Ag and Au NPs on triplet and singlet oxygen generation

Triplet state formation and fluorescence are competing processes. Pc conjugation to metallic NPs enhances ISC and hence increases triplet and singlet oxygen quantum yields. The number of Pc molecules loaded on the NP surface is positively correlated with the triplet quantum yield (Nwaji and Nyokong, 2017c).

An increase in triplet quantum yield is expected to decrease the triplet lifetime, as was observed for Pc complexes conjugated to Ag NPs. However, an opposite trend was observed when the same complexes were conjugated to Au NPs follow-

ing the same strategy (Nwaji and Nyokong, 2017c), which was attributed to the protective effect of larger (compared to Ag NPs) Au NPs (Idowu et al., 2008).

The effects of NP shape on Pc photophysical properties have been extensively investigated. When Au NSs and Au NRs with three different aspect ratios (2.0, 4.7, and 7.1) were conjugated to ZnPc (Mthethwa et al., 2014), both NSs and NRs with the smallest aspect ratio (2.0) afforded the same  $\Phi_{\Delta}$  of 0.23, although the number of Pc molecules loaded per NP equaled 27 and 49, respectively. In the case of higher-aspect-ratio NRs (4.7 and 7.1), the above number increased to 111 and 243, respectively, which induced a slight increase in the  $\Phi_{\Delta}$  of Pc-Au NRs (7.1) to 0.29 (Mthethwa et al., 2014). Higher values of  $\Phi_T$  and  $\Phi_{\Delta}$  were recorded for Au NS conjugates (more loaded Pc molecules) than for Au NT ones (less loaded Pc molecules) (Dube and Nyokong, 2019a).

Al-Pc complexes are characterized by low values of  $\Phi_{\Delta}$  due to the small size of Al atoms. However, when these complexes are conjugated to Au NPs,  $\Phi_{\Delta}$  increases. Mthethwa et al. conjugated Pcs to Au NSs, Au NRs, and Au BPs, showing that the asymmetric shape of these NPs resulted in a slight increase in the  $\Phi_{\Delta}$  of the corresponding conjugates compared to that observed for conjugates of symmetrical Au NSs (Mthethwa and Nyokong, 2015).

According to D'Souza et al., who studied the effects of Ag NSs, Ag NFs, and Ag NTs, the increase of  $\Phi_T$  is correlated to Pc loading, decreasing in the order of Ag NSs (7 Pcs/NP) > Ag NFs (4) > Ag NTs (3). All conjugates showed an increased triplet lifetime due to the protective effect of tetra-substituted Pc on Ag NPs. No clear trend was observed for the monosubstituted complex (D'Souza et al., 2015b).

The  $\Phi_{\Delta}$  of Pc was reported to increase upon conjugation to Fe<sub>3</sub>O<sub>4</sub>@Ag core-shell NPs (but not in case of the Ag-Fe<sub>3</sub>O<sub>4</sub> hybrid) because of the screening effect of magnetic NPs that possibly inhibited the interaction of the excited triplet state of the conjugates with the ground state of molecular oxygen (Magadla et al., 2019). The hybrid of a carboxy-functionalized asymmetric ZnPc complex with cysteine-functionalized Ag NPs showed a larger increase in  $\Phi_T$  and  $\Phi_{\Delta}$  than the hybrid of the corresponding complex with amino-functionalized magnetic NPs (Matlou et al., 2019).

Conjugation to bimetallic alloys can increase  $\Phi_T$ , and the extent of this increase was found to be positively correlated with Au content (Bankole et al., 2016c; Dube et al., 2017). Moreover, the choice of a suitable capping agent may also enhance the physical properties of Pcs, e.g., the presence of

bromide from TOABr was shown to promote the ISC of NPs (Hone et al., 2002) and facilitate energy transfer from the triplet state of the photosensitizer to molecular oxygen (Tombe et al., 2012). On the other hand, a decrease in  $\Phi_{\Delta}$  was observed when Pc was conjugated to a metal alloy capped with GSH (Dube et al., 2017), which was attributed to the screening effect of the correspondingly capped NPs that prevented the interaction between the excited triplet state of nanoconjugates and the ground state of molecular oxygen (Chadwick et al., 2016; Yin et al., 2015). Interestingly, the doping of this alloy onto Si NPs before Pc linking improved the  $\Phi_{\Delta}$  of Pc from 0.37 to 0.49. In this case, the porous silica acted as a hydrophobic molecule carrier and possibly protected the Pc from the degradation (Nguyen, 2012). Notably, Ke et al. synthesized Au NR@SiO<sub>2</sub>-Pc conjugates with silica shell thicknesses of 2.1, 10.6, and 28.2 nm, showing that the silica shell can increase  $\Phi_{\Delta}$ , which was maximal for a shell thickness of 28.2 nm (Ke et al., 2014). Conjugation of Pc to Ag NPs-GSH resulted in decreased  $\Phi_{T}$ , whereas an increase in  $\Phi_{T}$  was recorded when the same complex was conjugated to core-shell Ag<sub>2</sub>Se/ZnS-GSH QDs, which was attributed to the larger NP size (and hence, the larger number of heavy atoms) in the latter case. Both nanoconjugates showed lower triplet lifetimes than Pc alone (Oluwole et al., 2017a). The coupling of GSH-capped QDs, Au NPs, and Ag NPs to MnO<sub>2</sub> was shown to promote singlet oxygen generation in water (Nwahara et al., 2019).

### 3.3.4. Photothermal conversion efficiency

It is noteworthy to mention that PDT has a drawback of keeping the patients in dark during and after treatment to avoid any photosensitive reaction with their healthy tissues (Li et al., 2018b). On the other hand, photothermal therapy (PTT) is an oxygen-independent mechanism which was found to be effective in treatment of hypoxic tumors (Zheng et al., 2021). In PTT, heat is generated when a near-infrared (NIR) light is applied to a PTT agent through non-radiative relaxation pathways (Jung et al., 2018). This mechanism cannot be induced by sunlight or bright indoor light like in the case of PDT. And, therefore, the application of Pcs as PTT agents have been investigated by inhibiting or reducing fluorescence process and intersystem crossing through synthesis of aggregated Pcs and/or using a paramagnetic metal (Du et al., 2017; He et al., 2020; Li et al., 2017; Lim et al., 2012; Wu et al., 2020). Plasmonic nanomaterials like Au and Ag NPs have also been known as PTT agents (Kim et al., 2019) owing

to their strong absorption and scattering in the NIR region (Shibu et al., 2013). Since PTT was found to enhance the blood flow in tumor tissues, thereby improving the oxygen level in the tumor microenvironment (Zhang et al., 2019; Zheng et al., 2021; Zhou et al., 2019), conjugation of Au and Ag NPs to Pcs is expected to afford hybrids with combined PDT and PTT capabilities (Dube et al., 2018b; Nombona et al., 2011b; Oluwole et al., 2016).

### 3.4. Nonlinear optical limiting

#### 3.4.1. Background

Laser light finds diverse applications (e.g., CD players, scanners, laser pointers, spectroscopic studies, optical sensors, astronomy, and military). However, highly intense laser light can destroy optical sensors and skin tissues and cause blindness. When light hits an object, it can be absorbed, transmitted, reflected, refracted, or scattered, as illustrated in Fig. 16.

Since the birth of the laser in the 1960s, materials with NLO properties have been intensively investigated, finding use in higher harmonic frequency generation, frequency mixing, self-focusing electro-optic modulation (Dalton et al., 1999), optical parametric oscillators (Donaldson and Tang, 1984), photo refractivity (Kippelen et al., 1998), terahertz generators (Brahadeeswaran et al., 2006), etc. Optical limiters are materials that transmit light of low intensity (e.g., ambient light) while absorbing harmful high-intensity light (e.g., laser radiation). Such materials were discovered by J. Kerr, who noticed that the electric field can change the refractive indices of organic liquids and glasses (Crova, 1879; Kerr, 1875). Although NLO activity was observed for inorganic crystals such as LiNbO<sub>3</sub>, the use of these materials was limited either by their low NLO responses (as in the case of semiconductors) or the difficulty of processing into thin films and incorporation into micro-optoelectronic devices (as in the case of ferroelectric crystals) (Saleh and Teich, 2001; Zyss, 1994). By the mid-1980s, organic materials with NLO properties were discovered and attracted increased attention due to their comparatively low fabrication cost, fast response time, and large nonlinear susceptibility (Chemla and Zyss, 1987; Nalwa and Miyata, 1997).

**3.4.1.1. Definition of an optical limiter.** An optical limiter (OL) is a substance which displays a decrease in transmittance with increasing fluence or light intensity. An ideal optical limiter shows a fluence output linearly dependent on energy input below a certain threshold value and exhibits a constant fluence output above this threshold to protect the optical sensors (Fig. 17).

Good NLO materials should be highly soluble, feature a high linear transmission and a large nonlinear absorption, and exhibit a high damage threshold (Calvete et al., 2004), with fullerenes (Tutt and Kost, 1992), porphyrins (Calvete et al., 2004; Chen et al., 2005; Senge et al., 2007), carbon nanotubes (Senge et al., 2007), NPs, metal NWs (Han et al., 2011), and Pcs (Calvete et al., 2004; Chen et al., 2005) found to be good candidates. Specifically, Pcs with an 18  $\pi$ -electron system have been considered as promising NLO materials because of their large optical nonlinearities, ultrafast response times, and ease of processing (McKeown, 1998; Nalwa and Miyata, 1997). The optoelectronic properties of Pcs can be controlled by the

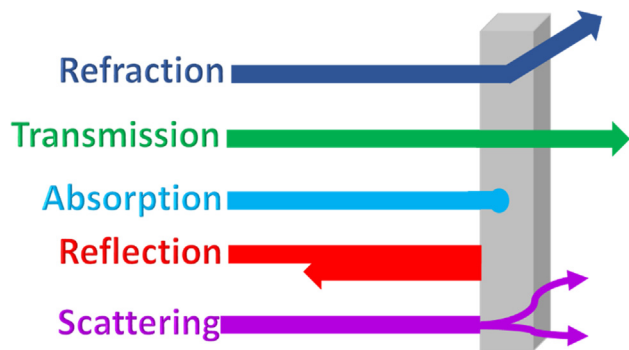


Fig. 16 Illustration of different optical responses of materials.

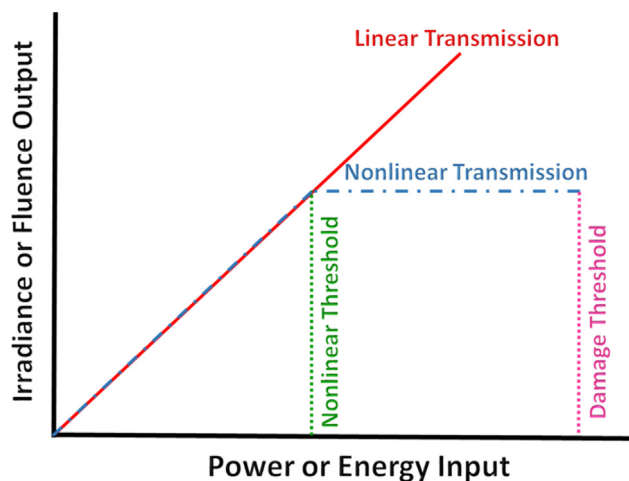


Fig. 17 Schematic representation of the ideal behavior for a passive optical limiter.

chemical modifications of the axial ligand, peripheral and non-peripheral substituents, and the central metal atom (O'Flaherty et al., 2003). The incorporation of heavy metal atoms was shown to increase the population of Pc excited states via ISC and thus lead to a large absorption cross-section of the excited state (Auger et al., 2003). Optical limiting with Pcs has been first reported for a chloroaluminum phthalocyanine (Coulter et al., 1989) and has since then been described for many other Pc complexes, e.g.,  $t\text{Bu}_4\text{-PcInCl}$ ,  $t\text{Bu}_4\text{PcIn}(p\text{-TMP})$  (Shirk et al., 2000), and  $\text{PbPc}(\beta\text{-CP})_4$  (Shirk et al., 1993).

**3.4.1.2. Z-scan technique used to study NLO properties.** Several characterization techniques are available for measuring third-order optical nonlinearities, e.g., degenerate four-wave mixing, nearly degenerate three-wave mixing, optical Kerr effect, ellipse rotation, interferometric methods, two-beam coupling, beam self-bending, and third harmonic generation, all of which are potentially sensitive yet complicated. Among these techniques, the Z-scan method offers simplicity and sensitivity in measuring the third-order optical nonlinearity and allows one to compute the contributions of nonlinear absorption and nonlinear refraction toward this nonlinearity. The basics of the Z-scan technique have been presented by Sheik-Bahae et al. (Sheik-Bahae et al., 1989, 1990).

The Z-scan method relies on the principle of moving the sample through the focus of a tightly focused Gaussian laser beam, the intensity of which changes as the sample is moved. When the sample is far from the focus and the incident intensity is low, the transmission is close to unity. However, when the sample approaches the focus ( $Z = 0$ ), the measured transmittance either increases to form a peak (saturable absorption, SA) or decreases to form a valley (reverse saturable absorption, RSA) (Fig. 18).

**3.4.1.3. SA and RSA.** Upon receiving energy, an NLO material undergoes transitions that can be explained in terms of the five-level diagram shown in Fig. 19. When interacting with laser radiation in the presence of strong electromagnetic fields, the highly conjugated Pc structure promotes preferable polarizability and fast charge distribution (Bilgin et al., 2007). Pcs are optical limiters of the RSA type (Venkatram et al.,

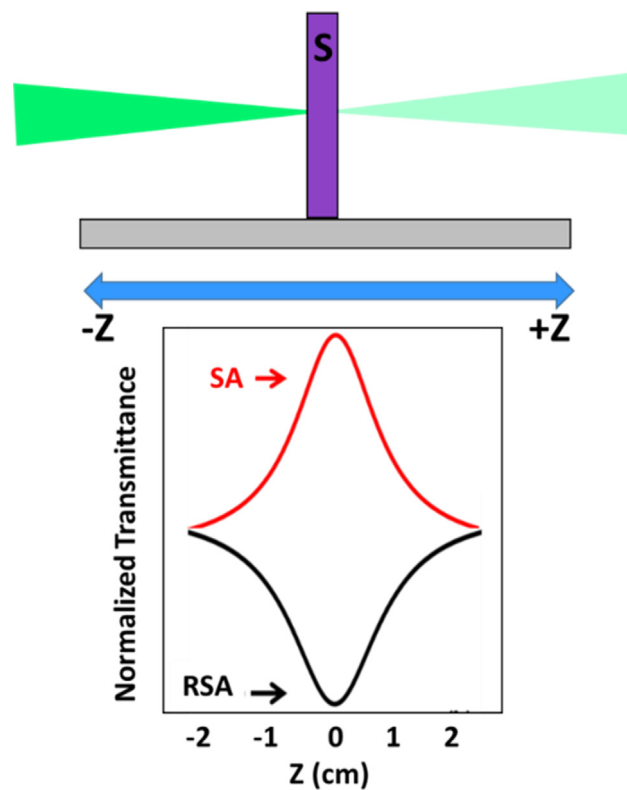
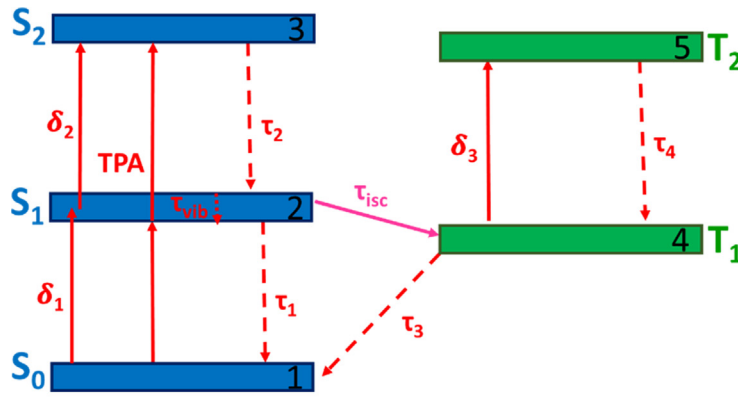


Fig. 18 Representative open-aperture Z-scans of SA and RSA materials.

2008), with the corresponding mechanism involving a sequential two-photon absorption of the ground state ( $S_0$ ) to afford a higher excited state ( $S_1$ ), which can further absorb photons to afford higher-lying excited states ( $S_n$ ). Pcs can absorb intense light, undergoing ISC to produce an excited triplet ( $T_1$ ) state from the  $S_1$  state upon their relaxation back to the ground state. At this point, irradiation with intense light would result in triplet-triplet absorption ( $T_1 \rightarrow T_n$ ). Large  $\delta_2$  and  $\delta_3$  as well as a long excited state lifetime are required for the largest nonlinear absorption, which makes Pcs excellent optical limiters (Fitzgerald et al., 2015; Zhang et al., 2014).

With increasing laser intensity, if the excited states show saturation due to their long lifetimes, the transmission exhibits SA behavior, whereas RSA behavior is observed if the excited state has a stronger absorption than the ground state (Srinivas et al., 2001). Materials showing RSA become more opaque as the incident optical intensity increases (Fig. 20) because of the enhanced absorption of the excited state, multi-photon absorption, or both (Srinivas et al., 2003). Such materials can be used for the protection of eyes and sensitive devices from intense radiation, also finding applications in passive mode locking and optical pulse shaping/processing (Harter et al., 1984; Tutt and Bogges, 1993). Conversely, SA materials, which become more transparent as the incident optical intensity increases (Fig. 20), are widely used in short-pulse lasers as crucial passive mode-locking or Q-switching elements (Wang et al., 2005). Notably, many materials simultaneously exhibit more than one nonlinear absorption process at different laser energies (Srinivas et al., 2003).



$S_0, S_1, S_2$  = ground, first and second singlet excited states, respectively.  
 $\delta_1, \delta_2, \delta_3$  = ground, singlet and triplet excited cross sections, respectively.  
 ISC = intersystem crossing.  
 $T_1$  and  $T_2$  = lower and higher energy triplet state, respectively.

**Fig. 19** Illustration of the five-level process used to describe the interaction of light with a molecule in terms of electronic transitions in NLO materials.

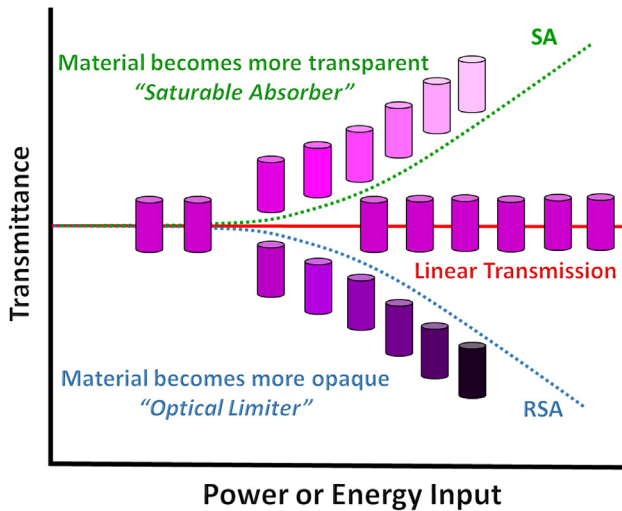


**Fig. 20** Illustration of the difference between RSA and SA materials.

#### 3.4.2. Calculation of NLO parameters

Open aperture Z-scan measurements are performed according to the method described by Sheik-Bahae et al. (Sheik-Bahae et al., 1989, 1990; Sheik-Bahae and Stryland, 1998):

$$T(z) = \frac{1}{\sqrt{\pi}q_0(z)} \int_{-\infty}^{\infty} \ln[1 + q_0(z)e^{-\tau^2}] d\tau \quad (14)$$

where

$$q_0(z) = \frac{\beta_{eff} I_{00} L_{eff}}{1 + z^2/z_0^2} \quad (15)$$

and

$$L_{eff} = \frac{1 - e^{(-zL)}}{\alpha} \quad (16)$$

$L$  and  $I_{00}$  are the path length and the on-focus peak input irradiance, respectively;  $\alpha$  and  $\beta_{eff}$  are the linear and effective nonlinear absorption coefficients, respectively; and  $L_{eff}$ ,  $z$ , and  $z_0$  are the effective path length, translation distance of the sample relative to the focal point of the Z-scan instrument, and the Rayleigh length, respectively. The Rayleigh length is defined as  $\pi w_0^2/\lambda$ , where  $w_0$  is the beam waist at the focus ( $Z = 0$ ), defined as the distance from the beam center to the point where the intensity decreases to  $1/e^2$  of its on-axis value, and  $\lambda$  is the wavelength of the laser beam. A numerical form of Eq. (14) is employed to fit experimental data (Sheik-Bahae et al., 1989, 1990; Sheik-Bahae and Stryland, 1998).

$$T(z) = 0.363e^{\left(\frac{-q_0(z)}{5.60}\right)} + 0.286e^{\left(\frac{-q_0(z)}{1.21}\right)} + 0.213e^{\left(\frac{-q_0(z)}{24.62}\right)} + 0.096e^{\left(\frac{-q_0(z)}{113.95}\right)} + 0.038e^{\left(\frac{-q_0(z)}{965.08}\right)} \quad (17)$$

The imaginary component of third-order susceptibility ( $\text{Im}[\chi^{(3)}]$ ) depends on the speed of the nonlinear absorption response and is related to  $\beta_{eff}$  as (Kadish et al., 2003)

$$\text{Im}[\chi^{(3)}] = \frac{n^2 \epsilon_0 c \lambda \beta_{eff}}{2\pi}, \quad (18)$$

where  $\epsilon_0$ ,  $n$ , and  $c$  are the permittivity of free space, the linear refractive index, and the speed of light in vacuum, respectively.

Second-order hyperpolarizabilities ( $\gamma$ ), related to the interaction between the incident photons and the permanent dipole moment of dyes, can be calculated as (Chen et al., 2005; Kadish et al., 2003)

$$\gamma = \frac{\text{Im}[\chi^{(3)}]}{f^4 C_{mol} N_A} \quad (19)$$

where  $N_A$  is Avogadro's constant,  $C_{mol}$  is the concentration of the active chromophore, and  $f$  is the Lorentz local field factor, defined as  $f = \frac{(n^2+2)}{3}$ .

### 3.4.3. Effect of Ag and Au NPs

The extended delocalized  $\pi$ -system of Pcs makes them promising NLO materials. For example, Pc complexes show low linear absorption at 532 nm and absorption cross-sections of the excited state that exceed those of the ground state. In recent years, many approaches have been used to conjugate Pc complexes to metallic (e.g., Ag and Au) NPs exhibiting SPR for enhancing Pc OL properties. SPR in Ag and Au NPs is an eminent spectroscopic feature that gives rise to absorption due to the oscillation of free electrons in the metal conduction band (Jain et al., 2006). When the surface geometry of metallic NPs is modified, the electric field density on the surface is shifted to afford an NLO response (Nwaji et al., 2018). Enhanced NLO responses are generally observed for Pc complexes conjugated to Au and Ag NPs because of the heavy atom effect, which is known to increase the triplet state population (Nwaji et al., 2017d). However, the performance of Ag NPs was found to be inferior to that of Au NPs, as the SPR band of the former is not resonant with 532 nm (Nwaji et al., 2017a), while that of the latter (530 nm) is in complete resonance with the wavelength used in Z-scan measurements. Thus, Au NPs are a better candidate for NLO property enhancement than Ag NPs (Nwaji et al., 2017b, 2017d; Nwaji and Nyokong, 2017c).

The Z-scan profile of Au NPs shows SA at low irradiance, while a complete shift to RSA is observed at higher irradiance, as has also been reported for other metal NPs (Bankole and Nyokong, 2017b; De Boni et al., 2008; Gao et al., 2003; Gurudas et al., 2008; Lee et al., 2009; Nwaji and Nyokong, 2017c; Oluwole et al., 2017a). When parameters such as laser input intensity and particle size/shape (e.g., Au/Ag core-shell NPs (Anija et al., 2003), Au-Ag alloy nanoclusters (Philip et al., 2000), and Au NRs (Elim et al., 2006)) were changed, the SA behavior of these NPs at moderate input intensities was assigned to ground-state plasmon bleaching due to intraband electron excitation. In contrast, RSA behavior at higher input intensities was assigned to the transient absorption of free carriers and/or the photoejection of electrons, in addition to two-photon absorption and nonlinear scattering (Philip et al., 2000). The conjugation of materials with RSA behavior (e.g., Pcs) to materials showing SA behavior (e.g., Au NPs) at low irradiance can produce promising optical limiting properties that can be used in technological applications such as laser pulse narrowing, optical switching, and optical pulse compression (Bankole and Nyokong, 2016b). Upon the conjugation of Pcs to metallic NPs, the minimum transmittance in the RSA dip dropped further, which indicated an enhancement of the nonlinear response (Bankole and Nyokong, 2017b; Nwaji and Nyokong, 2017c; Oluwole et al., 2017a, 2017b). However, conjugation of Au NPs to lanthanide (III) complexes of 3-(ethylthio)phenyl-substituted Pcs only weakly affected Z-scan curve intensity and position, as the decrease in Pc concentration in the hybrid led to a decrease in nonlinear response (Dubinina et al., 2018).

The properties of Pc-NP conjugates are affected by the type of link between Pcs and NPs, in particular, Pcs exerted a greater influence when they were covalently linked to NPs, while a weaker influence was observed for conjugates prepared via surface assembly and featuring M—N bonding (Nwaji et al., 2017b). However, the latter nanoconjugates showed a more pronounced RSA behavior with lower minimum trans-

mittance values that the former conjugates when surface assembly was achieved through M—S bonding (Nwaji and Nyokong, 2017c). Thus, NLO property enhancement was found to decrease in the order of M—S > M—amide > M—N bonds. Moreover, Au NS-Pc featuring an azide link (i.e., containing a triazole ring) featured a larger enhancement (Bankole and Nyokong, 2017b) than the corresponding conjugate featuring an amide linkage to the same Pc (Bankole and Nyokong, 2016b). The annealing process was also found to remarkably alter the optical and structure-dependent of metallophthalocyanine thin film (Zawadzka et al., 2014, 2013), with an increase in the values of optical parameters observed for those with liquid crystal and DNA-CTMA (Derkowska et al., 2007). This process has been found to result in the formation of nanostructures (Zawadzka et al., 2015), with their polarizing effect indicating the potential applicability in nonlinear optics (Zawadzka et al., 2018). It has also been proposed that copper phthalocyanine nanocrystals exhibiting the surface plasmon resonance-like behavior may be applicable in nonlinear optical devices (Zongo et al., 2015).

NP shape was found to affect NLO properties and, hence, the NLO responses of Pcs. Papagiannouli et al. probed the NLO properties of bimetallic NPs, observing SA and RSA behavior at different input intensities, e.g., Au- and Ag-rich bimetallic nano-alloys switched to RSA at  $\sim 83$  and  $220 \text{ MW cm}^{-2}$ , respectively (Papagiannouli et al., 2015). The above authors also found that the OL performance of Au-rich alloy NPs was red shifted compared to that of pure Au NPs, which led to enhanced third-order susceptibility of the former NPs (Papagiannouli et al., 2015). The OL properties of zinc diaminopyrimidin-2-ylthio Pc were enhanced in the presence of  $\text{Ag}_x\text{Au}_y$  alloy NPs (Bankole et al., 2016c). The larger enhancement recorded for Pc- $\text{Ag}_1\text{Au}_3$  than for Pc- $\text{Ag}_3\text{Au}_1$  was attributed to the higher Au content of the former conjugate, in line with the results of Papagiannouli et al. (Bankole et al., 2016c).

The conjugation of a low-symmetry Zn Pc to  $\text{Fe}_3\text{O}_4/\text{Ag}$  core-shell NPs enhanced NLO behavior more than the conjugation of this Pc to a  $\text{Fe}_3\text{O}_4$ -Ag hybrid, which was attributed to the tensile effect exerted by the  $\text{Fe}_3\text{O}_4$  core on the Ag shell due to the variations in the corresponding lattice parameters (Liu and Yang, 2014). Moreover, the coverage of the paramagnetic surface of  $\text{Fe}_3\text{O}_4$  with a diamagnetic Ag shell resulted in NLO property deterioration (Bankole and Nyokong, 2016a).

**OL parameters.** Beam waist ( $\omega_0$ ) was revealed to slightly change upon conjugation because of pulse fluctuation. Interband transitions and hot electron formation in metallic NPs were found to result in light scattering due to the proximity of the optical response to the SPR band (Elim et al., 2006; Philip et al., 2000). The slight increase in waist radius was attributed to the presence of aggregates in hybrids or to localized plasma creation due to the SPR of metallic NPs, which led to light scattering (Nwaji et al., 2018).

$\beta_{\text{eff}}$ , which describes nonlinearity strength, significantly increased upon conjugation (Bankole and Nyokong, 2017b; Oluwole et al., 2017a, 2017b). As  $\text{Im}[\chi^{(3)}]$  and  $\gamma$  are directly related to  $\beta_{\text{eff}}$  (Eqs. (15) and (16)), nanoconjugates with higher  $\beta_{\text{eff}}$  displayed higher  $\text{Im}[\chi^{(3)}]$  and  $\gamma$  values (Bankole and Nyokong, 2017b; Oluwole et al., 2017a, 2017b).

The limiting threshold ( $I_{\text{lim}}$ ) is defined as “the input fluence at which the transmittance is 50% of the linear transmittance”

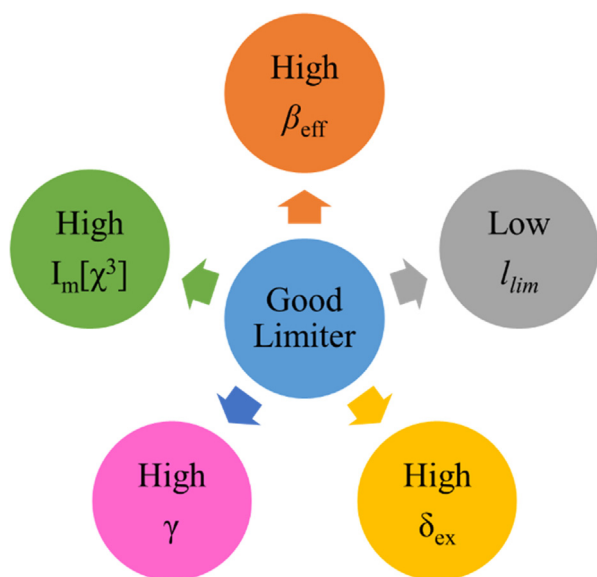


**Fig. 21** General OL parameters of a good limiter in nonlinear applications.

(Nwaji et al., 2018) and can be determined from the plot of transmittance against input fluence. Low values of  $I_{lim}$  represent good nonlinear optical absorbers well suited for sensor protection. Notably, nanoconjugates of Au NPs and Ag NPs featured lower  $I_{lim}$  than the corresponding free Pcs (Bankole and Nyokong, 2017b; Nwaji and Nyokong, 2017c; Nwaji et al., 2017d). Inorganic and organic complexes also exhibit the optical limiting process at the focal plane of the lens (Iliopoulos et al., 2010; Konstantinos Iliopoulos et al., 2012; Kulyk et al., 2016a, 2016b). The general OL parameters required for a good limiter are summarized in Fig. 21.

#### 4. Conclusion and future perspectives

Attempts to enhance the photophysical properties of Pc complexes have largely focused on conjugation to Ag and Au NPs of different shapes and sizes, as exemplified by Au NSs, NRs, BPs, and NSTs, and Ag NSs, NWS, NTs, and NFs. Conjugation of Pcs to variable-composition Ag-Au alloys has also been employed. Two main conjugation methods have been used, namely self-assembly through direct coordination of S and/or N to the metal surface and amide bond formation between Pcs and functionalized NP capping agents such as cysteamine, GSH, 3-azido-1-propylamine, and MPA. Other routes of conjugation include the click reaction between alkyne-functionalized Pcs and azide-functionalized Au NPs, donor-acceptor interactions, radical chain reactions, axial ligand exchange, and electrostatic attraction. Characterization of NPs and their conjugates by UV-Vis spectroscopy showed both red and blue shifts of NP SPR bands upon conjugation, depending on the NP shape and conjugation conditions. The Pc Q-band also showed variable behavior upon conjugation, i.e., blue, red, or no shift. Moreover, this band was reported to disappear when Pcs were saturated with NPs. NP size and the NP to Pc ratio were evaluated by PXRD, while XPS was used to compare the elemental compositions of NPs and their conjugates as well as to probe

links based on amide bond formation and/or self-assembly. The morphology and size distribution of bare NPs and their conjugates were studied by TEM, and the slight change in NP size after conjugation was attributed to factors such as aggregation and the presence of a shell around NPs. AFM revealed that some nanoconjugates deposited on thin films feature an island-type texture, additionally showing the different surface topographies of conjugated NPs and demonstrating that conjugation increases NP size. Finally, FT-IR spectroscopy was used to confirm amide bond formation between the amine and carboxylic groups of functionalized Pcs and capped NPs as well as to confirm self-assembly-based linking based on the disappearance of the S-H vibration.

A higher extent of fluorescence quantum yield quenching was recorded for covalently linked nanoconjugates than for self-assembled ones, which was ascribed to the higher aggregation of the former conjugates due to their higher loading of Pc molecules. Au NP shape was shown to affect the degree of fluorescence quenching, with Pc-Au NS conjugates featuring more pronounced quenching than conjugates of Au NTs, Au NRs, and Au BPs. Au NRs were shown to enhance hybrid fluorescence in pH 9 buffer and hence, metal-enhanced fluorescence was investigated. Fluorescence quantum yields were also affected by the nature of the functionalized capping agents. A general lowering of conjugate fluorescence lifetime was observed, and a bi-exponential decay curve was detected for some conjugates of nonspherical NPs. Increases in triplet quantum yields and decreases in triplet lifetimes were detected for Pcs conjugated to Ag NPs rather than for those conjugated to Au NPs. Singlet oxygen quantum yields showed a larger enhancement when Pcs were conjugated to higher-aspect-ratio NPs, and the extent of this enhancement was in the order of Au NRs ~ Au BPs > Au NSs > Au NTs. The triplet quantum yields of nanoconjugates were in the order of Ag NSs > Ag NFs > Ag NTs. Alloy- and other metal-based NPs were also described. Asymmetric Pcs were found to enhance intersystem crossing to the triplet state and thus quench fluorescence. Pcs are known to be good optical limiters, effectively absorbing high-intensity laser light. This behavior was improved in the presence of Au NPs more than in the presence of Ag NPs, as the SPR absorption of Au NPs was in complete resonance with the wavelength used in Z-scan measurements, unlike in the case of Ag NPs. Moreover, conjugation of RSA-type Pcs to SA-type (at low laser intensity) Au NPs can produce promising optical limiting properties for diverse applications. Finally, the effects of NP shape and conjugation approach on NLO responses were discussed.

The future perspectives can be summarized as follows:

- (1) With aggregation affecting optical parameters of some nanoconjugates due to  $\pi$ - $\pi$  stacking of Pcs, we opine that conjugation of Pc molecules with high-surface-area nanomaterials such as metal-organic frameworks, covalent organic frameworks, graphene layers, and carbon nanotubes may enhance the photochemicochemical and nonlinear optical properties.
- (2) Self-assembly is known to be highly effective in terms of therapeutic applications. When such nanostructures are conjugated to Ag NPs and Au NPs, it is expected that the new nanohybrids may exhibit enhanced photochemical properties for PDT and PTT applications.

- (3) This review is expected to facilitate the fabrication of novel (alternative) sensors for several areas of analytical chemistry, e.g., fluorescence spectroscopy, electrochemistry, Raman spectroscopy, and inductively coupled plasma mass spectrometry (ICP-MS). However, precautions concerning conjugation routes need to be considered. The fabrication of stable sensors capable of resisting strong acids and bases used for analyte adsorption-desorption remains a challenge, which, hopefully, can be overcome through the use of covalently linked hybrids.
- (4) The incorporation of functionalized Pcs into sol-gel composites is expected to produce a new generation of stable sorbents that can be used for coating fibers and capillaries to extract analytes by different methods of solid-phase microextraction hyphenated with chromatographic techniques such as high-performance liquid chromatography and gas chromatography.

### Declaration of Competing Interest

The authors declare that they have no known competing financial interests or personal relationships that could have appeared to influence the work reported in this paper.

### Acknowledgments

This study was supported by the National Unit for Environmental Research and Services (NUERS) at Kuwait University (SRUL 01/13) as well as by the University of South Africa. S. A.M. would like to express her deep gratitude to Dr. Abdullah Alhendal at Chemistry Department - Kuwait University for his help and support.

### References

- Achadu, O.J., Nyokong, T., 2017. Application of graphene quantum dots functionalized with thymine and thymine-appended zinc phthalocyanine as novel photoluminescent nanoprobes. *New J. Chem.* 41 (4), 1447–1458. <https://doi.org/10.1039/C6NJ03285K>.
- Albani, J.R., 2008. *Principles and Applications of Fluorescence Spectroscopy*. Wiley, Germany.
- Ali, I., Asim, M., Khan, T.A., 2012. Low cost adsorbents for the removal of organic pollutants from wastewater. *J. Environ. Manage.* 113 (Supplement C), 170–183. <https://doi.org/10.1016/j.jenvman.2012.08.028>.
- Allen, C.M., Sharman, W.M., Van Lier, J.E., 2001. Current status of phthalocyanines in the photodynamic therapy of cancer. *J. Porphyrins Phthalocyanines* 05 (02), 161.
- Alpugan, S., Topkaya, D., Verma, S., Atilla, D., Ahsen, V., Niazi, J. H., Dumoulin, F., 2019. Corrigendum to “Zn phthalocyanine conjugation to H2-ul aptamer for HER2-targeted breast cancer photodynamic therapy: Design, optimization and properties”. *J. Porphyrins Phthalocyanines* 23, 303. <https://doi.org/10.1142/S1088424619920019>.
- Alqadi, M.K., Abo Noqtah, O.A., Alzoubi, F.Y., Alzoubi, J., Aljarrah, K., 2014. pH effect on the aggregation of silver nanoparticles synthesized by chemical reduction. *Mater. Sci.-Poland* 32 (1), 107–111. <https://doi.org/10.2478/s13536-013-0166-9>.
- Alvarez, M.M., Khoury, J.T., Schaaff, T.G., Shafiqullin, M.N., Vezmar, I., Whetten, R.L., 1997. Optical absorption spectra of nanocrystal gold molecules. *J. Phys. Chem. B* 101 (19), 3706–3712. <https://doi.org/10.1021/jp962922n>.
- Anija, M., Thomas, J., Singh, N., Sreekumaran Nair, A., Tom, R.T., Pradeep, T., Philip, R., 2003. Nonlinear light transmission through oxide-protected Au and Ag nanoparticles: an investigation in the nanosecond domain. *Chem. Phys. Lett.* 380 (1), 223–229. <https://doi.org/10.1016/j.cplett.2003.09.023>.
- Ashjari, M., Dehfuly, S., Fatehi, D., Shabani, R., Koruji, M., 2015. Efficient functionalization of gold nanoparticles using cysteine conjugated protoporphyrin IX for singlet oxygen production in vitro. *RSC Adv.* 5 (127), 104621–104628. <https://doi.org/10.1039/C5RA15862A>.
- Ashokkumar, R., Kathiravan, A., Ramamurthy, P., 2014. Zn-phthalocyanine-functionalized nanometal and nanometal-TiO<sub>2</sub> hybrids: aggregation behavior and excited-state dynamics. *PCCP* 16 (27), 14139–14149. <https://doi.org/10.1039/C4CP00695J>.
- Auger, A., Blau, W.J., Burnham, P.M., Chambrier, I., Cook, M.J., Isare, B., et al., 2003. Nonlinear absorption properties of some 1,4,8,11,15,18,22,25-octaalkylphthalocyanines and their metallated derivatives. *J. Mater. Chem.* 13 (5), 1042–1047. <https://doi.org/10.1039/B300199G>.
- Bae, Y.J., Lee, N.J., Kim, T.H., Cho, H., Lee, C., Fleet, L., Hirohata, A., 2012. Growth and characterization of thin Cu-phthalocyanine films on MgO(001) layer for organic light-emitting diodes. *Nanoscale Res. Lett.* 7 (1), 650.
- Baldovi, H.G., Blas-Ferrando, V.M., Ortiz, J., Garcia, H., Fernandez-Lazaro, F., Sastre-Santos, A., 2016. Phthalocyanine-gold nanoparticle hybrids: modulating quenching with a silica matrix shell. *ChemPhysChem* 17 (11), 1579–1585. <https://doi.org/10.1002/cphc.201600136>.
- Banica, R., Ursu, D., Nyari, T., Kellenberger, A., 2017. Two step polyol-solvothermal growth of thick silver nanowires. *Mater. Lett.* 194, 181–184. <https://doi.org/10.1016/j.matlet.2017.02.045>.
- Bankole, O.M., Achadu, O.J., Nyokong, T., 2017a. Nonlinear Interactions of zinc phthalocyanine-graphene quantum dots nanocomposites: investigation of effects of surface functionalization with heteroatoms. *J. Fluorescence* 27 (2), 755–766. <https://doi.org/10.1007/s10895-016-2008-8>.
- Bankole, O.M., Nyokong, T., 2016a. Comparative studies on photophysical and optical limiting characterizations of low symmetry phthalocyanine linked to Fe<sub>3</sub>O<sub>4</sub>-Ag core-shell or hybrid nanoparticles. *New J. Chem.* 40 (12), 10016–10027. <https://doi.org/10.1039/C6NJ01511E>.
- Bankole, O.M., Nyokong, T., 2016b. Nonlinear optical response of a low symmetry phthalocyanine in the presence of gold nanoparticles when in solution or embedded in poly acrylic acid polymer thin films. *J. Photochem. Photobiol., A* 319–320, 8–17. <https://doi.org/10.1016/j.jphotochem.2015.12.014>.
- Bankole, O.M., Nyokong, T., 2017b. Azide-derivatized gold nanosphere “clicked” to indium and zinc phthalocyanines for improved nonlinear optical limiting. *J. Mol. Struct.* 1136, 309–320. <https://doi.org/10.1016/j.molstruc.2017.01.088>.
- Bankole, O.M., Osifeko, O., Nyokong, T., 2016c. Enhanced nonlinear optical responses of zinc diamminopyrimidin-2-ylthio phthalocyanine conjugated to Ag<sub>x</sub>Au alloy nanoparticles. *J. Photochem. Photobiol., A* 329, 155–166. <https://doi.org/10.1016/j.jphotochem.2016.06.025>.
- Bastys, V., Pastoriza-Santos, I., Rodríguez-González, B., Vaisnoras, R., Liz-Marzán, L.M., 2006. Formation of silver nanoprisms with surface plasmons at communication wavelengths. *Adv. Funct. Mater.* 16 (6), 766–773. <https://doi.org/10.1002/adfm.200500667>.
- Berberan-Santos, M.R.N., 2013. *Molecular fluorescence: principles and applications*. Wiley-VCH Verlag GmbH & Co. KGaA, Germany.
- Bilgin, A., Ertem, B., Gök, Y., 2007. Highly Organosoluble Metal-Free Phthalocyanines and Metallophthalocyanines: Synthesis and Characterization. *Eur. J. Inorg. Chem.* 2007 (12), 1703–1712. <https://doi.org/10.1002/ejic.200600943>.
- Bottari, G., Kahnt, A., Guldi, D.M., Torres, T., 2013. Protonation-induced changes in the photophysical properties of a phthalocya-



- nine and a covalently-linked, phthalocyanine-C60 fullerene dyad. *ECS J. Solid State Sci. Technol.* 2 (10), M3145.
- Brahadeeswaran, S., Onduka, S., Takagi, M., Takahashi, Y., Adachi, H., Yoshimura, M., et al, 2006. Growth of high-quality DAST crystals for THz applications. *J. Cryst. Growth* 292 (2), 441–444. <https://doi.org/10.1016/j.jcrysgro.2006.04.052>.
- Brannon, J.H., Magde, D., 1980. Picosecond laser photophysics. Group 3A phthalocyanines. *J. Am. Chem. Soc.* 102 (1), 62–65. <https://doi.org/10.1021/ja00521a011>.
- Brust, M., Walker, M., Bethell, D., Schiffrin, D.J., Whyman, R., 1994. Synthesis of thiol-derivatised gold nanoparticles in a two-phase Liquid-Liquid system. *J. Chem. Soc., Chem. Commun.* 7, 801–802. <https://doi.org/10.1039/C39940000801>.
- Calvete, M., Yang, G.Y., Hanack, M., 2004. Porphyrins and phthalocyanines as materials for optical limiting. *Synth. Met.* 141 (3), 231–243. [https://doi.org/10.1016/S0379-6779\(03\)00407-7](https://doi.org/10.1016/S0379-6779(03)00407-7).
- Camerin, M., Magaraggia, M., Soncin, M., Jori, G., Moreno, M., Chambrier, I., et al, 2010. The in vivo efficacy of phthalocyanine-nanoparticle conjugates for the photodynamic therapy of amelanotic melanoma. *Eur. J. Cancer* 46 (10), 1910–1918. <https://doi.org/10.1016/j.ejca.2010.02.037>.
- Carvalho, P.M., Felício, M.R., Santos, N.C., Gonçalves, S., Domingues, M.M., 2018. Application of light scattering techniques to nanoparticle characterization and development. *Front. Chem.* 6 (237). <https://doi.org/10.3389/fchem.2018.00237>.
- Castner, D.G., Hinds, K., Grainger, D.W., 1996. X-ray photoelectron spectroscopy sulfur 2p study of organic thiol and disulfide binding interactions with gold surfaces. *Langmuir* 12 (21), 5083–5086. <https://doi.org/10.1021/la960465w>.
- Castro-Latorre, P., Miranda-Rojas, S., Mendizabal, F., 2020. Theoretical exploration of the forces governing the interaction between gold-phthalocyanine and gold surface clusters. *RSC Adv.* 10 (7), 3895–3901. <https://doi.org/10.1039/C9RA07959A>.
- Cepak, V.M., Martin, C.R., 1998. Preparation and stability of template-synthesized metal nanorod sols in organic solvents. *J. Phys. Chem. B* 102 (49), 9985–9990. <https://doi.org/10.1021/jp982882i>.
- Chadwick, S.J., Salah, D., Livesey, P.M., Brust, M., Volk, M., 2016. Singlet oxygen generation by laser irradiation of gold nanoparticles. *J. Phys. Chem. C* 120 (19), 10647–10657. <https://doi.org/10.1021/acs.jpcc.6b02005>.
- Chandran, S.P., Pasricha, R., Bhatta, U.M., Satyam, P.V., Sastry, M., 2007. Synthesis of gold nanorods in organic media. *J. Nanosci. Nanotechnol.* 7 (8), 2808–2817. <https://doi.org/10.1166/jnn.2007.636>.
- Chemla, D.S., Zyss, J., 1987. In: *Nonlinear optical properties of organic molecules and crystals, Vol. 1 and 2. Academic Press, Orlando.*
- Chen, H.M., Liu, R.-S., Tsai, D.P., 2009. A Versatile Route to the Controlled Synthesis of Gold Nanostructures. *Cryst. Growth Des.* 9 (5), 2079–2087. <https://doi.org/10.1021/cg800396t>.
- Chen, H.M., Liu, R.S., Jang, L.Y., Lee, J.F., Hu, S.F., 2006. Characterization of core-shell type and alloy Ag/Au bimetallic clusters by using extended X-ray absorption fine structure spectroscopy. *Chem. Phys. Lett.* 421 (1), 118–123. <https://doi.org/10.1016/j.cplett.2006.01.043>.
- Chen, J., Glaus, C., Laforest, R., Zhang, Q., Yang, M., Gidding, M., et al, 2010. Gold nanocages as photothermal transducers for cancer treatment. *Small* 6 (7), 811–817. <https://doi.org/10.1002/smll.200902216>.
- Chen, L., Ji, F., Xu, Y., He, L., Mi, Y., Bao, F., et al, 2014. High-yield seedless synthesis of triangular gold nanoplates through oxidative etching. *Nano Lett.* 14 (12), 7201–7206. <https://doi.org/10.1021/nl504126u>.
- Chen, X., Ye, Q., Ma, D., Chen, J., Wang, Y., Yang, H., et al, 2018. Gold nanoparticles-pyrrolidinonyl metal phthalocyanine nanoconjugates: Synthesis and photophysical properties. *J. Lumin.* 195, 348–355. <https://doi.org/10.1016/j.jlumin.2017.11.047>.
- Chen, Y., Hanack, M., Araki, Y., Ito, O., 2005. Axially modified gallium phthalocyanines and naphthalocyanines for optical limiting. *Chem. Soc. Rev.* 34 (6), 517–529. <https://doi.org/10.1039/B416368K>.
- Cheng, H.-B., Li, X., Kwon, N., Fang, Y., Baek, G., Yoon, J., 2019. Photoswitchable phthalocyanine-assembled nanoparticles for controlled “double-lock” photodynamic therapy. *Chem. Commun.* 55 (82), 12316–12319. <https://doi.org/10.1039/C9CC03960K>.
- Choo, D.C., Kim, T.W., 2017. Degradation mechanisms of silver nanowire electrodes under ultraviolet irradiation and heat treatment. *Sci. Rep.* 7 (1), 1696. <https://doi.org/10.1038/s41598-017-01843-9>.
- Coulter, D.R., Miskowski, V.M., Perry, J.W., Wei, T.-H., Stryland, E.W.V., Hagan, D.J., 1989. Optical limiting in solutions of metallo-phthalocyanines and naphthalocyanines. Paper Presented at the SPIE 1989 Technical Symposium on Aerospace Sensing.
- Crova, A. (1879). JOHN KERR. — Electro-optic observations on various liquids (Observations électro-optiques sur divers liquides); *Phil. Magazine*, 5e série, t. VIII, p. 85-102; août 1879. *J. Phys. Theor. Appl.*, 8(1), 414-418. doi:10.1051/jphys:018790080041401
- D'Souza, S., Moeno, S., Antunes, E., Nyokong, T., 2013. Effects of gold nanoparticle shape on the aggregation and fluorescence behaviour of water soluble zinc phthalocyanines. *New J. Chem.* 37 (7), 1950–1958. <https://doi.org/10.1039/C3NJ00146F>.
- D'Souza, S., George, R., Göksel, M., Atilla, D., Durmuş, M., Nyokong, T., 2015a. Enhanced triplet state yields in aqueous media of asymmetric zinc phthalocyanines when conjugated to silver nanoflowers. *Polyhedron* 100, 296–302. <https://doi.org/10.1016/j.poly.2015.08.017>.
- D'Souza, S., Mashazi, P., Britton, J., Nyokong, T., 2015b. Effects of differently shaped silver nanoparticles on the photophysics of pyridylsulfanyl-substituted phthalocyanines. *Polyhedron* 99, 112–121. <https://doi.org/10.1016/j.poly.2015.06.038>.
- Das, S.K., Dickinson, C., Lafir, F., Brougham, D.F., Marsili, E., 2012. Synthesis, characterization and catalytic activity of gold nanoparticles biosynthesized with *Rhizopus oryzae* protein extract. *Green Chem.* 14 (5), 1322–1334. <https://doi.org/10.1039/C2GC16676C>.
- De Boni, L., Wood, E.L., Toro, C., Hernandez, F.E., 2008. Optical Saturable Absorption in Gold Nanoparticles. *Plasmonics* 3 (4), 171–176. <https://doi.org/10.1007/s11468-008-9071-1>.
- de Mello, J.C., Wittmann, H.F., Friend, R.H., 1997. An improved experimental determination of external photoluminescence quantum efficiency. *Adv. Mater.* 9 (3), 230–232. <https://doi.org/10.1002/adma.1997009308>.
- Dement'eva, O., M. Vinogradova, M., Lukyanets, E., I. Solov'eva, L., Ogarev, V. A., & M. Rudoy, V. (2014). Zinc Phthalocyanine-Based Water-Soluble Thiolated Photosensitizer and Its Conjugates with Gold Nanoparticles: Synthesis and Spectral Properties (Vol. 76).
- Derkowska, B., Wojdyła, M., Bała, W., Jaworowicz, K., Karpierz, M., Grote, J.G., et al, 2007. Influence of different peripheral substituents on the nonlinear optical properties of cobalt phthalocyanine core. *J. Appl. Phys.* 101, (8). <https://doi.org/10.1063/1.2719281> 083112.
- Donaldson, W.R., Tang, C.L., 1984. Urea optical parametric oscillator. *Appl. Phys. Lett.* 44 (1), 25–27. <https://doi.org/10.1063/1.94590>.
- Du, L., Qin, H., Ma, T., Zhang, T., Xing, D., 2017. In Vivo Imaging-Guided Photothermal/Photoacoustic Synergistic Therapy with Bioorthogonal Metabolic Glycoengineering-Activated Tumor Targeting Nanoparticles. *ACS Nano* 11 (9), 8930–8943. <https://doi.org/10.1021/acsnano.7b03226>.
- Dube, E., Nwaji, N., Mack, J., Nyokong, T., 2018a. The photochemical behavior of symmetric and asymmetric zinc phthalocyanines, surface assembled onto gold nanotriangles. *New J. Chem.* 42 (17), 14290–14299. <https://doi.org/10.1039/C8NJ02746C>.

- Dube, E., Nyokong, T., 2019a. Effect of gold nanoparticle shape on the photophysical properties of sulphur containing metallophthalocyanines. *J. Mol. Struct.* 1181, 312–320. <https://doi.org/10.1016/j.molstruc.2018.12.091>.
- Dube, E., Nyokong, T., 2019b. Effect of gold nanoparticles shape and size on the photophysical behaviour of symmetric and asymmetric zinc phthalocyanines. *J. Lumin.* 205, 532–539. <https://doi.org/10.1016/j.jlumin.2018.09.063>.
- Dube, E., Oluwole, D.O., Njemuwa, N., Prinsloo, E., Nyokong, T., 2019c. Photophysical and photodynamic therapy properties of metallophthalocyanines linked to gold speckled silica nanoparticles. *Photodiagn. Photodyn. Ther.* 25, 325–333. <https://doi.org/10.1016/j.pdpdt.2019.01.019>.
- Dube, E., Oluwole, D.O., Nwaji, N., Nyokong, T., 2018b. Glycosylated zinc phthalocyanine-gold nanoparticle conjugates for photodynamic therapy: Effect of nanoparticle shape. *Spectrochim. Acta Part A Mol. Biomol. Spectrosc.* 203, 85–95. <https://doi.org/10.1016/j.saa.2018.05.081>.
- Dube, E., Oluwole, D.O., Nyokong, T., 2017. Photophysical behaviour of anionic indium phthalocyanine when grafted onto AgxAu and porous silica nanoparticles. *J. Lumin.* 190, 353–363. <https://doi.org/10.1016/j.jlumin.2017.05.071>.
- Dube, E., Oluwole, D.O., Nyokong, T., 2018c. Improved photophysical and photochemical properties of thiopheneethoxy substituted metallophthalocyanines on immobilization onto gold-speckled silica nanoparticles. *Photochem. Photobiol.* 94 (3), 521–531. <https://doi.org/10.1111/php.12879>.
- Dubinina, T.V., Trashin, S.A., Borisova, N.E., Boginskaya, I.A., Tomilova, L.G., Zefirov, N.S., 2012. Phenyl-substituted planar binuclear phthalocyanine and naphthalocyanines: synthesis and investigation of physicochemical properties. *Dyes Pigm.* 93 (1), 1471–1480. <https://doi.org/10.1016/j.dyepig.2011.10.012>.
- Dubinina, T.V., Tychinsky, P.I., Borisova, N.E., Krasovskii, V.I., Ivanov, A.S., Savilov, S.V., et al, 2018. Lanthanide (III) complexes of 3-(ethylthio)phenyl-substituted phthalocyanines: Synthesis and physicochemical properties. *Dyes Pigm.* 156, 386–394. <https://doi.org/10.1016/j.dyepig.2018.04.028>.
- Elim, H.I., Yang, J., Lee, J.-Y., Mi, J., Ji, W., 2006. Observation of saturable and reverse-saturable absorption at longitudinal surface plasmon resonance in gold nanorods. *Appl. Phys. Lett.* 88, (8). <https://doi.org/10.1063/1.2177366> 083107.
- Esumi, K., Matsuhisa, K., Torigoe, K., 1995. Preparation of rodlike gold particles by UV irradiation using cationic micelles as a template. *Langmuir* 11 (9), 3285–3287. <https://doi.org/10.1021/la00009a002>.
- Faraday, M., 1857. The bakerian lecture: experimental relations of gold (and other metals) to light. *Philos. Trans. Roy. Soc. London Ser. I* 147, 145–181.
- Fashina, A., Antunes, E., Nyokong, T., 2013. Characterization and photophysical behavior of phthalocyanines when grafted onto silica nanoparticles. *Polyhedron* 53, 278–285. <https://doi.org/10.1016/j.poly.2013.01.037>.
- Fernández, L., Esteves, V.I., Cunha, Â., Schneider, R.J., Tomé, J.P. C., 2016. Photodegradation of organic pollutants in water by immobilized porphyrins and phthalocyanines. *J. Porphyrins Phthalocyanines* 20 (01n04), 150–166. <https://doi.org/10.1142/s108842461630007x>.
- Fery-Forgues, S., Lavabre, D., 1999. Are fluorescence quantum yields so tricky to measure? A demonstration using familiar stationary products. *J. Chem. Educ.* 76 (9), 1260. <https://doi.org/10.1021/ed076p1260>.
- Fitzgerald, J.P., Huffman, P.D., Brenner, I.A., Wathen, J.J., Beadie, G., Pong, R.G.S., et al, 2015. Synthesis, chemical characterization and nonlinear optical properties of thallium(III) phthalocyanine halide complexes. *Optical Mater. Express* 5 (7), 1560–1578. <https://doi.org/10.1364/OME.5.001560>.
- Fleger, Y., Rosenbluh, M., 2009. Surface plasmons and surface enhanced raman spectra of aggregated and alloyed gold-silver nanoparticles. *Res. Lett. Optics* 2009, 5. <https://doi.org/10.1155/2009/475941>.
- Fomo, G., Achadu, O.J., Nyokong, T., 2018. One-pot synthesis of graphene quantum dots-phthalocyanines supramolecular hybrid and the investigation of their photophysical properties. *J. Mater. Sci.* 53 (1), 538–548. <https://doi.org/10.1007/s10853-017-1539-y>.
- Forteach, S., Antunes, E., Chidawanyika, W., Nyokong, T., 2012. Unquenched fluorescence lifetime for  $\beta$ -phenylthio substituted zinc phthalocyanine upon conjugation to gold nanoparticles. *Polyhedron* 34 (1), 114–120. <https://doi.org/10.1016/j.poly.2011.12.015>.
- Frens, G., 1973. Controlled nucleation for the regulation of the particle size in monodisperse gold suspensions. *Nat. Phys. Sci.* 241 (105), 20–22. <https://doi.org/10.1038/physci241020a0>.
- Fullam, S., Cottell, D., Rensmo, H., Fitzmaurice, D., 2000. Carbon nanotube templated self-assembly and thermal processing of gold nanowires. *Adv. Mater.* 12 (19), 1430–1432. [https://doi.org/10.1002/1521-4095\(200010\)12:19 <1430::aid-adma1430 >3.0.co;2-8](https://doi.org/10.1002/1521-4095(200010)12:19 <1430::aid-adma1430 >3.0.co;2-8).
- Gao, Y., Wang, Y., Song, Y., Li, Y., Qu, S., Liu, H., et al, 2003. Strong optical limiting property of a novel silver nanoparticle containing C60 derivative. *Opt. Commun.* 223 (1), 103–108. [https://doi.org/10.1016/S0030-4018\(03\)01640-7](https://doi.org/10.1016/S0030-4018(03)01640-7).
- García Calavia, P., Marin, M.J., Chambrier, I., Cook, M.J., Russell, D.A., 2018. Towards optimisation of surface enhanced photodynamic therapy of breast cancer cells using gold nanoparticle-photosensitizer conjugates. *Photochem. Photobiol. Sci.* 17 (3), 281–289. <https://doi.org/10.1039/C7PP00225D>.
- Geddes, C.D., Lakowicz, J.R., 2002. Editorial: metal-enhanced fluorescence. *J. Fluorescence* 12 (2), 121–129. <https://doi.org/10.1023/A:1016875709579>.
- Ghadari, R., Sabri, A., Saei, P.-S., Kong, F.-T., Marques, H.M., 2020. Phthalocyanine-silver nanoparticle structures for plasmon-enhanced dye-sensitized solar cells. *Sol. Energy* 198, 283–294. <https://doi.org/10.1016/j.solener.2020.01.053>.
- Govindaraj, A., Satishkumar, B.C., Nath, M., Rao, C.N.R., 2000. Metal nanowires and intercalated metal layers in single-walled carbon nanotube bundles. *Chem. Mater.* 12 (1), 202–205. <https://doi.org/10.1021/cm990546o>.
- Gurudas, U., Brooks, E., Bubb, D.M., Heiroth, S., Lippert, T., Wokaun, A., 2008. Saturable and reverse saturable absorption in silver nanodots at 532 nm using picosecond laser pulses. *J. Appl. Phys.* 104, (7). <https://doi.org/10.1063/1.2990056> 073107.
- Han, Y.P., Luo, M.H., Wang, Q.W., Wang, J.X., Gao, X.L., 2011. Synthesis of silver nanowires and investigation of their optical limiting properties. *Adv. Mater. Res.* 295–297, 152–155. <https://doi.org/10.4028/www.scientific.net/AMR.295-297.152>.
- Harter, D.J., Shand, M.L., Band, Y.B., 1984. Power/energy limiter using reverse saturable absorption. *J. Appl. Phys.* 56 (3), 865–868. <https://doi.org/10.1063/1.334025>.
- He, Y., Wang, M., Fu, M., Yuan, X., Luo, Y., Qiao, B., et al, 2020. Iron(II) phthalocyanine loaded and AS1411 aptamer targeting nanoparticles: a nanocomplex for dual modal imaging and photothermal therapy of breast cancer. *Int. J. Nanomed.* 15, 5927–5949. <https://doi.org/10.2147/IJN.S254108>.
- Hone, D., Walker, P., Evans-Gowing, R., Fitzgerald, S., Beeby, A., Chambrier, I., et al, 2002. Generation of cytotoxic singlet oxygen via phthalocyanine-stabilized gold nanoparticles: a potential delivery vehicle for photodynamic therapy. *Langmuir* 18, 2985–2987. <https://doi.org/10.1021/la025623o>.
- Hong, S.-M., Son, H., Park, J.S., 2018. Preparation and electrochemical properties of cobalt-phthalocyanine-decorated Fe<sub>3</sub>O<sub>4</sub> nanoparticles. *J. Porphyrins Phthalocyanines* 22 (07), 611–618. <https://doi.org/10.1142/s1088424618500827>.
- Huang, X., El-Sayed, I.H., Qian, W., El-Sayed, M.A., 2007. Cancer cells assemble and align gold nanorods conjugated to antibodies to produce highly enhanced, sharp, and polarized surface raman spectra: a potential cancer diagnostic marker. *Nano Lett.* 7 (6), 1591–1597. <https://doi.org/10.1021/nl070472c>.

- Idowu, M., Chen, J.Y., Nyokong, T., 2008. Photoinduced energy transfer between water-soluble CdTe quantum dots and aluminium tetrasulfonated phthalocyanine. *New J. Chem.* 32 (2), 290–296. <https://doi.org/10.1039/B707808K>.
- Iliopoulos, K., Czaplicki, R., Ouazzani, H.E., Balandier, J.Y., Chas, M., Goeb, S., et al, 2010. Physical origin of the third order nonlinear optical response of orthogonal pyrrolo-tetrathiafulvalene derivatives. *Appl. Phys. Lett.* 97, (10). <https://doi.org/10.1063/1.3482943> 101104.
- Iliopoulos, K., El-Ghayoury, A., El Ouazzani, H., Pranaitis, M., Belhadj, E., Ripaud, E., et al, 2012. Nonlinear absorption reversing between an electroactive ligand and its metal complexes. *Opt. Express* 20 (23), 25311–25316. <https://doi.org/10.1364/OE.20.025311>.
- Ince, M., Yum, J.H., Kim, Y., Mathew, S., Grätzel, M., Torres, T., Nazeeruddin, M.K., 2014. Molecular engineering of phthalocyanine sensitizers for dye-sensitized solar cells. *J. Phys. Chem. C* 118 (30), 17166–17170.
- J., S. M., T., N., CC., L., & AB., L. (1989). Phthalocyanines. Properties and application. Weinheim VCH Publishers.
- Jain, P.K., Lee, K.S., El-Sayed, I.H., El-Sayed, M.A., 2006. Calculated absorption and scattering properties of gold nanoparticles of different size, shape, and composition: applications in biological imaging and biomedicine. *J. Phys. Chem. B* 110 (14), 7238–7248. <https://doi.org/10.1021/jp057170o>.
- Jana, N., Gearheart, L., Murphy, C., 2001. Seed-mediated growth approach for shape-controlled synthesis of spheroidal and rod-like gold nanoparticles using a surfactant template. *Adv. Mater.* 13, 1389–1393. [https://doi.org/10.1002/1521-4095\(200109\)13:18<1389::AID-ADMA1389>3.0.CO;2-F](https://doi.org/10.1002/1521-4095(200109)13:18<1389::AID-ADMA1389>3.0.CO;2-F).
- Jana, N.R., Gearheart, L., Obare, S.O., Murphy, C.J., 2002. Anisotropic chemical reactivity of gold spheroids and nanorods. *Langmuir* 18 (3), 922–927. <https://doi.org/10.1021/la0114530>.
- Jia, K., Wang, P., Wei, S., Huang, Y., Liu, X., 2017. Scalable creation of gold nanostructures on high performance engineering polymeric substrate. *Appl. Surf. Sci.* 426, 579–586. <https://doi.org/10.1016/j.apsusc.2017.07.116>.
- Jin, R., Cao, Y., Mirkin, C.A., Kelly, K.L., Schatz, G.C., Zheng, J. G., 2001. Photoinduced conversion of silver nanospheres to nanoprisms. *Science* 294 (5548), 1901–1903. <https://doi.org/10.1126/science.1066541>.
- Jung, H.S., Verwilst, P., Sharma, A., Shin, J., Sessler, J.L., Kim, J.S., 2018. Organic molecule-based photothermal agents: an expanding photothermal therapy universe. *Chem. Soc. Rev.* 47 (7), 2280–2297. <https://doi.org/10.1039/C7CS00522A>.
- Kadish, K.M., Smith, K.M., Guillard, R., 2003. *The Porphyrin Handbook* Vol. 17, 22–31.
- Kang, K.A., Wang, J., Jasinski, J.B., Achilefu, S., 2011. Fluorescence manipulation by gold nanoparticles: from complete quenching to extensive enhancement. *J. Nanobiotechnol.* 9, 16. <https://doi.org/10.1186/1477-3155-9-16>.
- Kao, P.C., Chu, S.Y., Liu, S.J., You, Z.X., Chuang, C.A., 2006. Improved performance of organic light-emitting diodes using a metal-phthalocyanine hole-injection layer. *J. Electrochem. Soc.* 153 (6), H122.
- Ke, X., Wang, D., Chen, C., Yang, A., Han, Y., Ren, L., et al, 2014. Co-enhancement of fluorescence and singlet oxygen generation by silica-coated gold nanorods core-shell nanoparticle. *Nanoscale Res. Lett.* 9, 666–673. <https://doi.org/10.1186/1556-276X-9-666>.
- Kerr, J., 1875. XL. A new relation between electricity and light: Dielectric media birefringent. *London, Edinburgh, Dublin Philos. Mag. J. Sci.* 50 (332), 337–348. <https://doi.org/10.1080/14786447508641302>.
- Khoza, P., Ndhunduma, I., Karsten, A., Nyokong, T., 2020. Photodynamic therapy activity of phthalocyanine-silver nanoparticles on melanoma cancer cells. *J. Nanosci. Nanotechnol.* 20 (5), 3097–3104. <https://doi.org/10.1166/jnn.2020.17398>.
- Khoza, P., Nyokong, T., 2014. Photocatalytic behavior of phthalocyanine-silver nanoparticle conjugates supported on polystyrene fibers. *J. Mol. Catal. A: Chem.* 395, 34–41. <https://doi.org/10.1016/j.molcata.2014.07.031>.
- Kim, M., Lee, J.-H., Nam, J.-M., 2019. Plasmonic photothermal nanoparticles for biomedical applications. *Adv. Sci.* 6 (17), 1900471. <https://doi.org/10.1002/advs.201900471>.
- Kippelen, B., Marder, S.R., Hendrickx, E., Maldonado, J.L., Guillemet, G., Volodin, B.L., et al, 1998. Infrared photorefractive polymers and their applications for imaging. *Science* 279 (5347), 54–57. <https://doi.org/10.1126/science.279.5347.54>.
- Knight, M.W., Grady, N.K., Bardhan, R., Hao, F., Nordlander, P., Halas, N.J., 2007. Nanoparticle-mediated coupling of light into a nanowire. *Nano Lett.* 7 (8), 2346–2350. <https://doi.org/10.1021/nl071001t>.
- Kossanyi, J., Chahraoui, D., 2000. Electron transfer reaction and demetalation of phthalocyanines. *Int. J. Photoenergy* 2 (1), 9–15. <https://doi.org/10.1155/s1110662x00000027>.
- Kotiaho, A., Lahtinen, R., Efimov, A., Metsberg, H.-K., Sariola, E., Lehtivuori, H., et al, 2010. Photoinduced charge and energy transfer in phthalocyanine-functionalized gold nanoparticles. *J. Phys. Chem. C* 114 (1), 162–168. <https://doi.org/10.1021/jp9087173>.
- Kou, X., Ni, W., Tsung, C.K., Chan, K., Lin, H.Q., Stucky, G.D., Wang, J., 2007. Growth of gold bipyramids with improved yield and their curvature-directed oxidation. *Small* 3 (12), 2103–2113. <https://doi.org/10.1002/sml.200700379>.
- Kou, X., Zhang, S., Tsung, C.-K., Yeung, M.H., Shi, Q., Stucky, G. D., et al, 2006. Growth of Gold Nanorods and Bipyramids Using CTEAB Surfactant. *J. Phys. Chem. B* 110 (33), 16377–16383. <https://doi.org/10.1021/jp0639086>.
- Kulyk, B., Guichaoua, D., Ayadi, A., El-Ghayoury, A., Sahraoui, B., 2016a. Metal-induced efficient enhancement of nonlinear optical response in conjugated azo-based iminopyridine complexes. *Org. Electron.* 36, 1–6. <https://doi.org/10.1016/j.orgel.2016.05.028>.
- Kulyk, B., Kerasidou, A.P., Soumahoro, L., Moussallem, C., Gohier, F., Frère, P., Sahraoui, B., 2016b. Optimization and diagnostic of nonlinear optical features of  $\pi$ -conjugated benzodifuran-based derivatives. *RSC Adv.* 6 (18), 14439–14447. <https://doi.org/10.1039/C5RA25889H>.
- Kulyk, B., Krupka, O., Smokal, V., Figà, V., Czaplicki, R., Sahraoui, B., 2019. Nonlinear optical behavior of DNA-functionalized gold nanoparticles. *Appl. Nanosci.* 9 (5), 703–708. <https://doi.org/10.1007/s13204-018-0704-1>.
- Kuzmina, E.A., Dubinina, T.V., Zasedatelev, A.V., Baranikov, A.V., Makedonskaya, M.I., Egorova, T.B., Tomilova, L.G., 2017. Hexadecachloro-substituted lanthanide(III) phthalocyaninates and their hybrid conjugates with gold nanoparticles: Synthesis and optical properties. *Polyhedron* 135, 41–48. <https://doi.org/10.1016/j.poly.2017.06.048>.
- Kuznetsova, N., Gretsova, N. S., Kalmykova, E. A., Makarova, E., Dashkevich, S. N., Negrimovsky, V., et al., 2000. Relationship between the photochemical properties and structure of porphyrins and related compounds, vol. 70.
- Lacey, J.A., Phillips, D., 2002. Fluorescence lifetime measurements of disulfonated aluminium phthalocyanine in the presence of microbial cells. *Photochem. Photobiol. Sci.* 1 (6), 378–383. <https://doi.org/10.1039/B108831A>.
- Lakowicz, J.R., 2005. Radiative decay engineering 5: metal-enhanced fluorescence and plasmon emission. *Anal. Biochem.* 337 (2), 171–194. <https://doi.org/10.1016/j.ab.2004.11.026>.
- Lee, E., Li, X., Oh, J., Kwon, N., Kim, G., Kim, D., Yoon, J., 2020. A boronic acid-functionalized phthalocyanine with an aggregation-enhanced photodynamic effect for combating antibiotic-resistant bacteria. *Chem. Sci.* 11 (22), 5735–5739. <https://doi.org/10.1039/D0SC01351J>.
- Lee, K.-C., Lin, S.-J., Lin, C.-H., Tsai, C.-S., Lu, Y.-J., 2008. Size effect of Ag nanoparticles on surface plasmon resonance. *Surf.*

- Coat. Technol. – Surf. Coat. Tech. 202, 5339–5342. <https://doi.org/10.1016/j.surfcoat.2008.06.080>.
- Lee, Y.H., Yan, Y., Polavarapu, L., Xu, Q.-H., 2009. Nonlinear optical switching behavior of Au nanocubes and nano-octahedra investigated by femtosecond Z-scan measurements. *Appl. Phys. Lett.* 95, (2). <https://doi.org/10.1063/1.3177064> 023105.
- Li, B., Lin, L., Lin, H., Wilson, B.C., 2016. Photosensitized singlet oxygen generation and detection: Recent advances and future perspectives in cancer photodynamic therapy. *J. Biophotonics* 9 (11–12), 1314–1325. <https://doi.org/10.1002/jbio.201600055>.
- Li, X., Kim, C.Y., Lee, S., Lee, D., Chung, H.-M., Kim, G., et al, 2017. Nanostructured phthalocyanine assemblies with protein-driven switchable photoactivities for biophotonic imaging and therapy. *J. Am. Chem. Soc.* 139 (31), 10880–10886. <https://doi.org/10.1021/jacs.7b05916>.
- Li, X., Lee, D., Huang, J.-D., Yoon, J., 2018a. Phthalocyanine-assembled nanodots as photosensitizers for highly efficient type I photoreactions in photodynamic therapy. *Angew. Chem. Int. Ed.* 57 (31), 9885–9890. <https://doi.org/10.1002/anie.201806551>.
- Li, X., Peng, X.-H., Zheng, B.-D., Tang, J., Zhao, Y., Zheng, B.-Y., et al, 2018b. New application of phthalocyanine molecules: from photodynamic therapy to photothermal therapy by means of structural regulation rather than formation of aggregates. *Chem. Sci.* 9 (8), 2098–2104. <https://doi.org/10.1039/C7SC05115H>.
- Li, X., Yu, S., Lee, Y., Guo, T., Kwon, N., Lee, D., et al, 2019a. In vivo albumin traps photosensitizer monomers from self-assembled phthalocyanine nanovesicles: a facile and switchable theranostic approach. *J. Am. Chem. Soc.* 141 (3), 1366–1372. <https://doi.org/10.1021/jacs.8b12167>.
- Li, X., Zheng, B.-D., Peng, X.-H., Li, S.-Z., Ying, J.-W., Zhao, Y., et al, 2019b. Phthalocyanines as medicinal photosensitizers: Developments in the last five years. *Coord. Chem. Rev.* 379, 147–160. <https://doi.org/10.1016/j.ccr.2017.08.003>.
- Lim, C.-K., Shin, J., Lee, Y.-D., Kim, J., Oh, K.S., Yuk, S.H., et al, 2012. Phthalocyanine-aggregated polymeric nanoparticles as tumor-homing near-infrared absorbers for photothermal therapy of cancer. *Theranostics* 2 (9), 871–879. <https://doi.org/10.7150/thno.4133>.
- Lim, J.S., Kim, S.M., Lee, S.Y., Stach, E.A., Culver, J.N., Harris, M. T., 2010. Biotemplated aqueous-phase palladium crystallization in the absence of external reducing agents. *Nano Lett* 10 (10), 3863–3867. <https://doi.org/10.1021/nl101375f>.
- Liu, H., Yang, J., 2014. Bimetallic Ag–hollow Pt heterodimers via inside-out migration of Ag in core–shell Ag–Pt nanoparticles at elevated temperature. *J. Mater. Chem. A* 2 (19), 7075–7081. <https://doi.org/10.1039/C4TA00243A>.
- Liu, J.-H., Tsai, C.-Y., Chiu, Y.-H., Hsieh, F.-M., 2009. The fabrication of polycrystalline silver nanowires via self-assembled nanotubes at controlled temperature. *Nanotechnology* 20, <https://doi.org/10.1088/0957-4484/20/3/035301> 035301.
- Liu, M., Guyot-Sionnest, P., 2005. Mechanism of silver(I)-assisted growth of gold nanorods and bipyramids. *J Phys Chem B* 109 (47), 22192–22200. <https://doi.org/10.1021/jp054808n>.
- Liu, S., Chen, G., Prasad, P.N., Swihart, M.T., 2011. Synthesis of Monodisperse Au, Ag, and Au–Ag Alloy Nanoparticles with Tunable Size and Surface Plasmon Resonance Frequency. *Chem. Mater.* 23 (18), 4098–4101. <https://doi.org/10.1021/cm201343k>.
- Liu, X., Atwater, M., Wang, J., Huo, Q., 2007. Extinction coefficient of gold nanoparticles with different sizes and different capping ligands. *Colloids Surf. B Biointerfaces* 58 (1), 3–7. <https://doi.org/10.1016/j.colsurfb.2006.08.005>.
- Liu, Z.-J., Liang, Y.-L., Geng, F.-F., Lv, F., Dai, R.-J., Zhang, Y.-K., Deng, Y.-L., 2012. Preparation of poly(N-isopropylacrylamide) brush grafted silica particles via surface-initiated atom transfer radical polymerization used for aqueous chromatography. *Front. Mater. Sci.* 6 (1), 60–68. <https://doi.org/10.1007/s11706-012-0161-9>.
- Lobo, A.C.S., Silva, A.D., Tomé, V.A., Pinto, S.M.A., Silva, E.F.F., Calvete, M.J.F., et al, 2016. Phthalocyanine labels for near-infrared fluorescence imaging of solid tumors. *J. Med. Chem.* 59 (10), 4688.
- Lokesh, K. S., Narayanan, V., Sampath, S., 2009. Phthalocyanine macrocycle as stabilizer for gold and silver nanoparticles, Vol. 167.
- Losev, A.P., Byteva, I.M., Gurinovich, G.P., 1988. Singlet oxygen luminescence quantum yields in organic solvents and water. *Chem. Phys. Lett.* 143 (2), 127–129. [https://doi.org/10.1016/0009-2614\(88\)87025-8](https://doi.org/10.1016/0009-2614(88)87025-8).
- Lovell, J.F., Jin, C.S., Huynh, E., Jin, H., Kim, C., Rubinstein, J.L., et al, 2011. Porphyrins nanovesicles generated by porphyrin bilayers for use as multimodal biophotonic contrast agents. *Nat. Mater.* 10 (4), 324–332. <https://doi.org/10.1038/nmat2986>.
- Lukyanets, E.A., 1999. Phthalocyanines as photosensitizers in the photodynamic therapy of cancer. *J. Porphyrins Phthalocyanines* 3 (6–7), 424.
- M., A. S., J., B.-A. C., V., S. V., M., R. J. M., S., N. M. G. P. M., S., V. A., & B., C. S. M. (2015). Anchoring of Gold Nanoparticles on Graphene Oxide and Noncovalent Interactions with Porphyrinoids. *ChemNanoMat*, 1(7), 502–510. doi:doi:10.1002/cnma.201500133
- Ma, X., Zhao, Y., 2015. Biomedical Applications of Supramolecular Systems Based on Host-Guest Interactions. *Chem. Rev.* 115 (15), 7794–7839. <https://doi.org/10.1021/cr500392w>.
- Mafukidze, D.M., Sindelo, A., Nyokong, T., 2019. Spectroscopic characterization and photodynamic antimicrobial chemotherapy of phthalocyanine-silver triangular nanoprisms conjugates when supported on asymmetric polymer membranes. *Spectrochim. Acta Part A Mol. Biomol. Spectrosc.* 219, 333–345. <https://doi.org/10.1016/j.saa.2019.04.054>.
- Magadla, A., Oluwole, D.O., Managa, M., Nyokong, T., 2019. Physicochemical and antimicrobial photodynamic chemotherapy (against *E. coli*) by indium phthalocyanines in the presence of silver–iron bimetallic nanoparticles. *Polyhedron* 162, 30–38. <https://doi.org/10.1016/j.poly.2019.01.032>.
- Majeed, S.A., 2020. Combining microextraction methods with surface-enhanced Raman spectroscopy towards more selective and sensitive analyte detection by plasmonic metal nanoparticles. *Analyst*. <https://doi.org/10.1039/D0AN01304H>.
- Majeed, S.A., Ghazal, B., Nevenon, D.E., Nemykin, V.N., Makhseed, S., 2019a. Spectroscopic and TDDFT studies on the charge-transfer properties of metallated Octa(carbazolyl)phthalocyanines. *Dyes Pigm.* 170, <https://doi.org/10.1016/j.dyepig.2019.107593> 107593.
- Majeed, S.A., Nwaji, N., Mack, J., Nyokong, T., Makhseed, S., 2019b. Nonlinear optical responses of carbazole-substituted phthalocyanines conjugated to graphene quantum dots and in thin films. *J. Lumin.* 213, 88–97. <https://doi.org/10.1016/j.jlumin.2019.04.034>.
- Maree, M.D., Nyokong, T., Suhling, K., Phillips, D., 2002. Effects of axial ligands on the photophysical properties of silicon octaphenoxyphtalocyanine. *J. Porphyrins Phthalocyanines* 06 (06), 373–376. <https://doi.org/10.1142/s1088424602000452>.
- Martin, B.R., Dermody, D.J., Reiss, B.D., Fang, M., Lyon, L.A., Natan, M.J., Mallouk, T.E., 1999. Orthogonal Self-Assembly on Colloidal Gold-Platinum Nanorods. *Adv. Mater.* 11 (12), 1021–1025. [https://doi.org/10.1002/\(sici\)1521-4095\(199908\)11:12<1021::aid-adma1021>3.0.co;2-s](https://doi.org/10.1002/(sici)1521-4095(199908)11:12<1021::aid-adma1021>3.0.co;2-s).
- Masilela, N., Nyokong, T., 2011. Conjugates of low-symmetry Ge, Sn and Ti carboxy phthalocyanines with glutathione capped gold nanoparticles: An investigation of photophysical behaviour. *J. Photochem. Photobiol., A* 223 (2), 124–131. <https://doi.org/10.1016/j.jphotochem.2011.08.009>.
- Matlou, G.G., Managa, M., Nyokong, T., 2019. Effect of symmetry and metal nanoparticles on the photophysicochemical and photodynamic therapy properties of cinnamic acid zinc phthalocyanine. *Spectrochim. Acta Part A Mol. Biomol. Spectrosc.* 214, 49–57. <https://doi.org/10.1016/j.saa.2019.02.005>.
- Matlou, G.G., Nyokong, T., 2020. Photophysico-chemical properties and photoinactivation of *Staphylococcus Aureus* using zinc phthalocyanines linked silver nanoparticles conjugates. *Dyes Pigm.* 176, <https://doi.org/10.1016/j.dyepig.2020.108237> 108237.

- Matshitse, R., Nyokong, T., 2020. Substituent effect on the photophysical and nonlinear optical characteristics of Si phthalocyanine – Detonated nanodiamond conjugated systems in solution. *Inorg. Chim. Acta* 504., <https://doi.org/10.1016/j.ica.2020.119447> 119447.
- McKeown, N. B. (1998). *Phthalocyanine materials: synthesis, structure and function* (J. W. G. B. Dunn, A. R. West Ed.). Cambridge: Cambridge University Press.
- Miller, J.D., Baron, E.D., Scull, H., Hsia, A., Berlin, J.C., McCormick, T., et al, 2007. Photodynamic therapy with the phthalocyanine photosensitizer Pc 4: The case experience with preclinical mechanistic and early clinical-translational studies. *Toxicol. Appl. Pharmacol.* 224 (3), 290.
- Ming, T., Zhao, L., Chen, H., Woo, K.C., Wang, J., Lin, H.-Q., 2011. Experimental Evidence of Plasmon-Directed Polarized Emission from Gold Nanorod-Fluorophore Hybrid Nanostructures. *Nano Lett.* 11 (6), 2296–2303. <https://doi.org/10.1021/nl200535y>.
- Mishra, N., Rathore, A., Prabhune, A., Kulkarni, S., 2010. Gold Nanoparticles for Colorimetric detection of hydrolysis of antibiotics by penicillin G acylase. *Adv. Biosci. Biotechnol.* 01, 322–329. <https://doi.org/10.4236/abb.2010.14042>.
- Mitchell, C.A., Yu, L., Ward, M.D., 2001. Selective Nucleation and Discovery of Organic Polymorphs through Epitaxy with Single Crystal Substrates. *J. Am. Chem. Soc.* 123 (44), 10830–10839. <https://doi.org/10.1021/ja004085f>.
- Moeno, S., Antunes, E., Nyokong, T., 2011. Synthesis and photophysical properties of a novel zinc photosensitizer and its gold nanoparticle conjugate. *J. Photochem. Photobiol., A* 222 (2), 343–350. <https://doi.org/10.1016/j.jphotochem.2011.07.007>.
- Moeno, S., Krause, R.W.M., Ermilov, E.A., Kuzyniak, W., Hopfner, M., 2014. Synthesis and characterization of novel zinc phthalocyanines as potential photosensitizers for photodynamic therapy of cancers. *Photochem. Photobiol. Sci.* 13 (6), 963.
- Moon, S., Tanaka, S.-I., Sekino, T., 2010. Crystal Growth of Thiol-Stabilized Gold Nanoparticles by Heat-Induced Coalescence. *Nanoscale Res. Lett.* 5, 813–817. <https://doi.org/10.1007/s11671-010-9565-6>.
- Mpeta, L., Sekhosana, K., Nyokong, T., 2020. Nonlinear optical response and electrocatalytic activity of cobalt phthalocyanine clicked zinc oxide nanoparticles. *Inorg. Chim. Acta* 119661. <https://doi.org/10.1016/j.ica.2020.119661>.
- Mphuthi, N., Adekunle, A., Fayemi, O., Olasunkanmi, L., Ebenso, E., 2017. Phthalocyanine Doped Metal Oxide Nanoparticles on Multiwalled Carbon Nanotubes Platform for the detection of Dopamine. *Sci. Rep.* 7, 43181. <https://doi.org/10.1038/srep43181>.
- Mthethwa, T., Antunes, E., Nyokong, T., 2014. Photophysical properties of a new water soluble tetra thiamine substituted zinc phthalocyanine conjugated to gold nanorods of different aspect ratios. *Dalton Trans.* 43 (22), 8230–8240. <https://doi.org/10.1039/C4DT00197D>.
- Mthethwa, T., Nyokong, T., 2015. Fluorescence behavior and singlet oxygen generating abilities of aluminum phthalocyanine in the presence of anisotropic gold nanoparticles. *J. Lumin.* 157, 207–214. <https://doi.org/10.1016/j.jlumin.2014.09.005>.
- Mthethwa, T.P., Arslanoglu, Y., Antunes, E., Nyokong, T., 2012. Photophysical behaviour of cationic 2-(dimethylamino) ethanethio tetrasubstituted phthalocyanine complexes in the presence of gold nanoparticles. *Polyhedron* 38 (1), 169–177. <https://doi.org/10.1016/j.poly.2012.03.002>.
- Mthethwa, T.P., Tuncel, S., Durmuş, M., Nyokong, T., 2013. Photophysical and photochemical properties of a novel thiol terminated low symmetry zinc phthalocyanine complex and its gold nanoparticles conjugate. *Dalton Trans.* 42 (14), 4922–4930. <https://doi.org/10.1039/C3DT32698E>.
- Murphy, C.J., Sau, T.K., Gole, A.M., Orendorff, C.J., Gao, J., Gou, L., et al, 2005. Anisotropic Metal Nanoparticles: Synthesis, Assembly, and Optical Applications. *J. Phys. Chem. B* 109 (29), 13857–13870. <https://doi.org/10.1021/jp0516846>.
- Nalwa, H.S., Miyata, S., 1997. *Nonlinear optics of organic molecules and polymers*. CRC Press, Boca Raton.
- Negrimovsky, V. M., Makarova, E. A., Mikhaleiko, S. A., Solov'eva, L. I., Yuzhakova, O. A., Donyagina, V. F., et al. (2015). The search for new synthetic photosensitizers. *Russ. J. Gen. Chem.*, 85(1), 240.
- Newman, J.D.S., Blanchard, G.J., 2006. Formation of Gold Nanoparticles Using Amine Reducing Agents. *Langmuir* 22 (13), 5882–5887. <https://doi.org/10.1021/la060045z>.
- Nguyen, T.-H. T. a. T.-D. (2012). *Practical Applications in Biomedical Engineering*: InTech Publisher, Croatia.
- Nikoobakht, B., El-Sayed, M.A., 2003. Preparation and Growth Mechanism of Gold Nanorods (NRs) Using Seed-Mediated Growth Method. *Chem. Mater.* 15 (10), 1957–1962. <https://doi.org/10.1021/cm020732l>.
- Nombona, N., Antunes, E., Litwinski, C., Nyokong, T., 2011a. Synthesis and photophysical studies of phthalocyanine-gold nanoparticle conjugates. *Dalton Trans.* 40 (44), 11876–11884. <https://doi.org/10.1039/C1DT11151E>.
- Nombona, N., Maduray, K., Beukes, E., Karsten, A., & Nyokong, T. (2011b). Synthesis of phthalocyanine conjugates with gold nanoparticles and liposomes for photodynamic therapy (Vol. 107). Nwahara, N., Managa, M., Prinsloo, E., Nyokong, T., 2019. Design of Phthalocyanine-Nanoparticle Hybrids for Photodynamic Therapy Applications in Oxygen-Deficient Tumour Environment. *ChemistrySelect* 4, 9084–9095. <https://doi.org/10.1002/slct.201901466>.
- Nwaji, N., Jones, B., Mack, J., Oluwole, D., & Nyokong, T., 2017a. Nonlinear optical dynamics of benzothiazole derivatized phthalocyanines in solution, thin films and when conjugated to nanoparticles (Vol. 346).
- Nwaji, N., Mack, J., Nyokong, T., 2017b. 4-Bis(4-aminophenoxy) phenoxy derivitized phthalocyanine conjugated to metallic nanoparticles: searching for enhanced optical limiting materials. *New J. Chem.* 41 (23), 14351–14363. <https://doi.org/10.1039/c7nj02718d>.
- Nwaji, N., Mack, J., Nyokong, T., 2018. Enhanced nonlinear optical response of benzothiazole substituted ball-type phthalocyanines in the presence of metallic nanoparticles. *Opt. Mater.* 82, 93–103. <https://doi.org/10.1016/j.optmat.2018.05.052>.
- Nwaji, N., Nyokong, T., 2017c. Nanosecond optical nonlinearities in low symmetry phthalocyanine nanoconjugates studied using the Z-scan technique. *J. Lumin.* 192, 1167–1179. <https://doi.org/10.1016/j.jlumin.2017.08.053>.
- Nwaji, N., Oluwole, D.O., Mack, J., Louzada, M., Khene, S., Britton, J., Nyokong, T., 2017d. Improved nonlinear optical behaviour of ball type indium(III) phthalocyanine linked to glutathione capped nanoparticles. *Dyes Pigm.* 140, 417–430. <https://doi.org/10.1016/j.dyepig.2017.01.066>.
- O'Flaherty, S.M., Hold, S.V., Cook, M.J., Torres, T., Chen, Y., Hanack, M., Blau, W.J., 2003. Molecular Engineering of Peripherally And Axially Modified Phthalocyanines for Optical Limiting and Nonlinear Optics. *Adv. Mater.* 15 (1), 19–32. <https://doi.org/10.1002/adma.200390002>.
- Ogunsipe, A., Chen, J.-Y., Nyokong, T., 2004. Photophysical and photochemical studies of zinc(ii) phthalocyanine derivatives-effects of substituents and solvents. *New J. Chem.* 28 (7), 822–827. <https://doi.org/10.1039/B315319C>.
- Ogunsipe, A., Maree, D., Nyokong, T., 2003. Solvent effects on the photochemical and fluorescence properties of zinc phthalocyanine derivatives. *J. Mol. Struct.* 650 (1), 131–140. [https://doi.org/10.1016/S0022-2860\(03\)00155-8](https://doi.org/10.1016/S0022-2860(03)00155-8).
- Oluwole, D.O., Ngxeke, S.M., Britton, J., Nyokong, T., 2017a. The effect of point of substitution and silver based nanoparticles on the photophysical and optical nonlinearity of indium carboxyphenoxy phthalocyanine. *J. Photochem. Photobiol., A* 347, 146–159. <https://doi.org/10.1016/j.jphotochem.2017.07.032>.
- Oluwole, D.O., Prinsloo, E., Nyokong, T., 2016. Photophysicochemical properties of nanoconjugates of zinc(II) 2(3)-mono-2-(4-oxy)

- phenoxy)acetic acid phthalocyanine with cysteamine capped silver and silver-gold nanoparticles. *Polyhedron* 119, 434–444. <https://doi.org/10.1016/j.poly.2016.09.034>.
- Oluwole, D.O., Yagodin, A.V., Britton, J., Martynov, A.G., Gorbunova, Y.G., Tsivadze, A.Y., Nyokong, T., 2017b. Optical limiters with improved performance based on nanoconjugates of thiol substituted phthalocyanine with CdSe quantum dots and Ag nanoparticles. *Dalton Trans.* 46 (46), 16190–16198. <https://doi.org/10.1039/C7DT03867D>.
- Osifeko, O., Nyokong, T., 2016. Synthesis and physicochemical properties of zinc and indium phthalocyanines conjugated to quantum dots, gold and magnetic nanoparticles. *Dyes Pigm.* 131, 186–200. <https://doi.org/10.1016/j.dyepig.2016.04.015>.
- Pansare, V. J., Hejazi, S., Faenza, W. J., Prud'homme, R. K., 2012. Review of Long-Wavelength Optical and NIR Imaging Materials: Contrast Agents, Fluorophores, and Multifunctional Nano Carriers. *Chem. Mater.*, 24(5), 812.
- Papagiannouli, I., Aloukos, P., Rioux, D., Meunier, M., Couris, S., 2015. Effect of the Composition on the Nonlinear Optical Response of  $\text{AuxAg}_{1-x}$  Nano-Alloys. *J. Phys. Chem. C* 119 (12), 6861–6872. <https://doi.org/10.1021/jp512404a>.
- Pastoriza-Santos, I., Liz-Marzán, L.M., 2008. Colloidal silver nanoplates. State of the art and future challenges. *J. Mater. Chem.* 18 (15), 1724–1737. <https://doi.org/10.1039/B716538B>.
- Philip, R., Kumar, G.R., Sandhyarani, N., Pradeep, T., 2000. Picosecond optical nonlinearity in monolayer-protected gold, silver, and gold-silver alloy nanoclusters. *Phys. Rev. B* 62 (19), 13160–13166. <https://doi.org/10.1103/PhysRevB.62.13160>.
- Pileni, M.P., Gulik-Krzywicki, T., Tanori, J., Filankembo, A., Dedieu, J.C., 1998. Template Design of Microreactors with Colloidal Assemblies: Control the Growth of Copper Metal Rods. *Langmuir* 14 (26), 7359–7363. <https://doi.org/10.1021/la980461m>.
- Pillay, J., Ozoemena, K.I., 2009. Layer-by-layer self-assembled nanostructured phthalocyaninatoiron(II)/SWCNT-poly(m-aminobenzenesulfonic acid) hybrid system on gold surface: Electron transfer dynamics and amplification of H<sub>2</sub>O<sub>2</sub> response. *Electrochim. Acta* 54 (22), 5053–5059. <https://doi.org/10.1016/j.electacta.2008.12.056>.
- Prabukumar, C., & Bhat, K. U. (2018). Purification of Silver Nanowires Synthesised by Polyol Method. *Mater. Today: Proc.* 5 (10, Part 3), 22487–22493. doi: <https://doi.org/10.1016/j.matpr.2018.06.620>.
- R. Dalton, L., H. Steier, W., H. Robinson, B., Zhang, C., Ren, A., Garner, S., et al. (1999). From molecules to opto-chips: organic electro-optic materials. *J. Mater. Chem.*, 9(9), 1905–1920. doi:10.1039/A902659B.
- Ramanathan, T., Fisher, F.T., Ruoff, R.S., Brinson, L.C., 2005. Amino-Functionalized Carbon Nanotubes for Binding to Polymers and Biological Systems. *Chem. Mater.* 17 (6), 1290–1295. <https://doi.org/10.1021/cm048357f>.
- Rapulenyane, N., Antunes, E., Nyokong, T., 2013. A study of the photophysical and antimicrobial properties of two zinc phthalocyanine-silver nanoparticle conjugates. *New J. Chem.* 37 (4), 1216–1223. <https://doi.org/10.1039/C3NJ41107A>.
- Ray, A., Pal, H., Ramanan, V., Bhattacharya, S., 2015. New photophysical insights on effect of gold nanoparticles on the interaction between phthalocyanine and PC70BM in solution. *Spectrochim. Acta Part A Mol. Biomol. Spectrosc.* 150, 992–1001. <https://doi.org/10.1016/j.saa.2015.05.075>.
- Ron Jenkins, R.S., 1996. *Introduction to X-Ray Powder Diffraction*. Wiley & Sons, New York.
- Saka, E.T., Durmuş, M., Kantekin, H., 2011. Solvent and central metal effects on the photophysical and photochemical properties of 4-benzyloxybenzoxy substituted phthalocyanines. *J. Organomet. Chem.* 696 (4), 913–924. <https://doi.org/10.1016/j.jorganchem.2010.10.024>.
- Saleh, B.E.A., Teich, M.C., 2001. *Photon Optics Fundamentals of Photonics*. John Wiley & Sons Inc., pp. 384–422.
- Selvakannan, P.R., Mandal, S., Pasricha, R., Adyanthaya, S.D., Sastry, M., 2002. One-step synthesis of hydrophobized gold nanoparticles of controllable size by the reduction of aqueous chloroaurate ions by hexadecylaniline at the liquid-liquid interface. *Chem. Commun.* 13, 1334–1335. <https://doi.org/10.1039/B203438G>.
- Senge, M.O., Fazekas, M., Notaras, E.G.A., Blau, W.J., Zawadzka, M., Locos, O.B., Ni Mhuirheartaigh, E.M., 2007. Nonlinear Optical Properties of Porphyrins. *Adv. Mater.* 19 (19), 2737–2774. <https://doi.org/10.1002/adma.200601850>.
- Seotsanyana-Mokhosi, I., Kuznetsova, N., Nyokong, T., 2001. Photochemical studies of tetra-2,3-pyridinoporphyrazines. *J. Photochem. Photobiol., A* 140 (3), 215–222. [https://doi.org/10.1016/S1010-6030\(01\)00427-0](https://doi.org/10.1016/S1010-6030(01)00427-0).
- Shaw, C.F., 1999. Gold-Based Therapeutic Agents. *Chem. Rev.* 99 (9), 2589–2600. <https://doi.org/10.1021/cr980431o>.
- Sheik-Bahae, M., Said, A. A., Van Stryland, E., 1989. High-sensitivity single-beam N<sub>2</sub> measurements (Vol. 14).
- Sheik-Bahae, M., Said, A.A., Wei, T., Hagan, D.J., Stryland, E.W.V., 1990. Sensitive measurement of optical nonlinearities using a single beam. *IEEE J. Quantum Electron.* 26 (4), 760–769. <https://doi.org/10.1109/3.53394>.
- Sheik-Bahae, M., Stryland, E. W. V., 1998. In *Characterization Techniques and Tabulations for Organic Nonlinear Materials*; In: M. G. K. a. C. W. Dirk (Ed.), (pp. 655–692). New York: Marcel Dekker.
- Shi, Y., He, L., Deng, Q., Liu, Q., Li, L., Wang, W., et al. 2019. Synthesis and Applications of Silver Nanowires for Transparent Conductive Films. *Micromachines* 10, 330. <https://doi.org/10.3390/mi10050330>.
- Shibu, E.S., Hamada, M., Murase, N., Biju, V., 2013. Nanomaterials formulations for photothermal and photodynamic therapy of cancer. *J. Photochem. Photobiol., C* 15, 53–72. <https://doi.org/10.1016/j.jphotochemrev.2012.09.004>.
- Shinohara, H., Tsaryova, O., Schnurpfeil, G., Wöhrle, D., 2006. Differently substituted phthalocyanines: Comparison of calculated energy levels, singlet oxygen quantum yields, photo-oxidative stabilities, photocatalytic and catalytic activities. *J. Photochem. Photobiol., A* 184 (1), 50–57. <https://doi.org/10.1016/j.jphotochem.2006.03.024>.
- Shirk, J.S., Pong, R.G.S., Bartoli, F.J., Snow, A.W., 1993. Optical limiter using a lead phthalocyanine. *Appl. Phys. Lett.* 63 (14), 1880–1882. <https://doi.org/10.1063/1.110635>.
- Shirk, J.S., Pong, R.G.S., Flom, S.R., Heckmann, H., Hanack, M., 2000. Effect of Axial Substitution on the Optical Limiting Properties of Indium Phthalocyanines. *J. Phys. Chem. A* 104 (7), 1438–1449. <https://doi.org/10.1021/jp993254j>.
- Singh, V.P., Singh, R.S., Parthasarathy, B., Aguilera, A., Anthony, J., Payne, M., 2005. Copper-phthalocyanine-based organic solar cells with high open-circuit voltage. *Appl. Phys. Lett.* 86, (8) 082106.
- Snow, A.W., Griffith, J.R., Marullo, N.P., 1984. Syntheses and characterization of heteroatom-bridged metal-free phthalocyanine network polymers and model compounds. *Macromolecules* 17 (8), 1614–1624. <https://doi.org/10.1021/ma00138a033>.
- Spiller, W., Kliesch, H., Wöhrle, D., Hackbarth, S., Röder, B., Schnurpfeil, G., 1998. Singlet oxygen quantum yields of different photosensitizers in polar solvents and micellar solutions. *J. Porphyrins Phthalocyanines* 2 (2), 145–158. [https://doi.org/10.1002/\(SICI\)1099-1409\(199803/04\)2:2 < 145::AID-JPP60 > 3.0.CO;2-2](https://doi.org/10.1002/(SICI)1099-1409(199803/04)2:2 < 145::AID-JPP60 > 3.0.CO;2-2).
- Srinivas, Naga, N. K. M., Rao, S. V., Rao, D. N., 2003. Saturable and reverse saturable absorption of Rhodamine B in methanol and water. *J. Opt. Soc. Am. B*, 20(12), 2470–2479. doi:10.1364/JOSAB.20.002470.
- Srinivas, Rao, S. V., Rao, D. V. G. L. N., Kimball, B. K., Nakashima, M., DeCristofano, B. S., Rao, D. N., 2001. Wavelength dependent studies of nonlinear absorption in zinc meso-tetra

- (p-methoxyphenyl)tetrabenzoporphyrin (Znmp TBP) using Z-scan technique. *J. Porphyrins Phthalocyanines*, 5(7), 549–554. doi: 10.1002/jpp.357.
- Stillman, M.J., Thomson, A.J., 1974. Assignment of the charge-transfer bands in some metal phthalocyanines. Evidence for the S=1 state of iron (II) phthalocyanine in solution. *J. Chem. Soc., Faraday Trans. 2: Mol. Chem. Phys.* 70, 790–804. <https://doi.org/10.1039/F29747000790>.
- Sun, X., 2010. Morphology and size-controllable preparation of silver nanostructures through a wet-chemical route at room temperature. *Inorg. Mater.* 46 (6), 679–682. <https://doi.org/10.1134/s0020168510060208>.
- Sun, X., Dong, S., Wang, E., 2004. Large-scale synthesis of micrometer-scale single-crystalline Au plates of nanometer thickness by a wet-chemical route. *Angew. Chem. Int. Ed. Engl.* 43 (46), 6360–6363. <https://doi.org/10.1002/anie.200461013>.
- Sun, X., Dong, S., Wang, E., 2005. Rapid preparation and characterization of uniform, large, spherical Ag particles through a simple wet-chemical route. *J. Colloid Interface Sci.* 290 (1), 130–133. <https://doi.org/10.1016/j.jcis.2005.04.016>.
- Sun, Y., Mayers, B., Herricks, T., Xia, Y., 2003. Polyol Synthesis of Uniform Silver Nanowires: A Plausible Growth Mechanism and the Supporting Evidence. *Nano Lett.* 3 (7), 955–960. <https://doi.org/10.1021/nl034312m>.
- Suzuki, K., Kobayashi, A., Kaneko, S., Takehira, K., Yoshihara, T., Ishida, H., et al, 2009. Reevaluation of absolute luminescence quantum yields of standard solutions using a spectrometer with an integrating sphere and a back-thinned CCD detector. *PCCP* 11 (42), 9850–9860. <https://doi.org/10.1039/B912178A>.
- Swierczewska, M., Lee, S., Chen, X., 2011. The design and application of fluorophore-gold nanoparticle activatable probes. *PCCP* 13 (21), 9929–9941. <https://doi.org/10.1039/C0CP02967J>.
- Syafuddin, A., Salmiati, S., Salim, M., Kueh, A., Hadibarata, T., 2017. A Review of Silver Nanoparticles: Research Trends, Global Consumption, Synthesis, Properties, and Future Challenges. *J. Chin. Chem. Soc.* 64, 732–756. <https://doi.org/10.1002/jccs.201700067>.
- Teixeira, R., Paulo, P.M.R., Costa, S.M.B., 2015. Gold Nanoparticles in Core-Polyelectrolyte-Shell Assemblies Promote Large Enhancements of Phthalocyanine Fluorescence. *J. Phys. Chem. C* 119 (37), 21612–21619. <https://doi.org/10.1021/acs.jpcc.5b04667>.
- Teixeira, R., Paulo, P.M.R., Viana, A.S., Costa, S.M.B., 2011. Plasmon-Enhanced Emission of a Phthalocyanine in Polyelectrolyte Films Induced by Gold Nanoparticles. *J. Phys. Chem. C* 115 (50), 24674–24680. <https://doi.org/10.1021/jp209605v>.
- Terentyuk, G., Panfilova, E., Khanadeev, V., Chumakov, D., Genina, E., Bashkatov, A., et al, 2014. Gold nanorods with a hematoporphyrin-loaded silica shell for dual-modality photodynamic and photothermal treatment of tumors in vivo. *Nano Res.* 7 (3), 325–337. <https://doi.org/10.1007/s12274-013-0398-3>.
- Thomas, S., Nair, S.K., Jamal, E.M.A., Al-Harhi, S.H., Varma, M. R., Anantharaman, M.R., 2008. Size-dependent surface plasmon resonance in silver silica nanocomposites. *Nanotechnology* 19, (7). <https://doi.org/10.1088/0957-4484/19/7/075710> 075710.
- Tombe, S., Antunes, E., Nyokong, T., 2013a. Electrospun fibers functionalized with phthalocyanine-gold nanoparticle conjugates for photocatalytic applications. *J. Mol. Catal. A: Chem.* 371, 125–134. <https://doi.org/10.1016/j.molcata.2013.01.033>.
- Tombe, S., Antunes, E., Nyokong, T., 2013b. The photophysical and photochemical behaviour of coumarin-derivatized zinc phthalocyanine when conjugated with gold nanoparticles and electrospun into polymer fibers. *New J. Chem.* 37 (3), 679–689. <https://doi.org/10.1039/C2NJ40984D>.
- Tombe, S., Chidawanyika, W., Antunes, E., Priniotakis, G., Westbroek, P., Nyokong, T., 2012. Physicochemical behavior of zinc tetrakis (benzylmercapto) phthalocyanine when used to functionalize gold nanoparticles and in electrospun fibers. *J. Photochem. Photobiol., A* 240, 50–58. <https://doi.org/10.1016/j.jphotochem.2012.05.011>.
- Topal, S.Z., Isci, U., Kumru, U., Atilla, D., Gurek, A.G., Hirel, C., et al, 2014. Modulation of the electronic and spectroscopic properties of Zn(II) phthalocyanines by their substitution pattern. *Dalton Trans.* 43 (18), 6897–6908. <https://doi.org/10.1039/C3DT53410C>.
- Tran Thi, T.H., Desforge, C., Thiec, C., Gaspard, S., 1989. Singlet-singlet and triplet-triplet intramolecular transfer processes in a covalently linked porphyrin-phthalocyanine heterodimer. *J. Phys. Chem.* 93 (4), 1226–1233. <https://doi.org/10.1021/j100341a013>.
- Turkevich, J., Stevenson, P.C., Hillier, J., 1951. A study of the nucleation and growth processes in the synthesis of colloidal gold. *Discuss. Faraday Soc.* 11, 55–75. <https://doi.org/10.1039/DF9511100055>.
- Tutt, L.W., Boggess, T.F., 1993. A review of optical limiting mechanisms and devices using organics, fullerenes, semiconductors and other materials. *Prog. Quantum Electron.* 17 (4), 299–338. [https://doi.org/10.1016/0079-6727\(93\)90004-S](https://doi.org/10.1016/0079-6727(93)90004-S).
- Tutt, L.W., Kost, A., 1992. Optical limiting performance of C60 and C70 solutions. *Nature* 356, 225. <https://doi.org/10.1038/356225a0>.
- van der Zande, B.M.I., Böhmer, M.R., Fokkink, L.G.J., Schönenberger, C., 2000. Colloidal Dispersions of Gold Rods: Synthesis and Optical Properties. *Langmuir* 16 (2), 451–458. <https://doi.org/10.1021/la9900425>.
- Venkatram, N., Narayana Rao, D., Giribabu, L., Venugopal Rao, S., 2008. Femtosecond nonlinear optical properties of alkoxy phthalocyanines at 800nm studied using Z-Scan technique. *Chem. Phys. Lett.* 464 (4), 211–215. <https://doi.org/10.1016/j.cplett.2008.09.029>.
- Vukovic, S., Corni, S., Mennucci, B., 2009. Fluorescence Enhancement of Chromophores Close to Metal Nanoparticles. Optimal Setup Revealed by the Polarizable Continuum Model. *J. Phys. Chem. C* 113 (1), 121–133. <https://doi.org/10.1021/jp808116y>.
- Walter, M.G., Rudine, A.B., Wamser, C.C., 2010. Porphyrins and phthalocyanines in solar photovoltaic cells. *J. Porphyrins Phthalocyanines* 14 (09), 759–792.
- Wang, Kang, B.S., Ren, F., Tien, L. C., Sadik, P. W., Norton, D. P., et al. (2005). Hydrogen-selective sensing at room temperature with ZnO nanorods. *Appl. Phys. Lett.*, 86(24), 243503. doi:10.1063/1.1949707
- Wang, B., Li, Z., Zuo, X., Wu, Y., Wang, X., Chen, Z., et al, 2010. Preparation, characterization and NO<sub>2</sub>-sensing properties of octa-iso-pentylxyphthalocyanine lead spin-coating films. *Sens. Actuators, B* 149 (2), 362–367. <https://doi.org/10.1016/j.snb.2010.06.051>.
- Wang, Y.L., Xu, J.J., Lin, Y.W., Chen, Q., Shan, H.Q., Yan, Y., et al, 2015. Tetra-methyl substituted copper (II) phthalocyanine as a hole injection enhancer in organic light-emitting diodes. *AIP Adv.* 5, (10) 107205.
- Waszkowska, K., Krupka, O., Kharchenko, O., Figà, V., Smokal, V., Kutsevol, N., Sahraoui, B., 2020. Influence of ZnO nanoparticles on nonlinear optical properties. *Appl. Nanosci.* <https://doi.org/10.1007/s13204-020-01373-3>.
- Weidner, T., Bretthauer, F., Ballav, N., Motschmann, H., Orendi, H., Bruhn, C., et al, 2008. Correlation between the molecular structure and photoresponse in aliphatic self-assembled monolayers with azobenzene tailgroups. *Langmuir: ACS J. Surf. Colloids* 24 (20), 11691–11700. <https://doi.org/10.1021/la802454w>.
- Widoniak, J., Eiden-Assmann, S., Maret, G., 2005. Silver particles tailoring of shapes and sizes. *Colloids Surf., A* 270–271, 340–344. <https://doi.org/10.1016/j.colsurfa.2005.09.004>.
- Wieder, M.E., Hone, D.C., Cook, M.J., Handsley, M.M., Gavriliovic, J., Russell, D.A., 2006. Intracellular photodynamic therapy with photosensitizer-nanoparticle conjugates: cancer therapy using a ‘Trojan horse’. *Photochem. Photobiol. Sci.* 5 (8), 727–734. <https://doi.org/10.1039/B602830F>.
- Williams, A.T.R., Winfield, S.A., Miller, J.N., 1983. Relative fluorescence quantum yields using a computer-controlled luminescence spectrometer. *Analyst* 108 (1290), 1067–1071. <https://doi.org/10.1039/AN9830801067>.
- Wu, F., Yue, L., Cheng, K., Chen, J., Wong, K.-L., Wong, W.-K., Zhu, X., 2020. Facile Preparation of Phthalocyanine-Based Nan-

- odots for Photoacoustic Imaging and Photothermal Cancer Therapy In Vivo. *ACS Biomater. Sci. Eng.* 6 (9), 5230–5239. <https://doi.org/10.1021/acsbiomaterials.0c00684>.
- Wu, H.-L., Chen, C.-H., Huang, M.H., 2009. Seed-Mediated Synthesis of Branched Gold Nanocrystals Derived from the Side Growth of Pentagonal Bipyramids and the Formation of Gold Nanostars. *Chem. Mater.* 21 (1), 110–114. <https://doi.org/10.1021/cm802257e>.
- Wu, X., Redmond, P.L., Liu, H., Chen, Y., Steigerwald, M., Brus, L., 2008. Photovoltage mechanism for room light conversion of citrate stabilized silver nanocrystal seeds to large nanoprisms. *J. Am. Chem. Soc.* 130 (29), 9500–9506. <https://doi.org/10.1021/ja8018669>.
- Xia, Y., Xiong, Y., Lim, B., Skrabalak, S.E., 2009. Shape-controlled synthesis of metal nanocrystals: simple chemistry meets complex physics? *Angew. Chem. Int. Ed. Engl.* 48 (1), 60–103. <https://doi.org/10.1002/anie.200802248>.
- Xue, C., Xue, Y., Dai, L., Urbas, A., Li, Q., 2013. Size- and Shape-Dependent Fluorescence Quenching of Gold Nanoparticles on Perylene Dye. *Adv. Opt. Mater.* 1 (8), 581–587. <https://doi.org/10.1002/adom.201300175>.
- Yam, C.M., Pradier, C.M., Salmain, M., Fischer-Durand, N., Jaouen, G., 2002. Molecular recognition of avidin on biotin functionalized gold surfaces detected by FT-IRRAS and use of metal carbonyl probes. *J. Colloid Interface Sci.* 245 (1), 204–207. <https://doi.org/10.1006/jcis.2001.7981>.
- Yam, C.M., Pradier, C.M., Salmain, M., Marcus, P., Jaouen, G., 2001. Binding of Biotin to Gold Surfaces Functionalized by Self-Assembled Monolayers of Cystamine and Cysteamine: Combined FT-IRRAS and XPS Characterization. *J. Colloid Interface Sci.* 235 (1), 183–189. <https://doi.org/10.1006/jcis.2000.7362>.
- Yang, Z.-L., Chen, H.-Z., Cao, L., Li, H.-Y., Wang, M., 2004. Synthesis and photoconductivity study of carbon nanotube bonded by tetrasubstituted amino manganese phthalocyanine. *Mater. Sci. Eng., B* 106 (1), 73–78. <https://doi.org/10.1016/j.mseb.2003.09.001>.
- Yin, R., Agrawal, T., Khan, U., Gupta, G.K., Rai, V., Huang, Y.-Y., Hamblin, M.R., 2015. Antimicrobial photodynamic inactivation in nanomedicine: small light strides against bad bugs. *Nanomedicine* 10 (15), 2379–2404. <https://doi.org/10.2217/nmm.15.67>.
- Yoshimoto, S., Honda, Y., Ito, O., Itaya, K., 2008. Supramolecular Pattern of Fullerene on 2D Bimolecular “Chessboard” Consisting of Bottom-up Assembly of Porphyrin and Phthalocyanine Molecules. *J. Am. Chem. Soc.* 130 (3), 1085–1092. <https://doi.org/10.1021/ja077407p>.
- Yu, Chang, S.-S., Lee, C.-L., & Wang, C. R. C. (1997). Gold Nanorods: Electrochemical Synthesis and Optical Properties. *J. Phys. Chem. B*, 101(34), 6661–6664. doi:10.1021/jp971656q.
- Yuen, A.P., Jovanovic, S.M., Hor, A.M., Klenkler, R.A., Devenyi, G.A., Loutfy, R.O., Preston, J.S., 2012. Photovoltaic properties of M-phthalocyanine/fullerene organic solar cells. *Sol. Energy* 86 (6), 1683–1688.
- Zasedatelev, A.V., Dubinina, T.V., Krichevsky, D.M., Krasovskii, V. I., Gak, V.Y., Pushkarev, V.E., et al, 2016. Plasmon-Induced Light Absorption of Phthalocyanine Layer in Hybrid Nanoparticles: Enhancement Factor and Effective Spectra. *J. Phys. Chem. C* 120 (3), 1816–1823. <https://doi.org/10.1021/acs.jpcc.5b08804>.
- Zawadzka, A., Karakas, A., Plóciennik, P., Szatkowski, J., Łukasiak, Z., Kapceoglu, A., et al, 2015. Optical and structural characterization of thin films containing metallophthalocyanine chlorides. *Dyes Pigm.* 112, 116–126. <https://doi.org/10.1016/j.dyepig.2014.06.029>.
- Zawadzka, A., Plóciennik, P., Strzelecki, J., Korcala, A., Arof, A.K., Sahraoui, B., 2014. Impact of annealing process on stacking orientations and second order nonlinear optical properties of metallophthalocyanine thin films and nanostructures. *Dyes Pigm.* 101, 212–220. <https://doi.org/10.1016/j.dyepig.2013.09.044>.
- Zawadzka, A., Plóciennik, P., Strzelecki, J., Pranaitis, M., Dabos-Seignon, S., Sahraoui, B., 2013. Structural and nonlinear optical properties of as-grown and annealed metallophthalocyanine thin films. *Thin Solid Films* 545, 429–437. <https://doi.org/10.1016/j.tsf.2013.07.042>.
- Zawadzka, A., Waszkowska, K., Karakas, A., Plóciennik, P., Korcala, A., Wisniewski, K., et al, 2018. Diagnostic and control of linear and nonlinear optical effects in selected self-assembled metallophthalocyanine chlorides nanostructures. *Dyes Pigm.* 157, 151–162. <https://doi.org/10.1016/j.dyepig.2018.04.048>.
- Zhang, Yun-Dong, Zhao, Z.-Y., Yao, C.-B., Yang, L., Li, J., Yuan, P., 2014. The nonlinear absorption and optical limiting in phenoxyphthalocyanines liquid in nano- and femto-second regime: Experimental studies. *Opt. Laser Technol.* 58, 207–214. <https://doi.org/10.1016/j.optlastec.2013.11.022>.
- Zhang, B., Xu, C., Sun, C., Yu, C., 2019. Polyphosphoester-Based Nanocarrier for Combined Radio-Photothermal Therapy of Breast Cancer. *ACS Biomater. Sci. Eng.* 5 (4), 1868–1877. <https://doi.org/10.1021/acsbiomaterials.9b00051>.
- Zhang, D., Zhou, X., Shou, H., He, X., Jia, K., Liu, X., 2018. Immobilization of Ag nanowire into zinc phthalocyanine doped copolyester elastomer for optoelectric flexible strain sensor. *Chem. Phys. Lett.* 693, 55–59. <https://doi.org/10.1016/j.cplett.2017.12.074>.
- Zhang, P., Wyman, I., Hu, J., Lin, S., Zhong, Z., Tu, Y., et al, 2017. Silver nanowires: Synthesis technologies, growth mechanism and multifunctional applications. *Mater. Sci. Eng., B* 223, 1–23. <https://doi.org/10.1016/j.mseb.2017.05.002>.
- Zharnikov, M., Frey, S., Heister, K., Grunze, M., 2000. Modification of Alkanethiolate Monolayers by Low Energy Electron Irradiation: Dependence on the Substrate Material and on the Length and Isotopic Composition of the Alkyl Chains. *Langmuir* 16 (6), 2697–2705. <https://doi.org/10.1021/la991034r>.
- Zheng, B.-D., He, Q.-X., Li, X., Yoon, J., Huang, J.-D., 2021. Phthalocyanines as contrast agents for photothermal therapy. *Coord. Chem. Rev.* 426. <https://doi.org/10.1016/j.ccr.2020.213548>
- Zhou, J., Wang, Q., Geng, S., Lou, R., Yin, Q., Ye, W., 2019. Construction and evaluation of tumor nucleus-targeting nanocomposite for cancer dual-mode imaging – Guiding photodynamic therapy/photothermal therapy. *Mater. Sci. Eng., C* 102, 541–551. <https://doi.org/10.1016/j.msec.2019.04.088>.
- Zhou, X., He, X., Wei, S., Jia, K., Liu, X., 2016. Au nanorods modulated NIR fluorescence and singlet oxygen generation of water soluble dendritic zinc phthalocyanine. *J. Colloid Interface Sci.* 482, 252–259. <https://doi.org/10.1016/j.jcis.2016.07.072>.
- Zhou, X., Jia, K., He, X., Wei, S., Wang, P., Liu, X., 2018. Assembly of carboxylated zinc phthalocyanine with gold nanoparticle for colorimetric detection of calcium ion. *J. Mater. Sci.: Mater. Electron.* 29 (10), 8380–8389. <https://doi.org/10.1007/s10854-018-8849-y>.
- Zongo, S., Dhlamini, M.S., Neethling, P.H., Yao, A., Maaza, M., Sahraoui, B., 2015. Synthesis, characterization and femtosecond nonlinear saturable absorption behavior of copper phthalocyanine nanocrystals doped-PMMA polymer thin films. *Opt. Mater.* 50, 138–143. <https://doi.org/10.1016/j.optmat.2015.10.013>.
- Zou, Q., Abbas, M., Zhao, L., Li, S., Shen, G., Yan, X., 2017. Biological Photothermal Nanodots Based on Self-Assembly of Peptide-Porphyrin Conjugates for Antitumor Therapy. *J. Am. Chem. Soc.* 139 (5), 1921–1927. <https://doi.org/10.1021/jacs.6b11382>.
- Zyss, J., 1994. *Molecular Nonlinear Optics: Materials, Physics, and Devices (Quantum Electronics-Principles and Applications)*. Academic Press, New York.